Ministère de l'Enseignement Supérieur et de la Recherche Scientifique

Université Hassiba Benbouali de Chlef

Faculté de Génie Civil et d'architecture.

Département de Génie civil.

THÈSE

Présentée pour l'obtention du diplôme de

DOCTORAT EN LMD

Spécialité : STRUCTURES

Par

ABDENNOUR LAKHAL

Thème :

Comportement au feu des dalles mixtes en béton léger

Soutenue le 03/07/2025, devant le jury composé de :

AIT ATMANE Hassen	Professeur	UHB Chlef	Président
HASSAINE DAOUADJI Tahar	Professeur	Université de Tiaret	Examinateur
BENSATALLAH Tayeb	Professeur	Université de Tiaret	Examinateur
ADJOUDJ M'hamed	Professeur	UHB Chlef	Examinateur
BOUGARA Abdelkader	Professeur	UHB Chlef	Rapporteur
BENLEKEHAL Nourredine	MCB	UHB Chlef	Co-Rapporteur

Ministry of Higher Education and Scientific Research.
Hassiba BenBouali University of Chlef.
Faculty of Civil Engineering and Architecture.
Department of Civil Engineering.

THESIS

Submitted for the award of the degree

DOCTORAT IN LMD

Specialty : STRUCTURES

By

ABDENNOUR LAKHAL

Theme:

Fire behaviour of composite slabs under fire conditions

Defended on 07/03/2025, before the jury composed of:

AIT ATMANE Hassen	Professor	UHB Chlef	President
HASSAINE DAOUADJI Tahar	Professor	Université of Tiaret	Examiner
BENSATALLAH Tayeb	Professor	Université of Tiaret	Examiner
ADJOUDJ M'hamed	Professor	UHB Chlef	Examiner
BOUGARA Abdelkader	Professor	UHB Chlef	Supervisor
BENLEKEHAL Nourredine	Senior lecturer	UHB Chlef	Co- Supervisor

ACKNOWLEDGEMENTS

I would like to express my deepest gratitude to my supervisors: Professor Abdelkader Bougara, and co-supervisor Dr. Noureddine Benlakehal. Their invaluable guidance, solid support, and generous investment of time and efforts have been instrumental in the completion of this thesis. I sincerely appreciate their encouragement alongside my university teachers throughout this journey.

Also, I would like to thanks my family and friends for their moral support during this journey. This accomplishment is as much theirs as it is mine.

I would like to express my deepest gratitude to my beloved wife, for her unwavering support throughout this journey. Her invaluable assistance in refining my English writing, along with her endless patience and encouragement, made this thesis possible.

Abstract

Composite structures are composed of two or more different materials called composite elements. These elements have many benefits due to their combined properties that allow them to behave as a single unit to perform better in overall this work is about the Composite slabs, which are horizontal elements used for many types of buildings. They are made by casting concrete above a profiled steel sheet. The main objective of this research is to study the influence of lightweight concrete on the thermal-mechanical behaviour of composite slabs by developing a 3D finite element model the study is divided into three major parts. Starting with a literature review of experimental and numerical works on the thermal-mechanical behaviour of Composite slabs passing to a thermal analysis using ANSYS; this study shows that the moisture content of lightweight concrete significantly impacts fire resistance time. When the moisture content exceeds 3%, the Eurocode method predicts a lower fire resistance time compared to the simulation method. The prediction models indicate that to achieve the same fire resistance time, a normal-weight concrete section must be 7% thicker than a lightweight concrete section. Finally, a thermal-mechanical analysis was conducted using a hybrid method based on the thermal results of the finite elements study and the analytical equations mentioned in the Eurocodes. The results of this study show that concretes with higher mechanical performances result in a significant residual moment after heating, while the stability is still monitored. The development of the deflection is more important in LWC than in NWC and the positions of the rebars have a significant impact on the thermal and mechanical results of the composite slab.

Keywords: composite slab, lightweight concrete, fire resistance, numerical simulation, Eurocode 4, moisture content, load bearing capacity, deflection.

Résumé

Les structures mixtes sont constituées de deux matériaux ou plus, appelées éléments mixtes, qui offrent des avantages grâce à leurs propriétés combinées permettant une performance globale optimisée. Cette étude se concentre sur les dalles mixtes, des éléments horizontaux largement utilisés dans le bâtiment à ossature en acier ou mixte, formées par du béton coulé sur une tôle d'acier profilée. L'objectif principal est d'étudier l'influence du béton léger sur leur comportement des dalles mixtes sollicité par des charges verticales et celle des hautes températures des incendies via un modèle 3D par éléments finis. Le travail débute par une revue de littérature des études expérimentales et numériques existantes, suivie d'une analyse thermique avec ANSYS. Les résultats montrent que la teneur en humidité du béton léger joue un rôle clé dans la résistance au feu : au-delà de 3%, l'Eurocode sous-estime cette résistance par rapport aux simulations. Pour une protection équivalente, le béton ordinaire nécessite une épaisseur 7% supérieure. Enfin, une analyse thermo-mécanique hybride (couplant éléments finis et équations Eurocodes) révèle que les bétons de haute caractéristiques mécaniques maintiennent un moment résiduel notable après chauffage, tandis que la déformation est plus prononcée pour les bétons légers. La position des armatures s'avère également déterminante pour les performances globales de la dalle.

Mots clés : Dalle mixte, béton léger, résistance au feu, simulation numérique, Eurocode 4, teneur en humidité, capacité portante, flèche.

ملخص

تكون الهياكل المركبة من مادتين أو أكثر تتميز بخصائص متكاملة تمنحها أداءً فريداً، حيث تركز هذه الدراسة على البلاطة المركبة المستخدمة في البناء والتي يتم تنفيذها بصب الخرسانة فوق صفائح فولاذية مموجة، من خلال نموذج ثلاثي الأبعاد بالمحاكاة العددية (العناصر المحددة). تم تحليل تأثير الخرسانة خفيفة الوزن على السلوك الحراري-الميكانيكي لهذه البلاطة المركبة، حيث أظهرت نتائج التحليل الحراري (باستخدام ANSYS) أن محتوى الرطوبة في الخرسانة خفيفة الوزن يؤثر بشكل كبير على مقاومة الحريق، فعند تجاوز نسبة 3% تتنبأ معايير كود الأوربي 4 بزمن مقاومة أقل مقارنة بنتائج المحاكاة، كما تتطلب الخرسانة العادية زيادة سماكتها بنسبة 7% لتحقيق نفس مقاومة الحريق. أما نتائج التحليل الحراري-الميكانيكي (باستخدام طريقة هجينة) فقد كشفت أن الخرسانة عالية الأداء تحتفظ بعزم مقاوم كبير بعد التعرض للحرارة، بينما تظهر انحرافات أكبر في الخرسانة خفيفة الوزن، مع التأكيد على الدور الحاسم لمواضع حديد التسليح في الأداء العام للبلاطة المركبة.

كلمات البحث: البلاطة المركبة، الخرسانة خفيفة الوزن، مقاومة الحريق، طريقة التحليل الرقمية، كود الأوربي 4، نسبة الرطوبة، قيمة التحمل، إنحناءات.

TABLE OF CONTENTS

LIST OF FIGURES

LIST OF TABLES

SYMBOLS NOMENCLATURE TABLE

Latin Letters

A_i A_j	Composite slab components Area.
A_p	Nominal cross-section of the steel deck.
A_s	Cross-sectional area of reinforcement.
b	Bond width of the loads.
b_m	The width of the rib at the half of the depth of the steel deck.
d_p	Position of the rebar relative to the upper side of the slab.
d_s	Position of the rebars relative to the upper side of the slab.
E	Young modulus of the material.
e_s	The cover distance of the reinforcement relative to the lower side of the slab.
f_y	Nominal yield strength for steel.
f_u	Ultimate yield strength for steel.
f_c	Mechanical resistance of the concrete.
G	Warping Coefficient.
h	Overall depth of slab.
h_c	Thickness of concrete above the main flat surface of the top of the ribs.
h_p	Height of the steel deck.
$\dot{h}_{net,r}$	Heat flux from radiation.
$\dot{h}_{net,c}$	Heat flux from convection.
$\dot{h}_{net,d}$	Design value of the density of heat flow per unit area.
I_c	Second moment of area for the section.
I_p	Second moment of inertia of the steel deck.
K_y	Reduction factor on effective yield strength.
K_E	Reduction factor on the elastic modulus.
K_p	Reduction factor on proportional limit of the yield strength.
K_u	Reduction factor on the ultimate tensile strength.
K_c	Reduction factor on the compressive strength of concretes.
L	Span of theyu slab between the supports.
L_1, L_2, L_3	**S**pecific dimensions of the trapezoidal or re-entrant steel deck profile.
M_{Rd}	The resisting moment of the slab.
M_{Ed}	The solicitating moment.
$M_{p,Rd}$	Positive sagging moment resistance.
$N_{p,pl}$	Plastic tensile force for the effective section.
$N_{s,pl}$	Plastic tensile force for the steel rebars.

q	Applied load on the slab.
T or θ	Temperature of the element.
T_g	Gas temperature.
T_m	Materials temperature.
$t_{\mathbf{fi,d}}$	Design value of the fire resistance.
$t_{\mathbf{fi,r}}$	Minimal required resistance.
x_c	Position of the elastic neutral axis relative to the upper side of the slab.
x_u	The position of the elastic neutral axis relative to the upper side of the slab.
x_{pl}	The plastic centroid of the effective section.
z_{pl}	The natural plastique axis of the rib.
z_i z_j	Distance between the natural axis of the components and natural plastique axis of the rib.
	Greek letters
α_c	Convection coefficient.
α_{slab}	Coefficient taking into account the assumption of the rectangular stress block when designing slabs
$\gamma_{M,fi}$	Security factor for steel components.
$\gamma_{M,fi,c}$	Security factor for concrete components.
$\Delta l/l$	Thermal elongation.
c	Specific heat of the material.
ε_c	Concrete Strain at Maximum Compressive Stress.
ε_{cu}	Ultimate Compressive Strain of Concrete.
$\varepsilon_{c,\theta}$	Thermal strain of concrete.
ε_f	The emissivity of the fire.
ε_m	The emissivity of the surface of the element.
$\varepsilon_{s,\theta}$	Thermal strain of steel.
λ	Thermal conductivity of the material.
ρ	Density of the material.
υ	Punching shear coefficient.
σ	Stefan-Boltzmann's constant.
ϕ	View factor.

GENERAL INTRODUCTION

1.1. General

Nowadays, there is a large trend toward the usage of composite structures, which are composed of two or more different martials named composite elements. These elements have many benefits due to the their combined properties that allow them to behave as a single unit to perform better in overall (better in both mechanical and thermal behaviours [1], [2]). The use of this structural system can be related to its many advantages such as hight stiffness with the regard to non-composite structural systems, light weighted, good behaviour against fire conditions and economic reasons [2]. Among the composite structures elements, there are composite slabs which function is to transmit the vertical loads and to contribute as an horizontal bracing element. Furthermore, these elements require satisfactory to fire resistance according to the standard fire.

Composite slabs are horizontal elements used for many types of buildings. They are made by the connection of steel-concrete, steel-timber or concrete-timber [1]. Steel-concrete composite slabs is made by casting a concrete above a profiled steel sheet which represents a permanent formwork and a safe working platform (see figure 1). The performance of these elements primarily depends on the properties of the two materials and their interaction. This system offers several benefits, such as reduced construction time, savings in concrete and reinforcing steel, and enhanced fire resistance [3]. Additionally, the steel deck acts as supplementary reinforcement for the slab.

In terms of designing a composite slab two main stages must be considered; the construction stage and the composite stage. At the construction stage, the steel deck acts as formwork [4]. The profiled sheeting has to carry its own weight, the wet concrete and the construction loads which is generally estimated between 150 to 250 kg/m². In the composite stage, the slab is loaded with its own weight, the floor finishes and the variable load. The composite slabs must resist for bending moment, deflections and longitudinal shear forces, the design resistance of the composite slabs against the latter is carried out by two major different methods, either the partial connection method or m-k method based on two empirical factors m and k, provided by the manufacturer. This method is used on both cases ductile and non-ductile behaviours regarding the first method which is used only in the case of ductile behaviour. This method is based on experimental carried out on composite slab to estimate the shear degree of connection [4].

Figure 1.1: Steel deck as a temporary working platform [5].

The main component of this type of slabs are steel deck regarding its shape, concrete regarding its type, reinforcing rebars anti crack-mesh and studs or connectors see figure 2.

Moreover, the shape of the steel deck can play a big role in improving the fire time resistance [6] there is many types of the profiled steel sheet such as the closed profile, re-entrant profile and trapezoidal profile and as shown in figure 3. All the surfaces of the profiled steel sheet are galvanized to prevent corrosion and insuring the durability [7].

The steel rebars are used in this type of slabs either as anti-crack mesh on the top side or as a reinforcement on the lower part of the slab to increase the resistance against, the bending moment, the deflection and the longitudinal shear. Also, the steel rebars increase the fire resisting time[8].

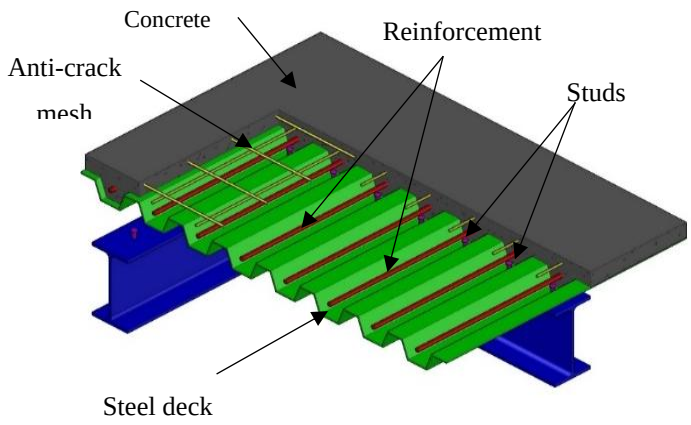

Figure 1.2: The different elements of a composted slab.

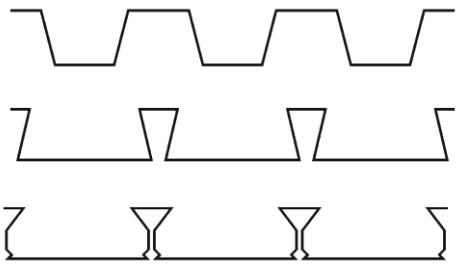

Figure 1.3: Steel deck profiles.

In the connection between steel and concrete, the type of concrete used has a significant influence on the thermo-mechanical behaviour of the composite element [9]. To enhance the fire resistance of the composite system, lightweight concrete (LWC) has been found to be an ideal choice due to its good thermal performances such as the low fire conductivity [10] which is always lower than 1 W/mK [11]. Lightweight concrete is a special concrete with low density and conductivity, it can be produced by incorporating gas bubbles or by replacing fine aggregates with lighter alternatives or by it substitution. It offers several advantages, making it suitable for use as an insulating or filling material, as well as for structural applications.

However, the lightweight concrete for structure must have at least a compressive strength of 17 MPa with a density below 1840 kN/m3 [12]. According to EN1994-1-2:2005 [11], the density of unreinforced LWC has to be in the range of 1600 to 2000 kN/m^3.

1.2. Problem statement

Slabs are among the heaviest structural elements in buildings and are typically constructed using normal-weight concrete (NWC). This significant weight increases the load on supporting structural elements, necessitating additional reinforcement and leading to higher construction costs. To address this issue, lightweight concrete (LWC) has been suggested as a potential replacement for NWC. While LWC reduces the overall weight of the slab, its lower mechanical properties with the regard to NWC raise concerns about its load-bearing capacity.

The use of a composite element; combining LWC with steel deck, offers a promising approach. This solution not only optimizes the weight of the slab but also increases its load-bearing capacity through the combination between the concrete and steel. However, the fire resistance of such composite slabs, mainly those made with LWC, remains a critical problem because of the lack of knowledge about the thermal behaviour of the LWC [13]. In a situation of a fire, the performance of the steel decking and its interaction with LWC under high temperatures are not yet fully explored. This study aims to examines the fire behaviour of composite slabs made with lightweight concrete, maintaining their structural stability and safety under fire conditions while keeping the benefits of weight optimization and enhanced load-bearing capacity.

1.3. Scoop and objectives

The primary goal of this study is to create three-dimensional thermal models based on the aforementioned concerns in order to perform a series of parametric studies that will examine the fire behaviour of composite steel-concrete slabs made with profiles steel sheet :

- Investigating the thermal and mechanical properties of lightweight concrete composite slabs under elevated temperatures.
- Comparing the fire performance of lightweight concrete composite slabs with those made with normal-weight concrete.
- Identifying key factors which influence the thermal and mechanical resistance of the slabs, such as material composition, slab thickness, shape of the steel deck and reinforcement details such as rebars diameter and its location in the rib.

The results performed by the numerical model should be validated and compared against experimental and numerical previous works.

1.4. Organisation of the thesis

The thesis is organised into eight chapters. A brief overview of the content of each chapter is given in the following paragraphs.

The thesis starts by a general introduction to the research work, where some definitions of the subject and the objectives and the motivations are introduced.

Chapter 2 presents the thermal behaviour of composite slabs and materials according to European standards. The thermal and mechanical properties of steel and concrete are mentioned. The definition of the thermal actions and the nominal and natural fire curves are also described. Finally, the different fire resistance criterions are highlighted.

In Chapter 3, we have summarized a state of the art on the experimental and numerical works dealing with the thermal mechanical behaviour of composite slabs at elevated temperature.

The analysis methods of composite slabs are presented in chapter 4. The first method deals with the simple calculation method according to EN 1994-1-2 [11]. This method is divided into two sections, the first section is about only the thermal analysis of the slab, and the second one treats the mechanical-thermal analysis. The numerical simulations are performed with the finite element ANSYS software with both thermal and mechanical analysis under standard fire ISO-834. Finally, a

hybrid method based on the analytical mechanical equations incorporated with the ANSYS thermal results is suggested.

The results of the thermal behaviour of composite slabs made by NWC and LWC using different steel deck geometries at different fire rating classes are discussed in chapter 5.

Chapter 6 includes the numerical results and discussion of the thermal-mechanical behaviour of composite slabs made by both trapezoidal and re-entrant steel deck according to the hybrid method.

The numerical method and the hybrid method results in this study are validated against the experimental and numerical works in chapter 7.

Finally, the main conclusions and recommendations for the future work are summarized in the chapter 8.

Thermal behaviour of composite structures

2.1. Introduction

This chapter focuses on the thermal behaviour of composite structures and its main inflowing parameters. It's divided into four main points which are: the thermal and mechanical properties of all the materials used in this study; explaining the fire actions on the buildings by explaining the heat transfer and the thermal actions passing to the different fire curves ending with the deferent fire resistance criterions.

2.2. Thermal and mechanical properties of the materials

The numerical simulation of the behaviour of structural members under fire conditions is influenced by the properties of each material which forms these members. These properties are dependent on the raise of the temperature and are categorised on two groups, thermal properties including, specific heat c, and thermal expansion, density ρ, thermal conductivity λ and mechanical properties which contains strain-stress, the strength reduction factors.

The thermal conductivity λ is the aptitude of a material to conduct heat", The specific heat can be defined as "the energy required to raise the temperature of a unit mass of a substance by 1 °C in a specified manner." [14]. The density is a physical property of matter, represents the mass per unit volume of a substance. It is a measure of how much mass is contained in a given volume and is denoted by the symbol "ρ". The common unit of the density is expressed in kg/m^3.

These thermal and mechanical properties vary according to the standards used for composite slabs [11], steel structures [15] and concrete structures [16]. In the following subsections, a brief discussion on the thermal properties of each material of interest is given.

2.2.1. Thermal properties of the materials

2.2.1.1. Carbon steel for the steel deck and reinforcement rebars

a) Thermal conductivity

Figure 2.1 illustrates the relationship between carbon steel's thermal conductivity and temperature. As shown, this property decreases linearly until reaching 800 °C, beyond which it stabilizes at a constant value. Notably, the thermal conductivity of steel returns to its original state after cooling post-fire, demonstrating reversible behaviour [17].

The thermal conductivity of the carbon steel λ_a (W/mK) should be determined from the following equations [15]:

$$\lambda_a = 54 - 3.33 \times 10^{-2}.\theta_a \qquad for\ 20\ °C \leq \theta_a < 800\ °C \qquad (2.1)$$

$$\lambda_a = 27.3 \qquad for\ 800\ °C \leq \theta_a \leq 1200\ °C \qquad (2.2)$$

In the equations above, θ_a is the steel temperature (°C).

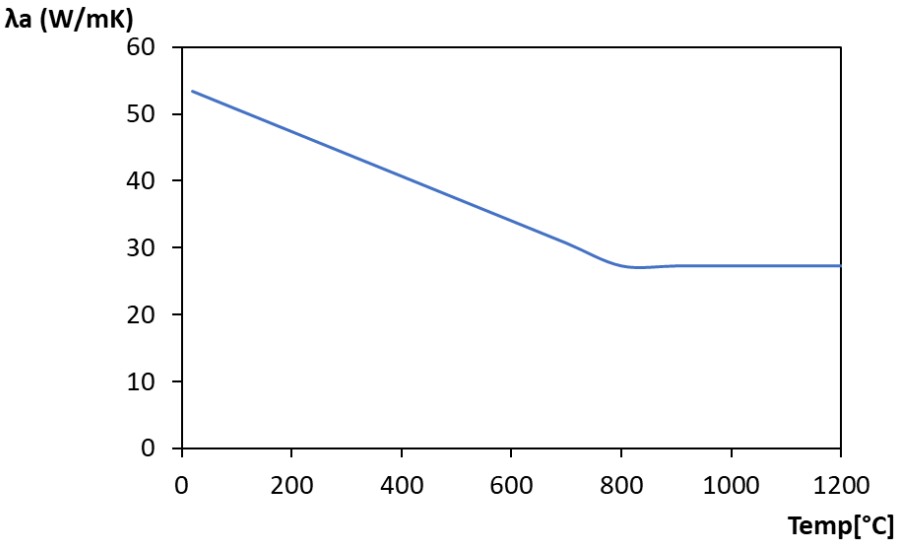

Figure 2.1: Variation of carbon steel's thermal conductivity with temperature.

b) Specific heat

Figure 2.2 shows the variation of carbon steel's specific heat with temperature. A sharp increase is observed between 700 °C and 800 °C, attributed to allotropic phase transformation. This change can influence the temperature evolution in steel components.

The specific heat of the carbon steel c_a (J/kg K) should be determined from the following equations [15]:

$$c_a = 425 + 7.73 \times 10^{-1}\theta_a - 1.69 \times 10^{-3}{\theta_a}^2 + 2.22 \times 10^{-6}{\theta_a}^3 \qquad for\ 20\ °C \leq \theta_a < 600\ °C \qquad (2.3)$$

$$c_a = 666 + \frac{13002}{738 - \theta_a} \qquad for\ 600\ °C \leq \theta_a < 735\ °C \qquad (2.4)$$

$$c_a = 545 + \frac{17820}{\theta_a - 731} \qquad for\ 735\ °C \leq \theta_a < 900\ °C \qquad (2.5)$$

$$c_a = 650 \qquad for\ 900\ °C \leq \theta_a \leq 1200\ °C \qquad (2.6)$$

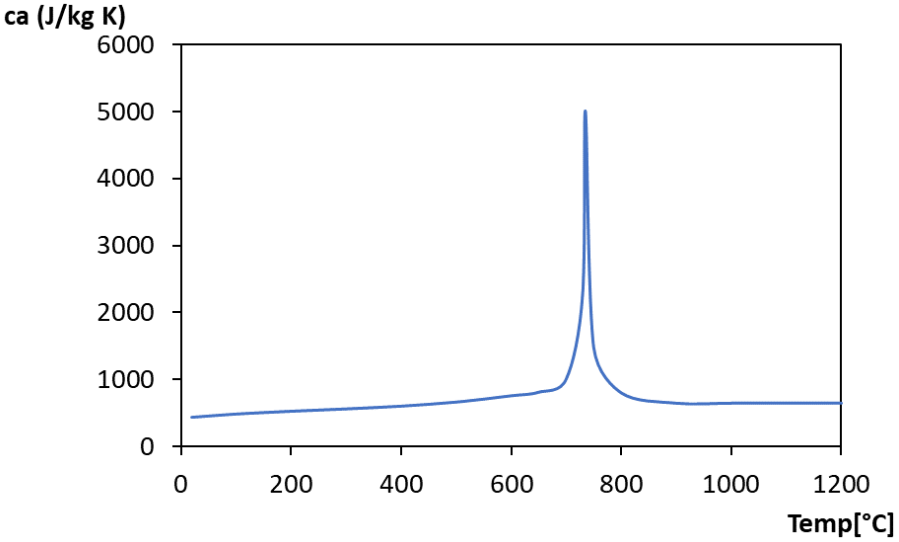

Figure 2.2: Variation of carbon steel's specific heat as function of temperature.

c) Density

As specified in EN 1993-1-2, the unit mass of carbon steel (ρ_a) can be assumed constant regardless of temperature. Therefore, a fixed value of ρ_a = 7850 kg/m³ is adopted, as illustrated in Figure 2.3.

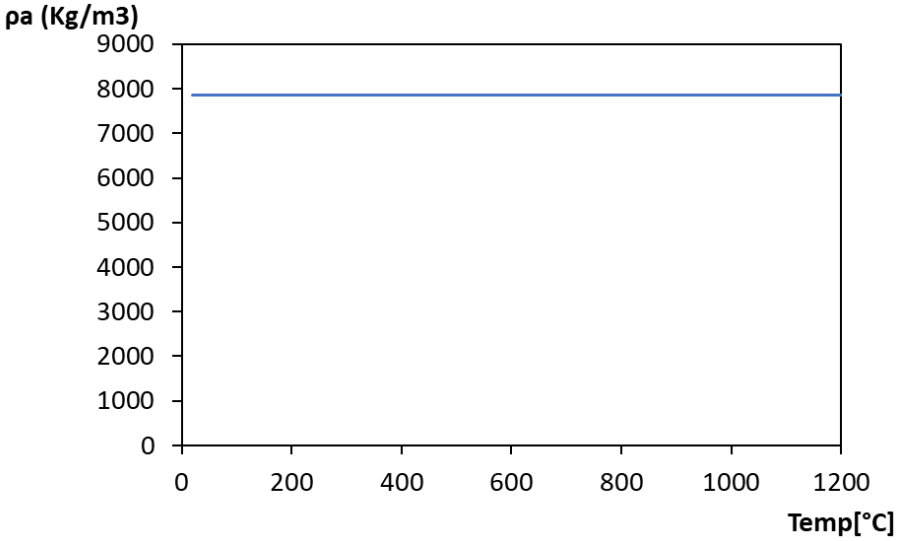

Figure 2.3: Variation of carbon steel's density as function of temperature.

d) Thermal expansion

The thermal expansion of carbon steel increases with temperature as illustrated Figure 2.4. It can be seen from the graph that the thermal elongation increases linearly until it reaches a value of 11×10^{-6} at 750°C, then remains constant up to 860°C at the same value of 11×10^{-6}. After that, it increases again to reach a value of 18×10^{-6} at 200°C.

The thermal elongation of the carbon steel $\Delta l/l$ (dimensionless) can be determined from the following equations [15]:

$$\Delta l/_l = 1.2 \times 10^{-5}\theta_a + 0.4 \times 10^{-8}{\theta_a}^2 - 2.416 \times 10^{-4} \qquad for\ 20\ °C \leq \theta_a < 750\ °C \qquad (2.7)$$

$$\Delta l/_l = 1.110^{-2} \qquad for\ 750\ °C \leq \theta_a < 860\ °C \qquad (2.8)$$

$$\Delta l/_l = 2 \times 10^{-5}\theta_a - -6.2 \times 10^{-3} \qquad for\ 760\ °C \leq \theta_a \leq 1200\ °C \qquad (2.9)$$

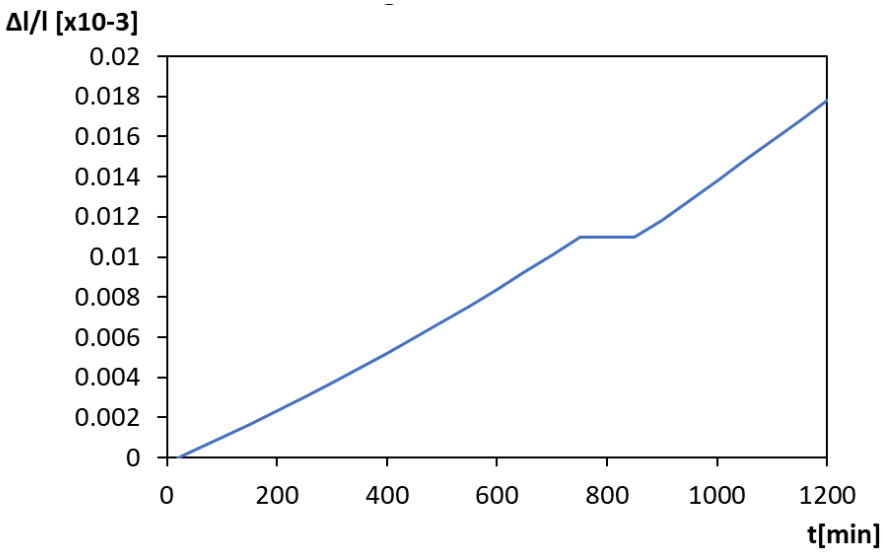

Figure 2.4: Variation of carbon steel's thermal elongation as function of temperature.

The following figure 2.5 brings together the thermal properties of the carbon steel. It is to be noted that tall the thermal properties of the carbon steel become constant over 800 °C.

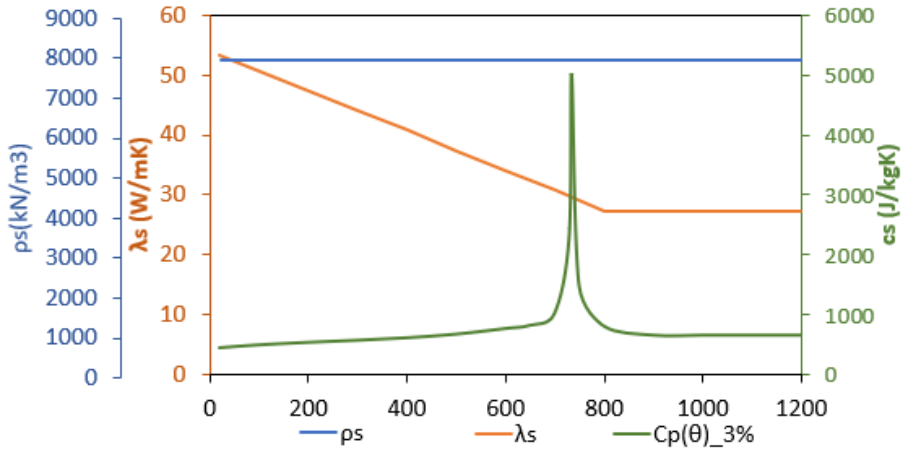

Figure 2.5: Variation of carbon steel's thermal properties as function of temperature.

2.2.1.2. Lightweight and Normal weight concrete for the slab

a) Thermal conductivity

Concrete's thermal conductivity λc is influenced by both the kind of aggregate and its temperature. It may be determined within the range of the lower and upper limit values for the NWC or directly from Figure 2.6 for the LWC. One can see from the graph that the thermal conductivity of NWC decreases linearly with the temperature up to 800 °C, then becomes constant at a value of 0.5 W/(m.K.

The upper limit and the lower limit of the thermal conductivity λ_c [W/mK] of the NWC and the LWC concrete should be calculated using to the equations bellow [11]:

-Upper limit for the NWC

$$\lambda_c = 2 - 0.2451\left(\frac{\theta_C}{100}\right) + 0.0107\left(\frac{\theta_C}{100}\right)^2 \qquad for\ 20\ °C \le \theta_C \le 1200\ °C \qquad (2.10)$$

-Lower limit for NWC

$$\lambda_c = 1.36 - 0.136\left(\frac{\theta_C}{100}\right) + 0.0057\left(\frac{\theta_C}{100}\right)^2 \qquad for\ 20\ °C \le \theta_C \le 1200\ °C \qquad (2.11)$$

-LWC

$$\lambda_c = 1 - \left(\frac{\theta_C}{100}\right)^2 \qquad for\ 20\ °C \le \theta_C < 800\ °C \qquad (2.12)$$

$$\lambda_c = 0.5 \qquad for\ 800\ °C \le \theta_C \le 1200\ °C \qquad (2.13)$$

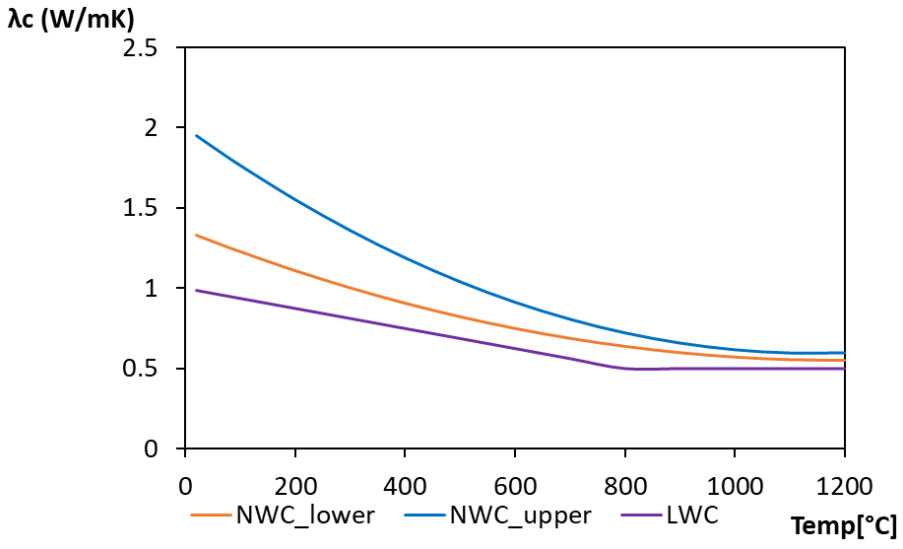

Figure 2.6: Variation of concretes thermal conductivity as function of temperature.

b) Specific heat

The specific heat of concrete varies primarily with its moisture content. As the temperature increases, the moisture within the concrete causes a peak in specific heat between 100 °C and 200 °C, due to the evaporation of water. Figure 2.7 illustrates how this property changes with temperature. The peak value depends on the amount of moisture (u); in this case, a moisture content of 3% was assumed for the normal-weight concrete (NWC), while no peak was considered for the lightweight concrete (LWC).

The determination of the specific heat (J/kg K) of dry concrete (u = 0%), with either siliceous or calcareous aggregates; for the LWC, should be determined according to the following equations [11], [16]:

-NWC

$$c_c = 900 \qquad for\ 20\ °C \leq \theta_C \leq 100\ °C \qquad (2.14)$$

$$c_c = 900 + (\theta_C - 100) \qquad for\ 100\ °C < \theta_C \leq 200\ °C \qquad (2.15)$$

$$c_c = 1000 + (\theta_C - 200)/2 \qquad for\ 200\ °C < \theta_C \leq 400\ °C \qquad (2.16)$$

$$c_c = 1100 \qquad for\ 400\ °C < \theta_C \leq 1200\ °C \qquad (2.17)$$

-LWC

$$c_c = 840 \qquad for\ 800\ °C \leq \theta_C \leq 1200\ °C \qquad (2.18)$$

Also, according to the codes, when the moisture content of the concrete is not taken into account in the computing, the function of the specific heat of the concrete should be modeled using a constant value of 2000 J/kg K. This corresponds to a temperature range between 100°C and 115°C, followed by a linear decrease in the curve for the temperature range between 115°C and 200°C.

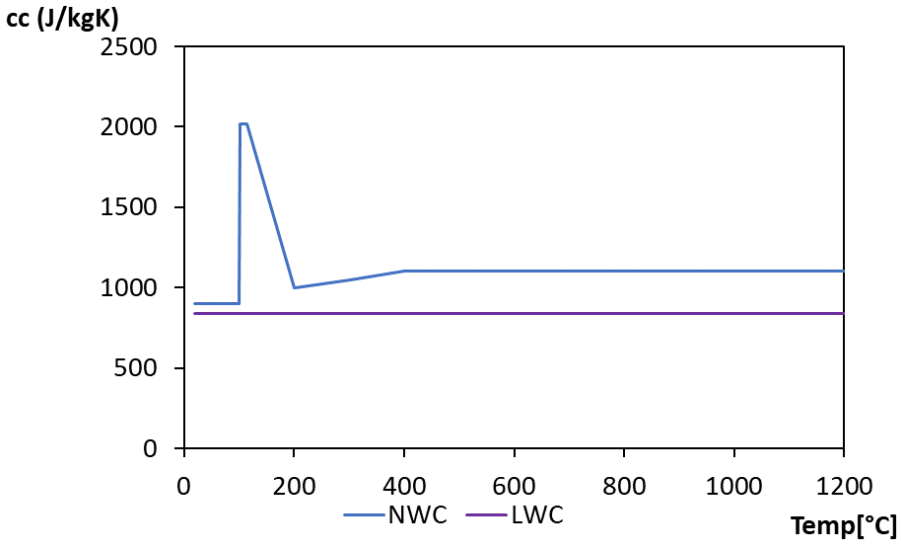

Figure 2.7: Variation of concretes specific heat as function of temperature.

c) Density

According to EN 1992 – 1-2, the density of concretes is temperature dependent and it is influenced by the water vaporization. This variation is defined in the equations below. At ambient temperature ρc (20 °C), The density of the normal weight concrete is equal to 2300 kg/m^3. For lightweight concrete, the density is below 1840 kN/m^3 and it must have a minimum of compressive strength of 17 MPa [12]. According EN1994-1-2, the density of unreinforced LWC has to be in the range of 1600 to 2000 kN/m^3. Figure 2.8 illustrates the density loss during the heating due to the free water loss.

For NWC and LWC

$$\rho(\theta) = \rho(20°C) \qquad for\ 20\ °C \leq \theta_C \leq 115\ °C \qquad (2.19)$$

$$\rho(\theta) = \rho(20°C).(1 - 0.02(\theta - 115)/85) \qquad for\ 115\ °C < \theta_C \leq 200\ °C \qquad (2.20)$$

$$\rho(\theta) = \rho(20°C).(0.98 - 0.03(\theta - 200)/200) \qquad for\ 200\ °C < \theta_C \leq 400\ °C \qquad (2.21)$$

$$\rho(\theta) = \rho(20°C).(0.95 - 0.07(\theta - 400)/800) \qquad for\ 400\ °C < \theta_C \leq 1200\ °C \qquad (2.22)$$

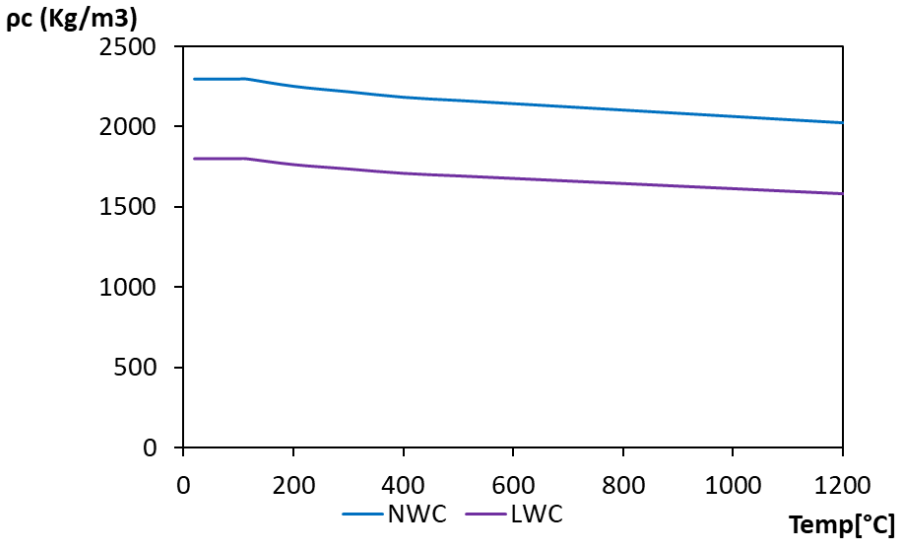

Figure 2.8: Variation of concretes densities as function of temperature.

d) Thermal expansion

The variation of the thermal expansion of the concretes with temperature as illustrated in Figure 2.9. As depicted, the thermal expansion of normal-weight concrete (NWC) varies depending on the aggregate type. Concretes made with siliceous aggregates exhibit greater thermal expansion compared to those with calcareous aggregates. In contrast, lightweight concrete (LWC) demonstrates lower thermal expansion than both types of NWC. The figure below shows that the elongation of the NWC increases with temperature, reaching 700 °C and 805°C for concretes made with siliceous and calcareous aggregates respectively, then after, they will be constant at the value of $14 \times 10^{-3}$for siliceous aggregates and 12×10^{-4} for the calcareous aggregates. Moreover, the elongation of the LWC is only increasing till the temperature of 1200°C, reaching the value of 9.6×10^{-3}.

The thermal elongation of concretes $\Delta l/l$ (dimensionless) may be determined from the following equations[11]:

-Siliceous aggregates:

$$\Delta l/_l = -1.8 \times 10^{-4} + 9 \times 10^{-6}\theta_C + 2.3 \times 10^{-11}{\theta_C}^3 \qquad for\ 20\ °C \leq \theta_C \leq 700\ °C \qquad (2.23)$$

$$\Delta l/_l = 14 \times 10^{-3} \qquad for\ 700\ °C < \theta_C \leq 1200\ °C \qquad (2.24)$$

-Calcareous aggregates:

$$\Delta l/_l = -1.2 \times 10^{-4} + 6 \times 10^{-6}\theta_C + 1.4 \times 10^{-11}{\theta_C}^3 \qquad for\ 20\ °C \le \theta_C \le 805\ °C \qquad (2.25)$$

$$\Delta l/_l = 12 \times 10^{-3} \qquad for\ 805\ °C < \theta_C \le 1200\ °C \qquad (2.26)$$

-LWC

$$\lambda_c = 1 - \left(\frac{\theta_C}{100}\right)^2 \qquad for\ 20\ °C \le \theta_C < 800\ °C \qquad (2.27)$$

$$\lambda_c = 0.5 \qquad for\ 800\ °C \le \theta_C \le 1200\ °C \qquad (2.28)$$

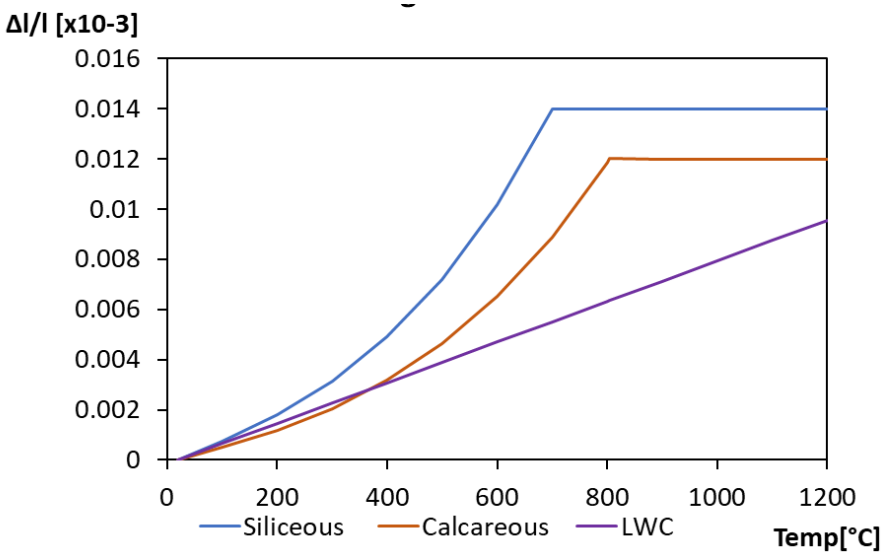

Figure 2.9: Variation of concretes thermal elongations as function of temperature.

The following figures 2.10 and 2.11 represent a summary for all the concretes thermal properties, in which we observe that all the concrete thermal properties are temperature dependent except for the specific heat of the LWC because the moisture is not considered.

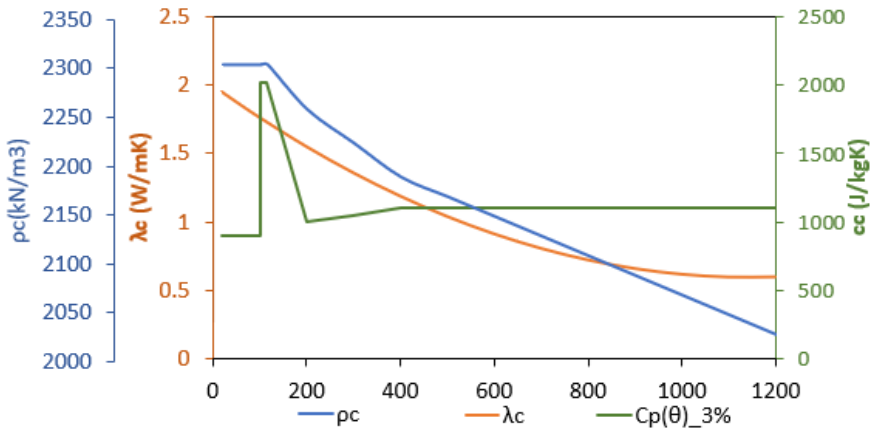

Figure 2.10: Variation of NWC thermal properties of the as function of temperature.

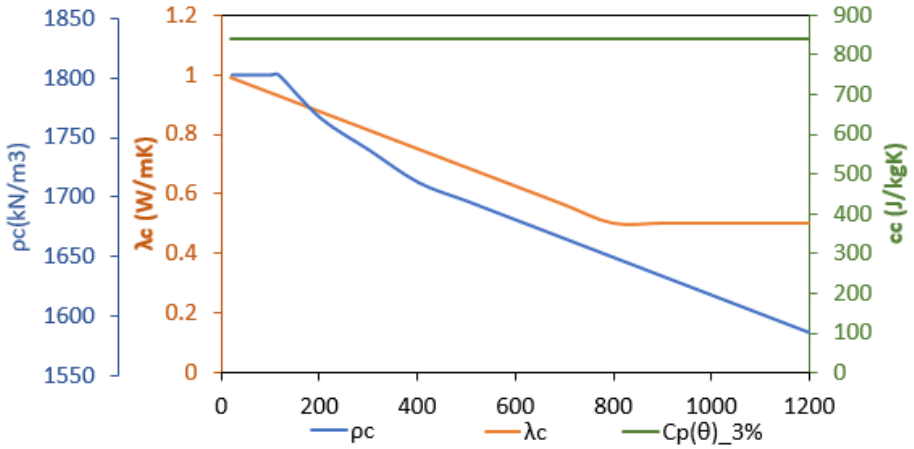

Figure 2.11: Variation of LWC thermal properties of the as function of temperature.

2.2.1.3. Air for the airgap

The thermal properties of the airgap are temperature-dependent and must be taken into account when modelling the detachment between the steel deck and the concrete. Furthermore, these properties also vary with air pressure. This study examines the thermal properties of the air at a pressure of 1 atm [14].

Currently, no standardized specifications exist for the thermal properties of air. Nevertheless, reliable data for numerical analyses can be obtained from validated computer programs and experimental studies. Figure 2.12 and Table 2.1 illustrate how the key thermal properties of air vary with temperature, namely the specific heat cair (J/kgK), the thermal conductivity λair (W/mK) and the density ρair (kg/m^3). From the graph we can see that all the three properties exhibit a nonlinear increase with temperature.

Table 2.1: Thermal properties of the airgap.

θair (°c)	cair (KJ/kgK)	ρair (Kg/m^3)	λair (W/mK)
20	1.007	1.204	0.02514
30	1.007	1.164	0.02588
60	1.007	1.059	0.02808
100	1.009	0.9458	0.03095
200	1.023	0.7459	0.03779
300	1.044	0.6158	0.04418
400	1.069	0.5243	0.05015
500	1.093	0.4565	0.05572
600	1.115	0.4042	0.06093
700	1.135	0.3627	0.06581
800	1.153	0.3289	0.07037
900	1.169	0.3008	0.07465
1000	1.184	0.2772	0.07868
1500	1.234	0.199	0.09599

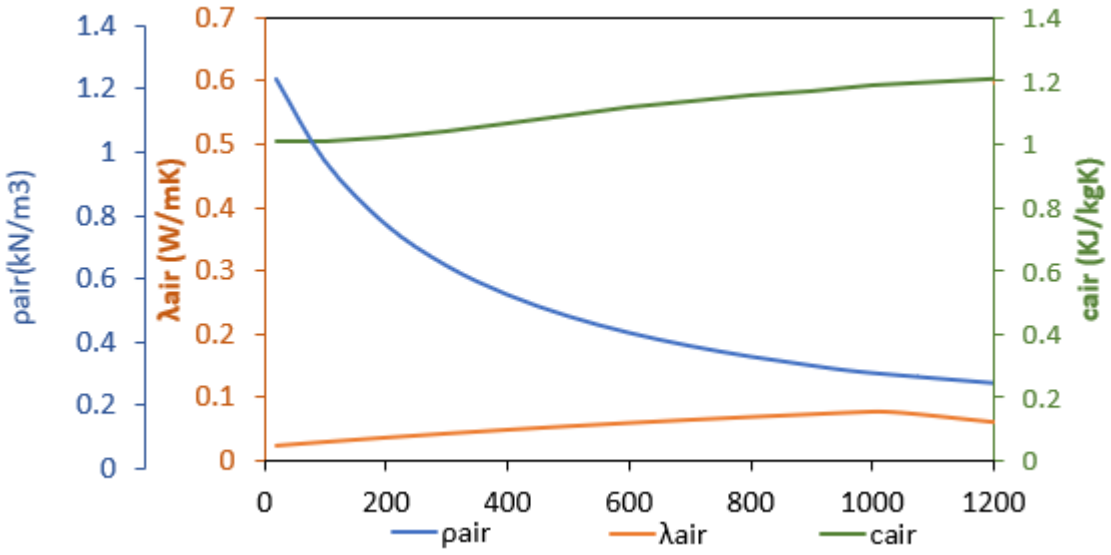

Figure 2.12: Variation of airgap thermal properties with temperature.

2.2.2. Mechanical properties of the materials

2.2.2.1. Carbon steel for the steel deck

The stress-strain relationship is used to determine the strength of structural elements in compression, tensile, shear and bending efforts. EN-1993-1-1 [18, p. 3] defines the mechanical properties at ambient temperature for the steel used for the deck, the mechanical properties of the steel used in this study are shown in Table 2.2.

Table 2.2: Mechanical properties of the steel used for the profiled sheet.

Ea[GPa]	fy[MPa]	fu[MPa]	Ga[GPa]	υ
210	275	430	81	0,3

Reduction coefficients are suggested to consider the effect of high temperatures on the mechanical properties of the steel as elaborated by EN 1993-1-2 [15] (see Figure 2.13) Reduction coefficients represent the degradation effect on the steel related to the temperature evolution in fire situation. These reduction factors are namely, K_y which defines the reduction on effective yield strength, K_E shows the reduction for the elastic modulus and K_p illustrates the proportional limit of the yield strength lastly the K_u outlines the ultimate tensile strength.

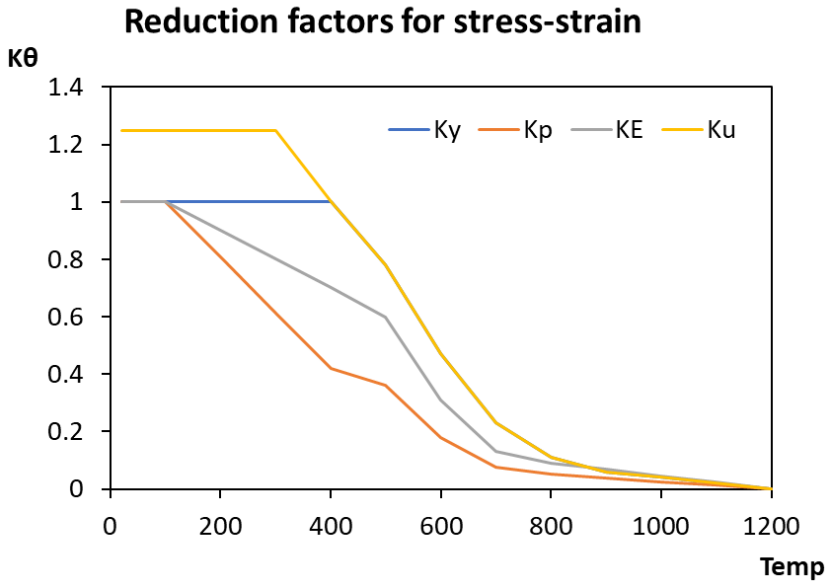

Figure 2.13: Reduction factors for the steel deck.

During the heating phase of the steel, it experiences a reduction in its bearing resistance and rigidity. To take this phenomena into account, the EN 1993-1-2 standard [15] proposes the following relationships for the stress-strain curves presented in table 2.3 figure 2.14. As it can be seen in the

Table 2.3: Mathematical model for stress-strain relationships of steel used for the seel deck at elevated temperatures.

Strain range $\varepsilon \leq \varepsilon_{p.\theta}$	Stress σ $\varepsilon\, E_{a.\theta}$	Tangent modulus $E_{a.\theta}$
$\varepsilon_{p.\theta} < \varepsilon < \varepsilon_{y.\theta}$	$f_{p.\theta} - c + \left(b/a\right)\left[a^2 - (\varepsilon_{y.\theta} - \varepsilon)^2\right]^{0.5}$	$\frac{b(\varepsilon_{y.\theta} - \varepsilon)}{a\left[a^2 - (\varepsilon_{y.\theta} - \varepsilon)^2\right]^{0.5}}$
$\varepsilon_{y.\theta} < \varepsilon < \varepsilon_{t.\theta}$	$f_{y.\theta}$	0
$\varepsilon_{t.\theta} < \varepsilon < \varepsilon_{u.\theta}$	$f_{y.\theta}\,[1 - (\varepsilon - \varepsilon_{t.\theta})/(\varepsilon_{u.\theta} - \varepsilon_{t.\theta})]$	-
$\varepsilon = \varepsilon_{u.\theta}$	0.00	-
parameters	$\varepsilon_{p.\theta} = f_{p.\theta}/E_{a.\theta}\ \ \varepsilon_{y.\theta} = 0.02$ $\varepsilon_{t.\theta} = 0.15\ \ \varepsilon_{u.\theta} = 0.20$	
Functions	$a^2 = (\varepsilon_{y.\theta} - \varepsilon_{p.\theta})(\varepsilon_{y.\theta} - \varepsilon_{p.\theta} + c/E_{a.\theta})$ $b^2 = c(\varepsilon_{y.\theta} - \varepsilon_{p.\theta})E_{a.\theta} + c^2$ $c = \frac{(f_{y.\theta} - f_{p.\theta})^2}{(\varepsilon_{y.\theta} - \varepsilon_{p.\theta})E_{a.\theta} - 2(f_{y.\theta} - f_{p.\theta})}$	

figures, the properties of the steel become weak and losses a big amount of its initial resistance at the elevated temperatures.

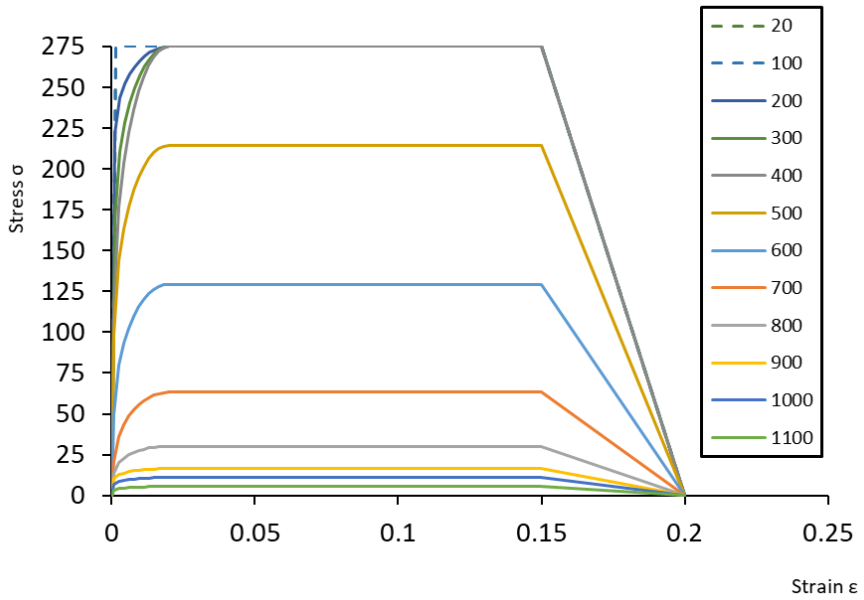

Figure 2.14: Reduction factors for the steel used for the steel deck.

2.2.2.2. Carbon steel for the reinforcement rebars

The characteristics of the steel reinforcement at ambient temperature are described in EN-1992-1-1 [16]. Steel S500 with the properties described in Table 2.4 is used in this study.

Table 2.4: Mechanical properties of the steel used for reinforcement rebars.

Ea[GPa]	fy[MPa]	fu[MPa]	Ga[GPa]	υ
210	500	540	81	0,3

When the steel reinforcement is subjected to high temperatures, the stress-strain relationship is reduced. EN-1992-1-2 [19, p. 2] defines some reduction factors represented in figure 2.15 which are applied to the mechanical properties.

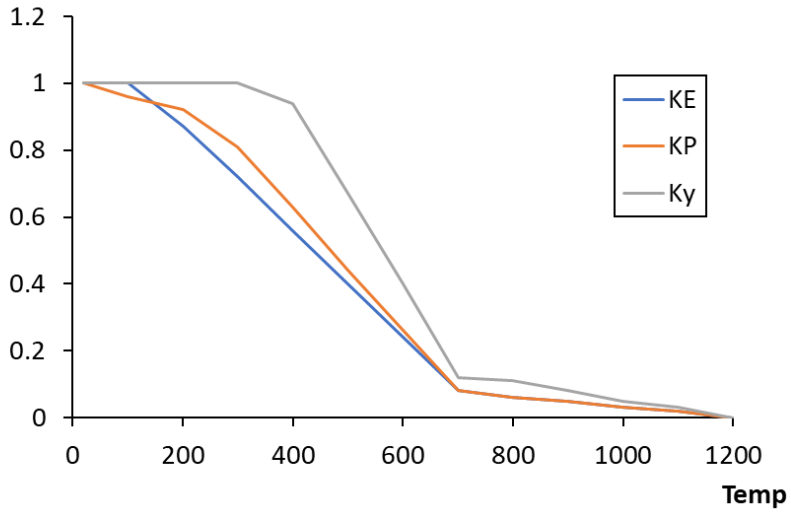

Figure 2.15: Reduction factors for the steel used for the reinforcement rebars.

EN-1992-1-2 [19, p. 2] standards establish the following equations to determine the stress-strain relationships (see Table 2.5). Figure 2.16 shows the variation of stress-strain curves plotted according to the following equations.

Table 2.5: Temperature-Dependent Stress–Strain Model for Steel Used in Steel Deck Applications.

Strain range $\boldsymbol{\varepsilon \leq \varepsilon_{p.\theta}}$	Stress σ $\varepsilon E_{a.\theta}$	Tangent modulus $E_{a.\theta}$
$\boldsymbol{\varepsilon_{p.\theta} < \varepsilon < \varepsilon_{y.\theta}}$	$f_{p.\theta} - c + \left(b/a\right)\left[a^2 - (\varepsilon_{y.\theta} - \varepsilon)^2\right]^{0.5}$	$\frac{b(\varepsilon_{y.\theta} - \varepsilon)}{a\left[a^2 - (\varepsilon_{y.\theta} - \varepsilon)^2\right]^{0.5}}$
$\boldsymbol{\varepsilon_{y.\theta} < \varepsilon < \varepsilon_{t.\theta}}$	$f_{y.\theta}$	0
$\boldsymbol{\varepsilon_{t.\theta} < \varepsilon < \varepsilon_{u.\theta}}$	$f_{y.\theta}\left[1 - (\varepsilon - \varepsilon_{t.\theta})/(\varepsilon_{u.\theta} - \varepsilon_{t.\theta})\right]$	-
$\boldsymbol{\varepsilon = \varepsilon_{u.\theta}}$	0.00	-
parameters	$\varepsilon_{p.\theta} = f_{p.\theta}/E_{a.\theta}$ $\varepsilon_{y.\theta} = 0.02$ $\varepsilon_{t.\theta} = 0.15$ $\varepsilon_{u.\theta} = 0.20$	
Functions	$a^2 = (\varepsilon_{y.\theta} - \varepsilon_{p.\theta})(\varepsilon_{y.\theta} - \varepsilon_{p.\theta} + c/E_{a.\theta})$ $b^2 = c(\varepsilon_{y.\theta} - \varepsilon_{p.\theta})E_{a.\theta} + c^2$ $c = \frac{(f_{y.\theta} - f_{p.\theta})^2}{(\varepsilon_{y.\theta} - \varepsilon_{p.\theta})E_{a.\theta} - 2(f_{y.\theta} - f_{p.\theta})}$	

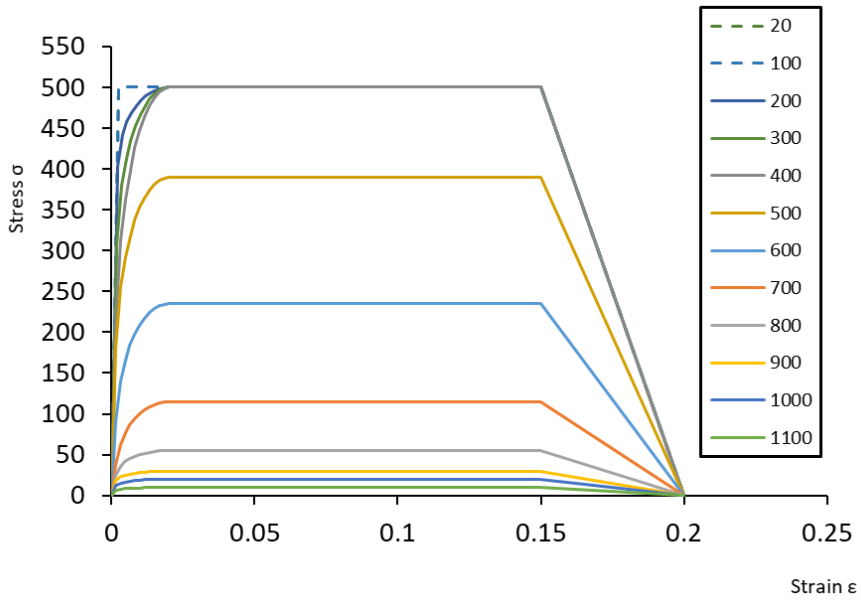

Figure 2.16: Strain-stress for the steel used for the reinforcement rebars.

2.2.2.3. Lightweight and normal weight concrete

The compressive strength of the concrete is the most basic and important mechanical behaviour. It acts as a fundamental property to identify the strength grade and quality index of the concrete, and to determine the values of other aspects of the mechanical behaviour. Stress-strain curve of concrete at

elevated temperatures has crucial influence on the fire response of structural systems. The properties of both concretes at room temperature are established in EN-1992-1-1 [16]. The mechanical characteristics of concretes used in this study is represented in Table 2.6.

Table 2.6: Mechanical characteristics of concrete the concretes.

Type of the concrete	F_{ck} [mPa]	E_{cm}[GPa]	εc [$^0/_{00}$]	εcu [$^0/_{00}$]
NWC	25	3.15	2	3.5
LWC	17	2.89	2	3.5

EN-1992-1-2 [19, p. 2] is the reference document for NWC and LWC materials under fire conditions. A reduction factor K_c, defined as the reduction of the characteristic compressive strength of concretes with the increase of the temperature, is introduced and can be represented in Figure 2.17.

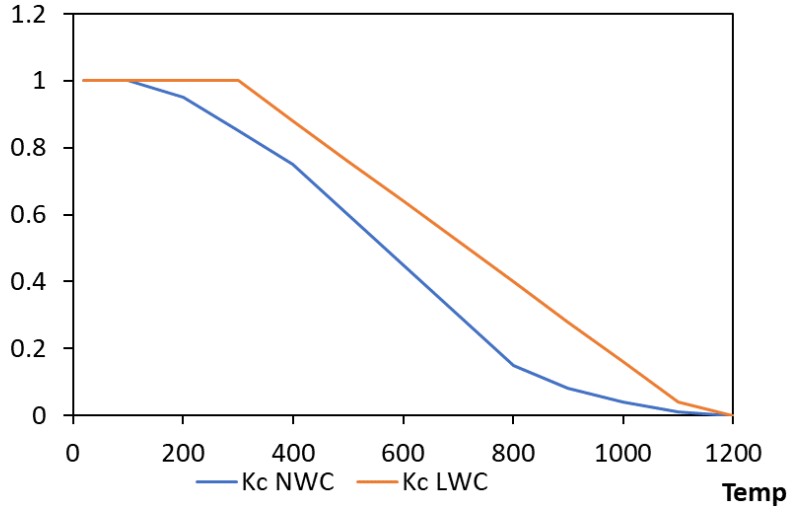

Figure 2.17: Reduction factors for the concretes.

The stress-strain relationship for concrete at elevated temperatures is illustrated in Table 2.7 according to EN-1994-1-2 [11]. The expected nonlinear variation of stress-strain for NWC and LWC at elevated temperatures is illustrated in Figure 2.18. According the latter Figure, both NWC and LWC concrete strengths present a relatively higher ductility at high temperatures with the decrease of the pic value of the compressive strength.

Table 2.7: Stress–Strain modelling of concrete in compression under elevated temperature conditions.

Range	Stress σ
$\varepsilon \leq \varepsilon_{C1,.\theta}$	$\dfrac{3\,\varepsilon\, f_{c.\theta}}{\varepsilon_{C1,.\theta}\left(2+\left(\dfrac{\varepsilon}{\varepsilon_{C1,.\theta}}\right)^3\right)}$

$\varepsilon_{C1,\theta} < \varepsilon \leq \varepsilon_{y.\theta}$	For numerical purposes a descending branch should be adopted. Linear or non-linear models are permitted.

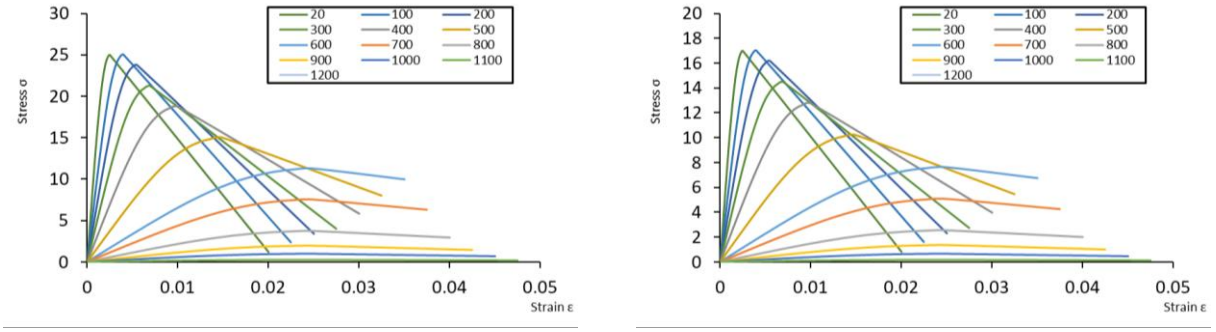

(a) NWC (b) LWC

Figure 2.18: Stress-strain for the concretes.

2.3. Fire actions on the buildings

Before performing any calculations, analyses, or designing structures to withstand fire loads, it is crucial to understand the mechanisms of heat transfer through the structural members and the various modes of heat transmission. The parameters which determine the fire development include the fire load density, combustion characteristics of materials, compartment shape and dimensions, ventilation conditions and the thermal properties of the boundary of enclosure; these are the most important factors [20].

The standard EC1 part 1-2 [21, p. 1] classifies the fire action as an accidental actions. The fire action affects the temperature of the elements causing loss of their initial load bearing capacities, this will be resulted in an additional deflections and external loads. These additional loads may lead to the failure of an element or to the total collapse of the building. So this part of the fire design must not be ignored by the structural designers [17].

The concept of the fire design for structural elements can be defined through a transient regime by the satisfaction of the equation below:

$$t_{\mathbf{fi,d}} \geq t_{\mathbf{fi,r}} \qquad (2.29)$$

Where $t_{\mathbf{fi,d}}$ represents the design value of the fire resistance and $t_{\mathbf{fi,r}}$ is the minimal required imposed by the standard. Both parameters are expressed as function of time.

2.3.1. Heat transfer and thermal actions

In order to well understand heat transfer mechanisms, it is essential to first establish some fundamental concepts “Temperature” can be determined as a measure of the warmth or coldness of a

substance. According to Çengel and Ghajar [14] heat represents a form of energy transferred between systems due to temperature differences. This energy transfer occurs through three distinct modes namely conduction, convections and radiation. It is to be noted that the heat distribution inside a system is dependent on the combination of these three modes.

The standard EC1 part 1-2 [21, p. 1] defines the heat transfer as the net heat flux to unit of surface area of the element and it is expressed by $\dot{h}_{net,d}\left[{}^{W}/_{m^2}\right]$. In addition, all the surfaces exposed to fire, must assume the transfer of heat by convection and rations according to the equation bellow:

$$\dot{h}_{net,d} = \dot{h}_{net,r} + \dot{h}_{net,c} \tag{2.30}$$

Where in this latter equation, $\dot{h}_{net,r}$ and $\dot{h}_{net,c}$ represent the heat flux from radiation and convection respectively.

Convection heat transfer refers to the thermal energy exchange between a solid surface and an adjacent moving fluid or gas when they are at different temperatures. Newton's law of cooling quantifies the rate of this energy transfer, expressed as:

$$\dot{h}_{net,c} = \alpha_c(T_g - T) \tag{2.31}$$

Where, α_c is the heat transfer coefficient by convection [w/m2k], T is the surface temperature of the member [°C] and T_g is the gas temperature in the vicinity of the fire exposed member [°C].

The heat transfer by radiation represents the energy transfer between two bodies through electromagnetic waves. This form of energy transfer, is exhibited by all bodies, and requires no medium for the heat to be transferred. It can even occur in a vacuum the amount of energy that can be radiated by a surface as expressed by Stefen-Boltzmann law equation.

$$\dot{h}_{net,r} = \sigma\phi\varepsilon_m\varepsilon_f\left[\left(T_g + 273\right)^4 - (T_m + 273)^4\right] \tag{2.32}$$

Where ε_f represents the emissivity of the fire; ε_m is the emissivity of the surface of the element; σ is the Stephan Boltzmann constant 5,67x10^{-8} [w/m^{2}k^4]; ϕ represents the view factor; T_m represents the surface temperature of the member [°C] T_g represents the effective radiation temperature of the fire environment [°C].

2.4. Fire curves

As known the fires occur with the existence of the three factors simultaneously which are the heat source; fuel and oxygen. Whether one of these factors is missing, the fire does not ignite or reach a

significant level. According to the Eurocode 1 part 1-2 a fire can be represented by temperature-time curves.

The following subsection deals with the most usually used fire curves.

2.4.1. Natural fire curve

In realistic natural fire scenarios, the full progression of fire development typically comprises four distinct stages (see Figure 2.19). However, not all fires strictly follow this curve, because there is more than one scenario of the colling phase, in some situations, it may disappear naturally or do not reach flashover, mainly if the fuel materials are isolated or if there is not enough air to maintain the combustion [22].

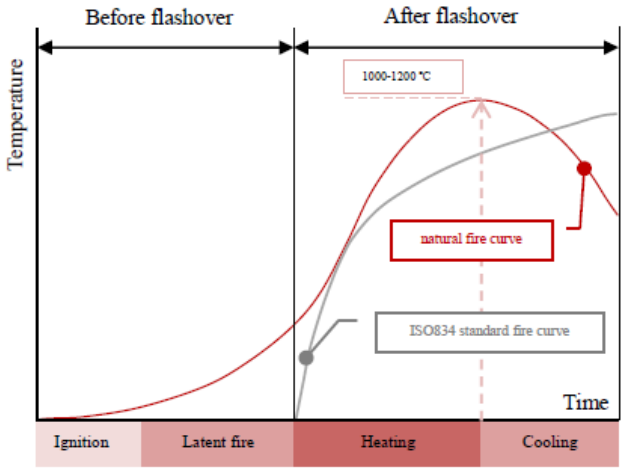

Figure 2.19: Different stages in the evolution of a real fire [23].

The fire process begins with the incipient stage, where materials heat up. Ignition marks the transition to the growth stage, where the fire spreads slowly at first and then more rapidly as it gains strength. Flashover occurs when the fire transitions to the burning period, characterized by a rapid increase in burning rate and ignition of all exposed surfaces. Finally, in the decay period, the fire dies down as temperatures drop after all fuel has burned [22].

These curves, derived from experimental fire tests in compartments under real fire conditions, display both an ascending and a descending phase.

2.4.2. Nominal standard fire curves

Standard fire curves were created to provide consistency in numerical simulations and experimental fire tests, focusing on the heating phase and independent of compartment characteristics. Eurocode 1 – Part 1-2 [21] defines three nominal fire curves for structural fire design: the standard temperature-

time curve, the external fire curve, and the hydrocarbon curve, which help calculate compartment temperature over time. The equations which describe these curves are presented below, where T_g represents the gas temperature (°C), and t is the time (min).

Standard fire curve (ISO 834)

$$T_g = 20 + 345.log_{10}(8t + 1) \quad (2.33)$$

External fire curve

$$T_g = 660.(1 - 0.687e^{-0.32t} - 0.313e^{-3.8t}) + 20 \quad (2.34)$$

Hydrocarbon curve

$$T_g = 1080.(1 - 0.325e^{-0.167t} - 0.675e^{-2.5t}) + 20 \quad (2.35)$$

The American Society for Testing and Materials (ASTM) presents a fire curve through the ASTM E119 [24] which is defined by a number of discrete points. There are several equations that approximate this curve; one of the most used is given by Lie [25], as presented bellow :

$$T_g = 20 + 750.\left(1 - e^{-3.79553\sqrt{t}}\right) + 170.41\sqrt{t} \quad (2.36)$$

These equations are plotted in the figure 2.20 bellow :

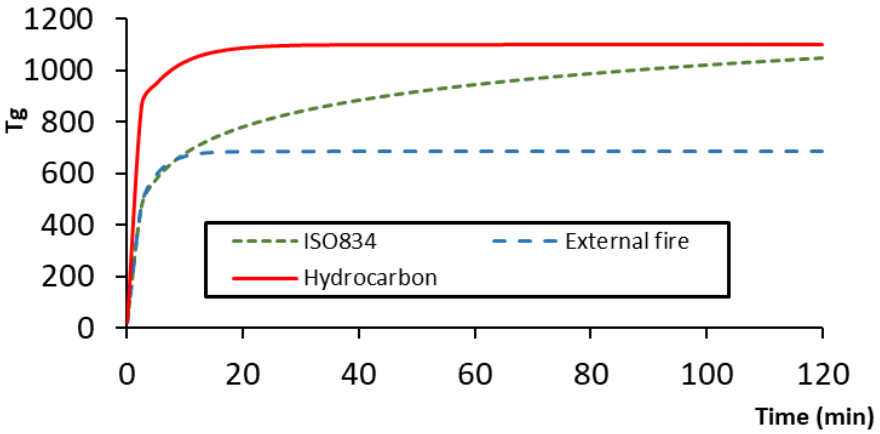

Figure 2.20: Nominal standard fire curves.

2.5. Fire resistance criteria

Structural elements must comply with fire-safety requirements set by building codes. For composite slabs, these requirements are typically specified by fire ratings R30 R60 R90 and finally R120 or more. The fire rating is generally determined through standard fire tests and should assess the criteria of Insulation (I), Integrity (E), and Load Bearing (R). Experimental full scale fire tests are typically costly and time-consuming. As an alternative, fire resistance can be assessed through numerical simulations and simplified calculation methods presented in standard. The fire resistance of

composite slabs is evaluated under standard fire exposure ISO834 from below. This study focuses on evaluating fire resistance in terms of both load-bearing (R) and thermal insulation (I) criteria. The thermal insulation criterion (I) refers to the ability of a structure to resist fire on one side and limit excessive heat transmission. The assessment is based on either the average temperature rise on the unexposed surface, which should not exceed 140°C above the initial average temperature, or the maximum temperature rise at any point on the unexposed surface, which should be limited to 180°C above the initial average temperature. The integrity criterion (E) refers to the ability to withstand fire on one side while preventing the penetration of hot gases and flames. The assessment is based on measuring cracks or openings exceeding specified dimensions, ignition of a cotton pad, or sustained flaming on the unexposed side. For cast-in-situ composite slabs, the integrity criterion is typically met as long as the joints are properly sealed. . Finally, the load bearing resistance for flexural loaded elements (R) is the ability to support the loading during the test without collapsing.

2.6. Conclusion

From the literature presented in this chapter, it's became clear the main keys of how does the heat transfer into the elements. This chapter presented the thermal and mechanical properties data used in this study for the different material components of the composite slabs (steel; concrete; carbon steel and the air) at elevated temperatures. Additionally, the thermal action; heat transfer according to EN-1991-1-2 and the fire resistance criterions exposed in this chapter, will be used in the parametric study in chapter 5 and chapter 6.

The material reviewed in this chapter illustrates the primary mechanisms/main keys of heat transport/mobility/flow into the elements.

Literature review of experimental and numerical works on the thermal mechanical behaviour of Composite slabs

3.1. Introduction

This chapter provides a scope on the previous research works, which are relevant to this investigation study. The literature review consists of three main parts. The first section treats the experimental works. The second exposes the numerical woks, and finally the third section demonstrates the works which has conducted with an experimental work validated with numerical simulations.

3.2. Experimental works

In 2013 Yu-Cheng Kan et al. [26], presented a mechanical experimental test of composite slabs made with both NWC and LWC. The specimens were simply supported and two concentrated loads were applied as shown in figure 3.1. The main objective of this study was to compare the mechanical behaviour of both concretes.

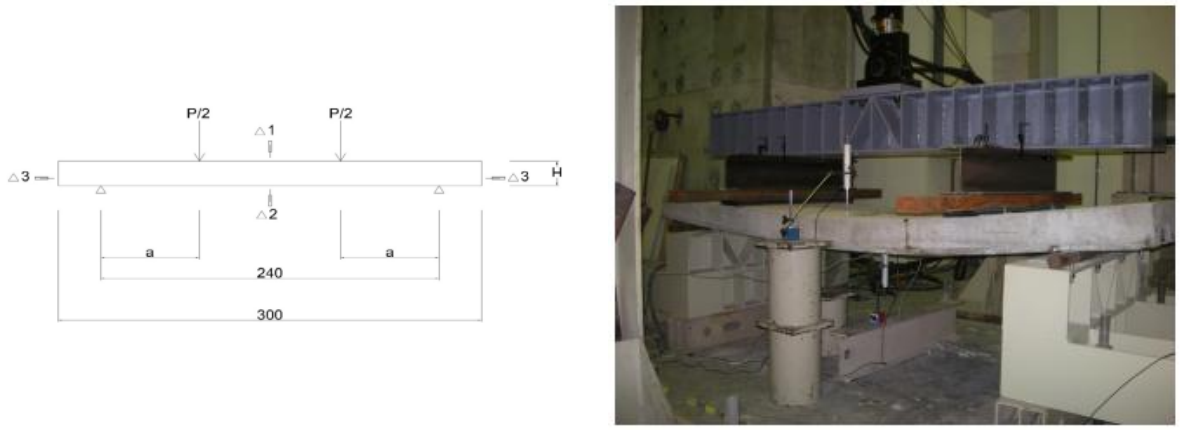

(a) Scheme of the simply supported setup (b) overview on the setup

Figure 3.1: The setup of the experiments.

These experiments gave rise to the following finding and observation: both concretes had the same mechanical behaviour, and a debonding between steel deck and concrete had place as illustrated in Figure 3.2. This debonding results in a peak load at the location where the moment occurs, and the load decreases rapidly thereafter. Subsequently, the load capacity of the steel deck increases again, and the ultimate load capacity may exceed the first peak load as shown in figure 3.2.

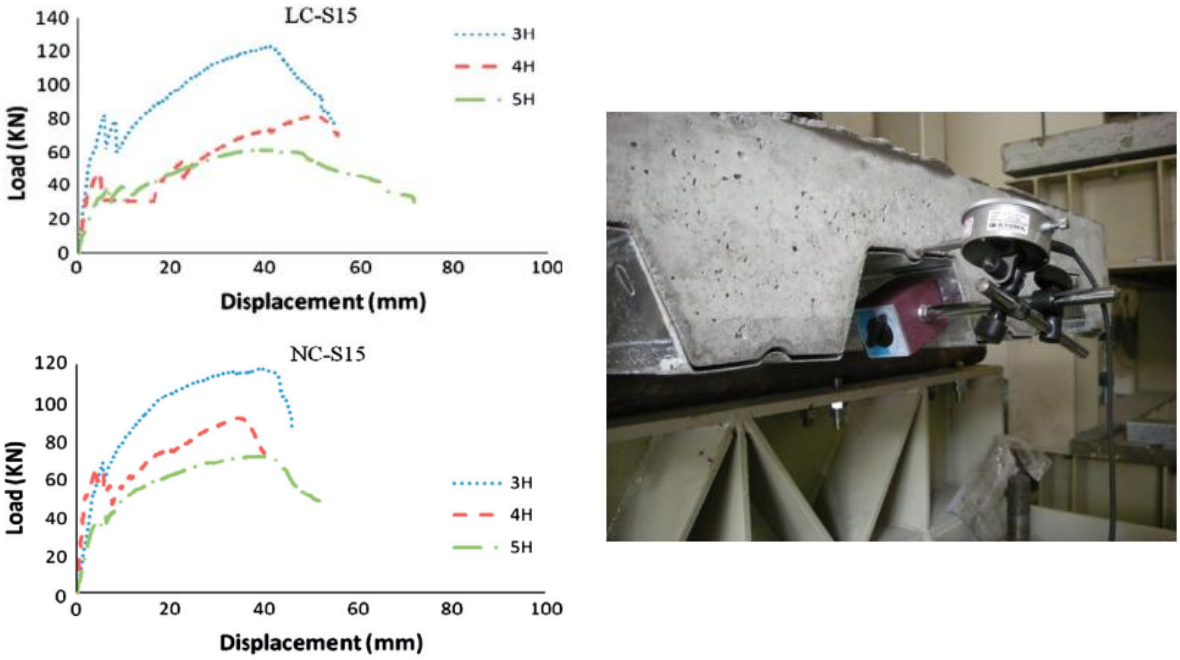

(a) Results for displacement for NC and LC (b) Real photo of the depending

Figure 3.2: Observation and result for LWC displacement.

In 2017 G.Q. Li et al [28], carried out an experimental work on four composite slabs supported by one unprotected secondary beam or not tasted with different ribs orientation and locations of the reinforcement rebars as presented in Figure 3.3 below.

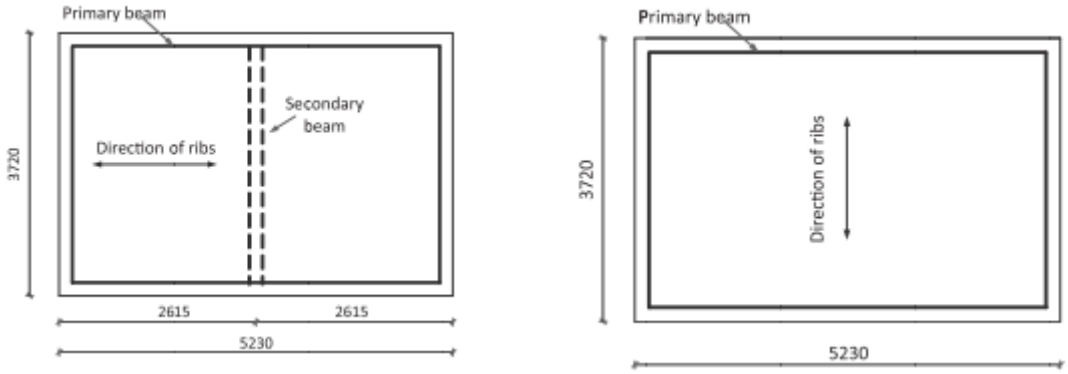

(a) Supported specimens (S1 and S2) (b) Unsupported specimens (S3 and S4)

Figure 3.3: Proposed model for the parametric studies [28].

The four slabs were tested in the furnace of State Key Laboratory for Disaster Reduction in Civil Engineering in Tongji University (see Figure 3.4). The key parameters of the parametric study were the boundary conditions, the shape of the slab, location of the rebars withing the slab and lastly the unprotected secondary beams on the development of tensile membrane action.

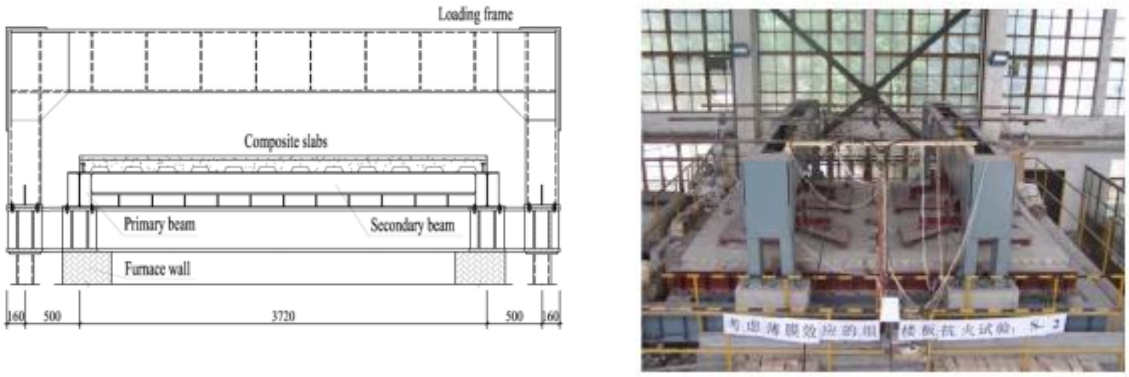

(a) Test setup for S1 and S2 (b) Overview of the test setup

Figure 3.4: The setup of the experiments [28].

In this investigation, it was concluded that the highest temperatures in the reinforcement and steel deck occurred during the cooling phase. The location of the reinforcement played a significant role in its temperature. Regarding the fire insulation criterion, the temperature on the unexposed side of all tested slabs remained below 100°C for a heating duration of up to 100 minutes, compared to a calculated fire resistance of 93 minutes based on the EC4 method. The temperature also varied depending on the position of the lower and upper flanges of the steel deck (see Figure 3.5).

(a) Debonding at the lower flange for S1 (b) Debonding at the upper flange for S2

Figure 3.5: Debonding between the steel deck and the concrete [28].

In 2017 D. Waldmann et al [27]. Elaborated a mechanical experiment on 22 specimens made with a renewable concrete which is the dense lightweight woodchip concrete with a minimum mechanical strength up to LC 20/22 the mixture of this concrete which is presented in Figure 3.6 below.

(a) Dense lightweight woodchip concrete (b) Porous lightweight woodchip concrete

Figure 3.6: Mixture of Dense lightweight woodchip concrete [27].

In these tests, the shear spans, profiled sheet types, and sheet thicknesses (types A and B) were the variable parameters. The specimens were tested using an experimental setup configured according to the guidelines of EC 4-1-1:2004 Annex B.3 [29]. A schematic overview of the setup is presented in Figure 3.7.

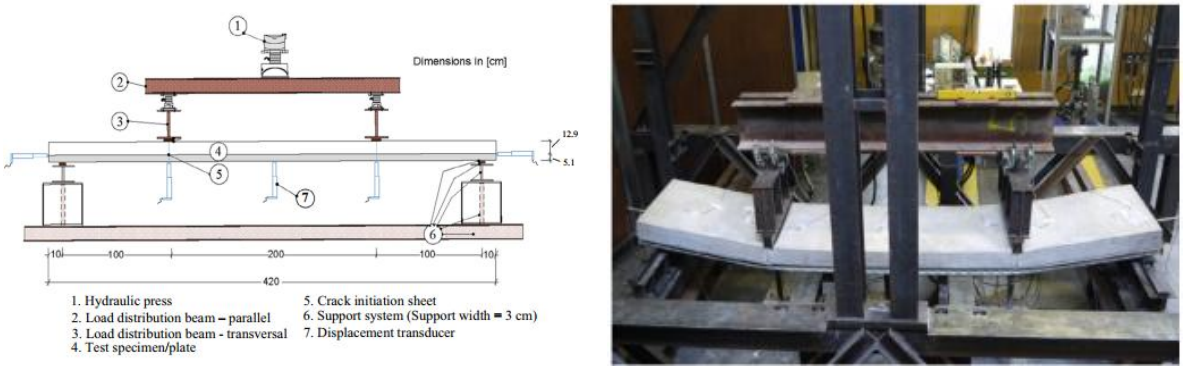

(a) Scheme of the experimental setup (b) overview on the setup

Figure 3.7: The setup of the experiments [27].

Through their study they conducted the following results: a dead load reduction up to 50% was measured while using the renewable concrete instead of the normal weight concrete, and loss of 20% in load bearing capacity were estimated. Type A composite plates cross-sectional area is about 77% lower than type B and the same for the moment of area is lower by 34%. Hence, by comparing the load bearing capacity of composite plates, type A is higher by 22-26% for a sheet of 0.75 mm thickness and up to 47% for 1 mm sheet thickness more than type B.

In 2019 Arrayago et al [30]. Conducted an experimental study on the trapezoidal ferritic steel decks. The ferritic steel is relatively new metallic material characterised by the absence of the nickel. The goal of their study was to determine the banding moment resistance of such elements on the construction phase of the project, The steel deck as mentioned above can be used as a safe working platform. In order to do the verifications, six simply supported decks were tested under different load conditions and positive and negative bending moments (see Figure 3.8), while three other continuous steel decks over two spans were tested (see Figure 3.9).

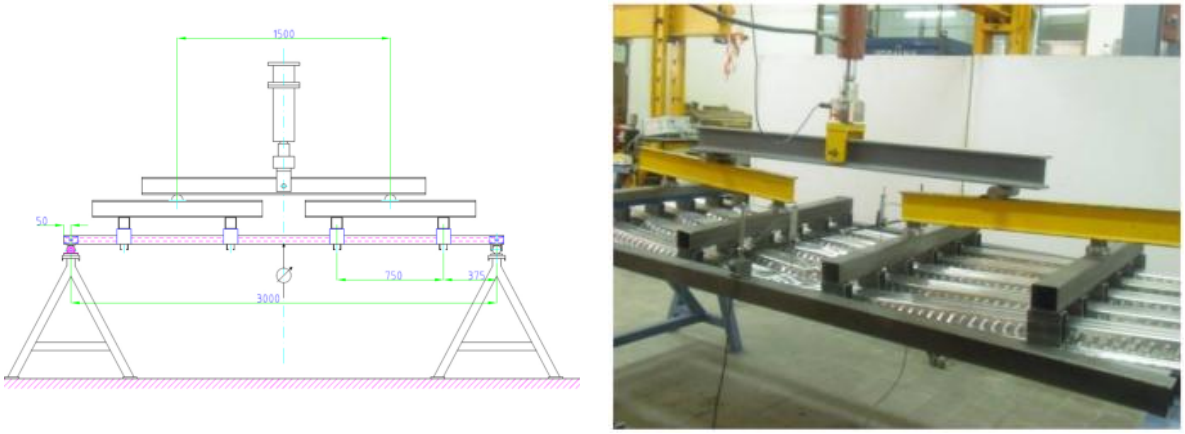

(a) Scheme of the simply supported setup (b) overview on the setup

Figure 3.8: The setup of the simply supported experiments.

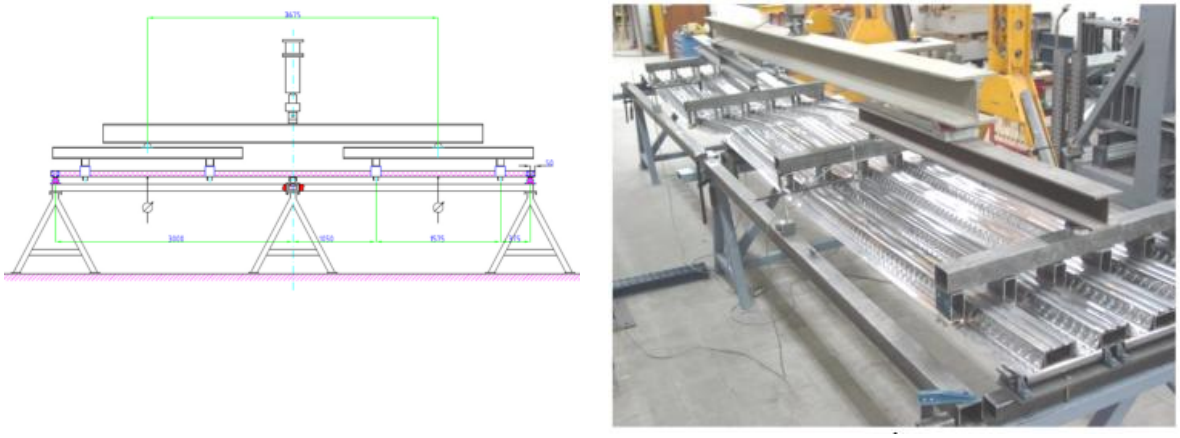

(a) Scheme of the two spans setup (b) overview on the setup

Figure 3.9: The setup of the continuous deck experiments.

For validation purposes, the ultimate loads have been compared to other experimental results conducted on a three-carbon steel deck under the same load condition, and the results were found similar. From their experiments, they concluded that for the simply supported decks the ultimate load predicted by the current standards for carbon steel provided safe results and it might be used for the

ferric steel. But regarding to the continuous deck, the interaction between the moment and the reaction caused the collapse and they proposed equation by Gozzi [31] for cold-firmed stainless steel provided more accurate and safe results.

In 2020 Del Coz-Díaz et al [10], carried out an experimental study on composite slabs made with NWC and LWC using a manufactured furnace built for both vertical elements and horizontal elements test (see figure 3.10).

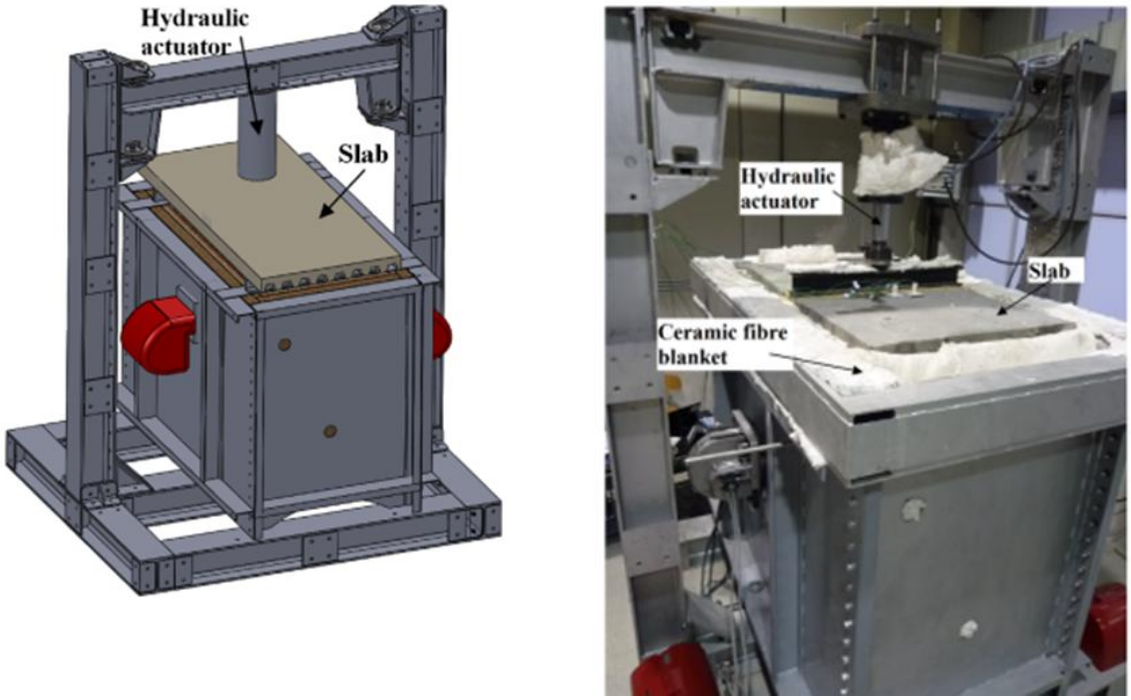

(a) Scheme of the setup (b) overview on the setup

Figure 3.10: The setup of the experiment [10].

They concluded that the heat transfer process is influenced by the moisture content and permeability of the concrete. The temperature does not rise until all the water is evaporated, and the evaporation process in lightweight concrete (LWC) slabs is much slower compared to normal concrete (NC) slabs. This is due to the higher permeability of LWC, which offers more resistance than normal-weight concrete (NWC). Additionally, the steel decking profile serves as a barrier, preventing explosive spalling. However, they observed that debonding of the steel profile occurs (see Figure 3.11).

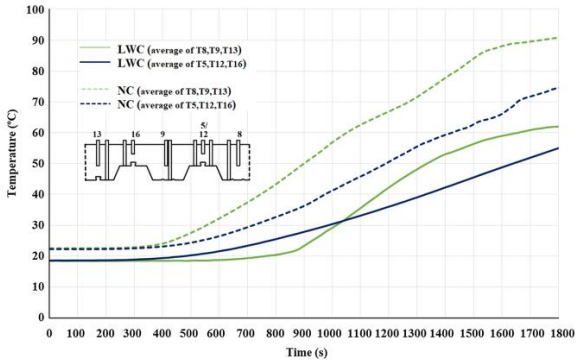

(a) Temperature measured in the concrete

(b) Debonding of the steel deck at the end of the experiment.

Figure 3.11: Excremental results [10].

3.3. Numerical works

In 2017 J. Jiang et al [6]. presented a numerical analysis to develop a reduced-order modelling approach to analyse both heat transfer inside the composite slabs and the structural analysis. To achieve that, they used two models based on solid elements for modelling the slab components in which it was validated against experimental results, and the second model in question made with shell layers only. The models are represented in Figure 3.12 below. The key elements of the parametric study were studying the effect of the influence of the thermal boundary conditions, thermal proproteins of the materials, and slab geometry (trapezoidal only) on the temperature inside the slab. They draw the following conclusions for the detailed model: the heat transfer analysis was not particularly affected by the mesh size a mesh size of 4x4 was sufficient to lead to an accurate result. Also, the temperature distribution in the cross section was non uniform due to the ribs. Besides, the thermal conductivity had a larger influence on the temperature evolution inside the slab. Furthermore, for the reduced-order model they concluded that to input the heat through the web a variable specific heat of the concrete is accounted for.

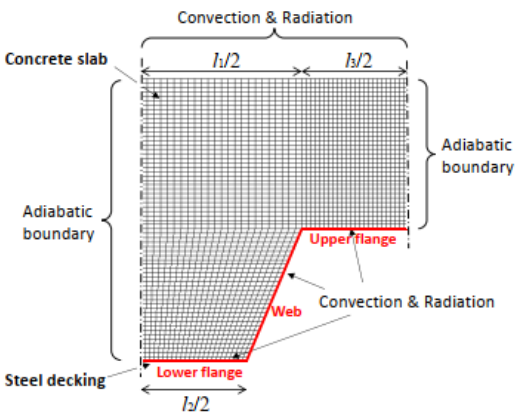

(a) Detailed model

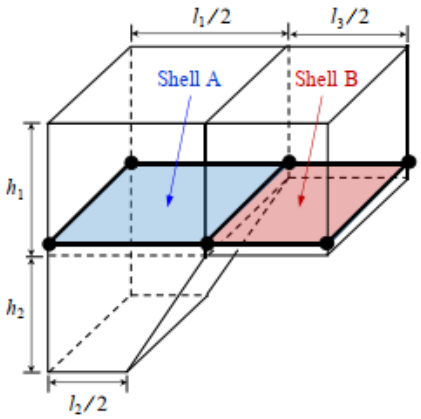

(b) Reduced-order

Figure 3.12: Proposed model for the parametric studies [6].

In 2018 P.A.G Piloto et al [32], evaluated the fire resistance of slabs with trapezoidal rib using two geometries with eight slab thicknesses of a normal weight concrete using numerical simulation and simple method presented in EC4 part 1-2 Annexe D [11]. The finite element method uses a 2D model developed using ANSYS [33] (See figure 3.13).

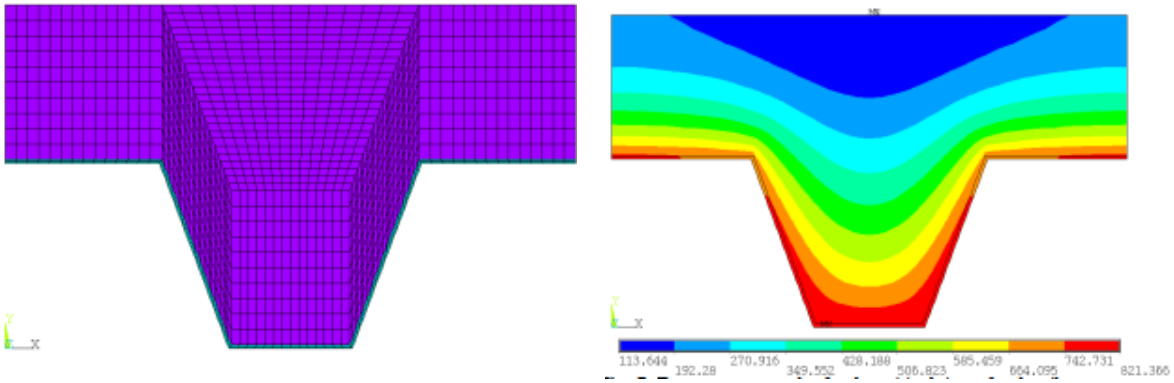

(a) finite element model (b) Temperature Distribution

Figure 3.13: Proposed model for the parametric studies [32].

They found that the simulation method gives a lower fire resistance compared to the Annex D [11] as it is shown in the figure 3.14 below. method in most cases. From their results, they proposed a new safer formula (3.1) to define fire resistance.

$$t_i = 0.0058.{h_e}^2 + 0.10710.h_e - 6.9976 \quad (3.1)$$

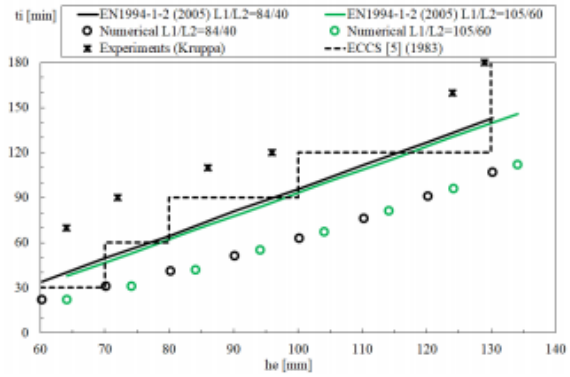

Figure 3.14: Proposed model for the parametric studies [32].

In 2018, J. Jinag [34] presented a numerical investigation on the influence of various of parameters such as thermal boundary conditions, thermal properties of concrete, and slab geometry on the temperature distribution within composite slabs. Using the same detailed model presented in [6]. After validating the model, they conducted the parametric studies using the parameters mentioned above. Out of their investigation, they draw the following conclusions: the most parameters

influencing the fire resistance of the slab were: the thickness of topping concrete, the emissivity of the steel deck, the view factor of the upper flange and the moisture concrete of the concrete. The convective heat transfer coefficient had little effect on the temperature distribution of composite slabs.

In 2019, Jiang et al. [35] conducted a numerical study on 54 composite slabs made with NWC and LWC taking into account the effect of the moisture content (in the range of 3% to 10 %). Using the same detailed model presented in [6]. The main focus of their investigation was to improve the calculation method for insulation-based fire resistance of composite slabs they concluded that the method given in the EC4 was unconservative up to 35% and over conservative up to 46% predictions of fire resistance of composite slabs. Thus, a new safer formula has proposed, and its results are presented in Figure 3.15.

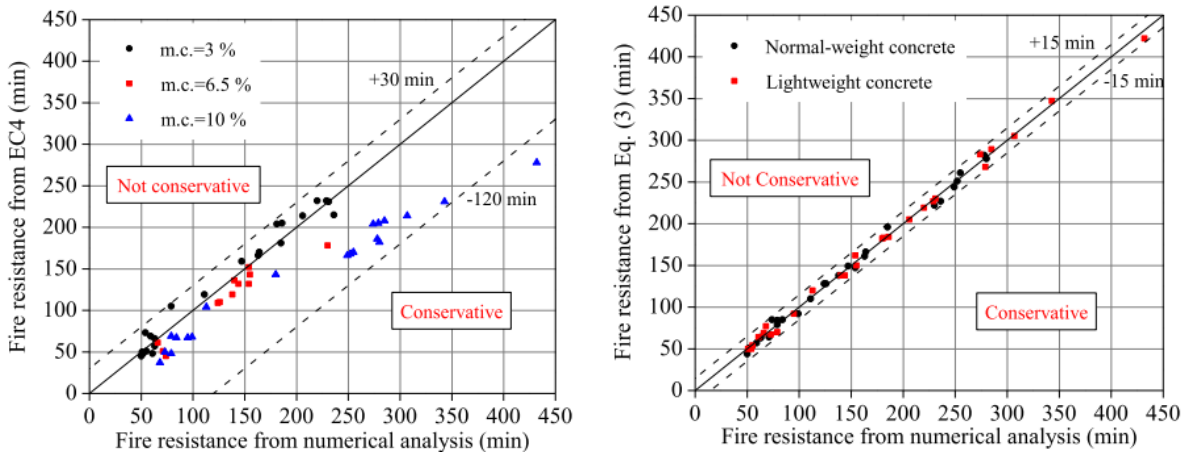

(a) Results of EC4 equation. (b) Results of the proposes equation.

Figure 3.15: Comparison of the results between the EC4 equation and proposed equation [35].

In 2019, P.A.G Piloto et al. [36] presented a three-dimensional numerical models to investigates the thermal and mechanical behaviour of composite slabs made with normal weight concrete and trapezoidal steel deck. The models were built in two different software ANSYS [37] and MATLAB [38]. These models were validated against experimental results. The thermal and mechanical result of the slabs is presented in Figure 3.16 and 3.17 below.

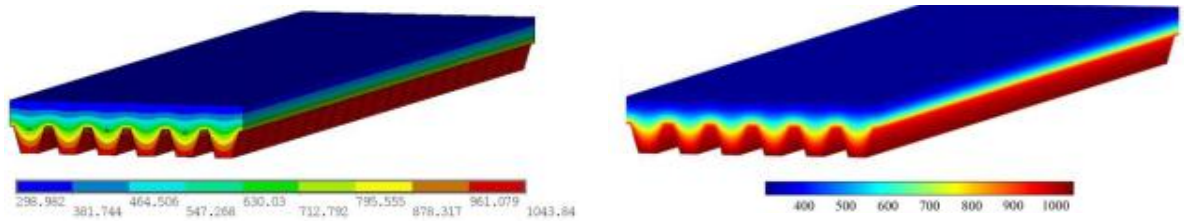

(a) ANSYS (b) MATLAB

Figure 3.16: Temperature Field of the Slab at 120 min of Simulation [36].

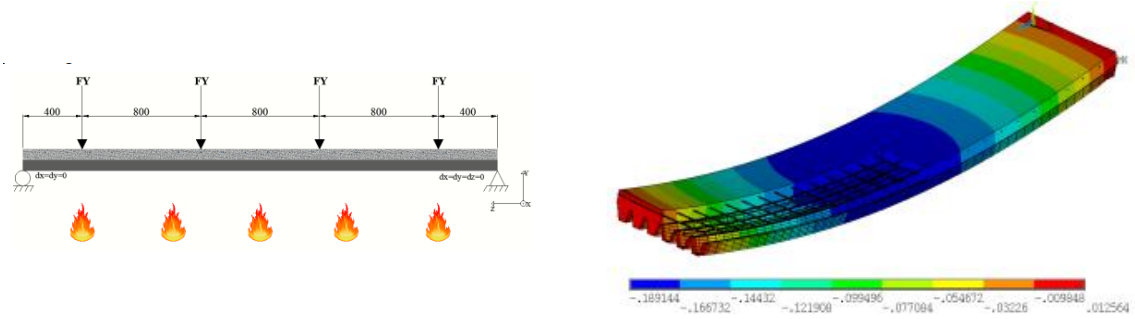

(a) Scheme of the support and loads (b) Slab deformation

Figure 3.17: Temperature Field of the Slab at 120 min of Simulation [36].

Out of their study, they came up with new proposals for the calculation of both thermal insulation criteria I, and load bearing resistance criteria R, these proposals provide better results for the evaluation of the fire resistance as it is shown in the Figure 3.18.

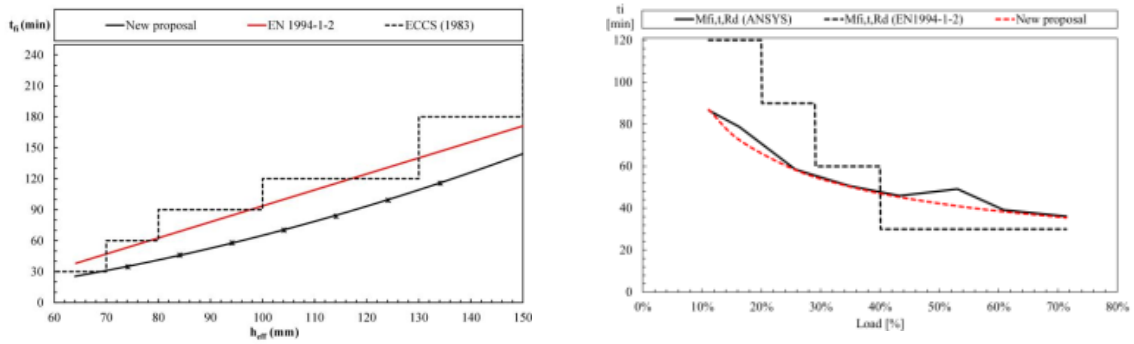

(a) New proposal Results For criteria I. (b) New proposal Results For criteria R.

Figure 3.18: Comparison of the results between the EC4 equation and proposed equation [36].

In 2019, S. Sharma et al. [39] presented a numerical Investigation using the ABAQUS software about the insulation effect of the concrete slab-steel deck interface due to the debouncing which occurs during the heating phase of fire. In order to study this phenomenon, an interface element was modeled to simulate the gap. To conduct their study, they used two different slab types namely the trapezoidal and the flat slab as presented in Figure 3.19. For the parametric study they used one type of concrete and they varied the geometrical parameters.

(a) Flat steel deck slab. (b) Trapezoidal steel deck slab.

Figure 3.19: Comparison of the results between the EC4 equation and proposed equation [39].

Out of their study they could establish a new formula to predict the concrete bottom surface temperature for a given slab, and the accuracy of the equation was validated against several examples as shown in the following Figure 3.20.

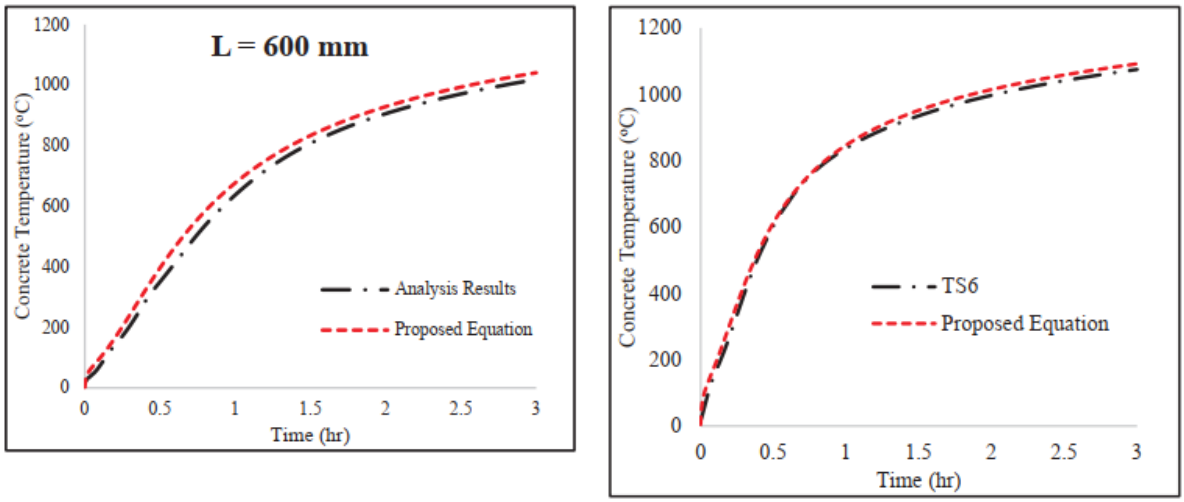

(a) Equation validation for the flat slab. (b) Equation validation for the flat slab.

Figure 3.20: Comparison of the results between the EC4 equation and proposed equation [39].

In 2020, a three-dimensional simulations based on full-scale and multi-domain slabs applying both ANSYS and MATLAB software programs were performed by Piloto et al [40]. They evaluated the thermal effect on the composite slabs with trapezoidal steel decks using NWC, taking into account the impact of the debonding between the concrete and the steel deck. This debonding was simulated by an airgap (see figure 3.21 for the model used).

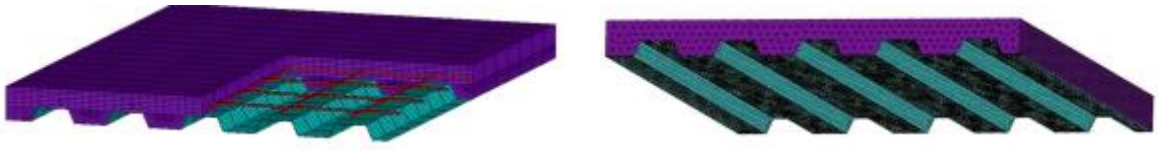

(a) ANSYS slab model. (b) MATLAB slab model.

Figure 3.21: Finites elements model used [39].

Out of the 40 simulation runed, they concluded that when considering the airgap effect, the numerical results are close to those of the experimental results. Thus, a new formula has been proposed for the calculation of the fire resistance.

In 2020, P.A.G Piloto et al. [41] presented a description for the thermal mechanical Fire resistance time for both criterion I and R for composite slabs with NWC. The 3D finite elements model presented

in Figure 3.22 below, were devolved using ANSYS and the result was validated against experimental results. The effect of the thickness of the airgap was tasted using two model with 0.5 mm and 1 mm.

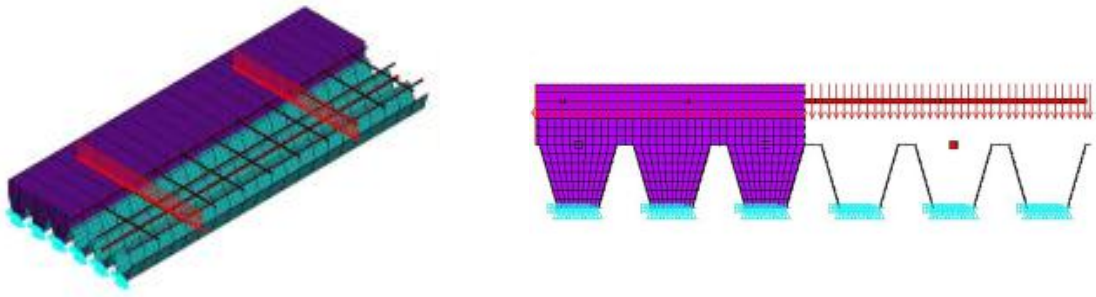

(a) 3d view of the model. (b) Front view of the model.

Figure 3.22: Finites elements model used [39].

From their investigations they could determine the following results: the fire resistance according the insulation criterion I was under estimated by the numerical model with perfect contact and better agreement were obtained with the airgap model (see Table 3.1 below). Concerning the results related to the R criterion, the fire resistance was consistently governed by the maximum displacement criterion. However, the simulation tended to underestimate the fire resistance time due to the higher temperature field. (see Table 3.2 below).

Table 3.1: Fire resistance for insulation condition (I): numerical, experimental and analytical result [39]

	Model PERF_C	Model 0.5 mm GAP	Model 1.0 mm GAP	EXP result	EN 1994-1-2 result
$t_{fi\ Ave}$ (min)	75.3	84.9	93.1	88.3	106.5
$t_{fi\ Max}$ (min)	85.3	96.4	105.92	102.0	

Table 3.2: Fire resistance for load-bearing condition (R): experimental, numerical and analytical result [39].

	Model PERF_C	Model 0.5 mm GAP	Model 1.0 mm GAP	EXP result	EN 1994-1-2 result
t_{fi} D (min)	54.5	69.1	81.1	97.6	120
t_{fi} dD/dt (min)	Not achieved	Not achieved	Not achieved	Not achieved	

In 2021, Balsa et al. [42] presented a more advanced models to represent the behaviour of composite slabs under fire conditions using MATLAB as it is represented in Figure 3.23 below. The main objective of this study was to determine the temperature distribution on the slab elements and to compare them with the Eurocode 4. Forty numerical simulations were performed to analyse the composite slabs made with NWC and LWC considering the effect of the airgap with different slab configurations.

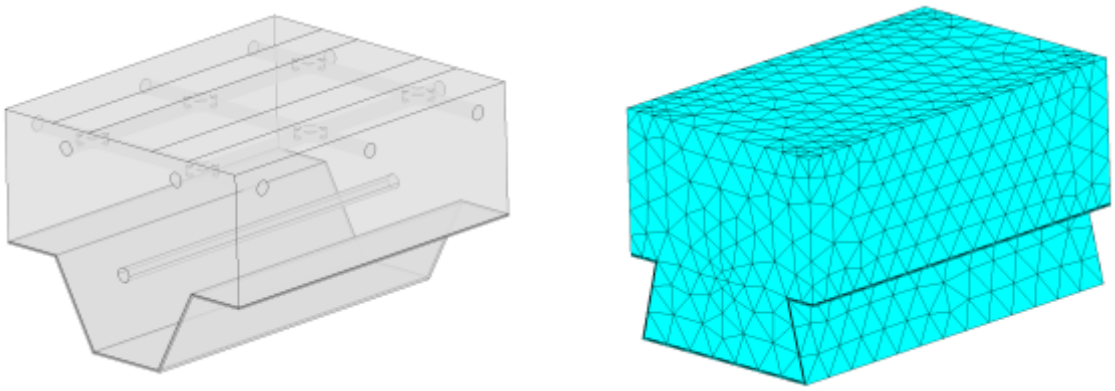

(a) 3d view of the model. (b) 3d view of the meshed model.

Figure 3.23: Finites elements model used [42].

This study led to a new calculation method for determining the temperature in the steel deck components. It was recommended to consider the moisture content of LWC and the mechanical effects of the airgap in future research.

The EC4 analytical method presented in Annex D has its own applicable field, it is also suitable for some slab geometries which satisfies the conditions of applicability. The question asked here is this method suitable for the composite slabs which are beyond the range of applicability? This problematic pushed J.Jiang et al [43] in 2021 to investigate this point. For their studies they used a detailed Two-Dimensional model with trapezoidal ribs for both NWC and LWC and the results were compared with the Analytical ones after validating the numerical result with the excremental ones presented in literature. At the end, they draw the following conclusions: the results of the analytic method were unreasonable, and that the effect of the Moisture content cannot be ignored because this latter parameter has a significant effect on the temperature distribution. Last but not least, the EC4 method provides no information about the temperature of the reinforcement placed on top of the slab.

In 2021, P.A.G Piloto et al. [44] presented a new calculation method for the temperature of the components of composite slabs under fire conditions based on an Investigation using finite elements method devolved with Ansys and validated successful. They claimed that no revision has been made

for the analytical method temperature calculation for the slab components. In their study, they proposed a new methodology to evaluate these temperatures. They noticed that the results obtained for the steel contents were unsafe for most of the analysis (see Figure 3.24). Thus, New calculation method was presented taking into account other parameters not included in the current equation of the EC4.

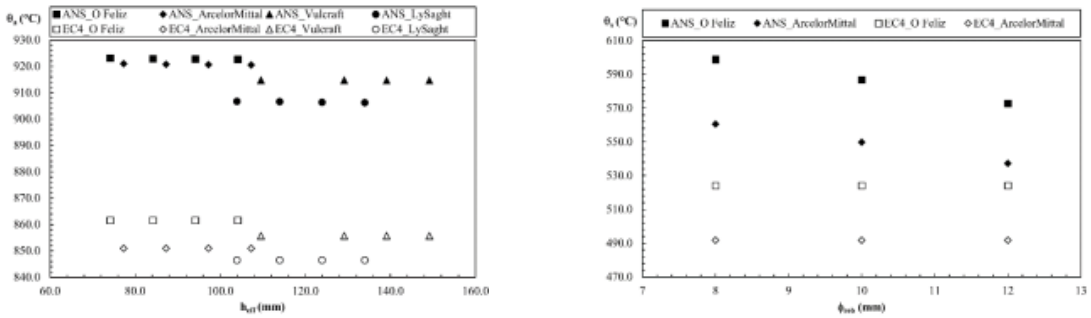

(a) Temperature of the lower flange. (b) Temperature of the rebars.

Figure 3.24: Comparison between the numerical and the analytical results [44].

In 2021, P.A.G Piloto et al. [45] presented another Computational Simulation of the Thermal analysis. By investigating further, the effect of the airgap on the trapezoidal composite slabs made with NWC, using different contact models (see Figure 3.25) with ANSYS (one with perfect contact and the other with different airgap thickness).

(a) Perfect contact model. (b) Airgap model (3mm).

Figure 3.25: Comparison between the numerical and the analytical results [45].

This study leads to the following conclusion: the use of grater airgap thickness led to a big enhance for fire resistance which led to unpleasant results. Plus, a new formula has been presented in which it takes the thickness of the airgap into account.

In 2022 Balsa et al [46], presented an update for their work, using a new and more realistic model for the thermal distribution inside the rib (see Figure 3.26 below) and considering two slab geometries and two concretes LWC and NWC. The main goal of this study was the optimization of the analytical calculation method.

(a) Trap-Final temperature distribution.

(b) Re-entrant-Final temperature distribution.

Figure 3.26: Temperature distribution inside the ribs [46].

Out of this work new calculation proposal for determining the temperature in the steel deck components and the rebars based on the numerical results is presented. The new formulation includes in the actual formula, provided by Eurocode, an additional term in order to include the effect of the concrete thickness. The new coefficients were determined by fitting the new proposal to the numerical results by non-linear least-squares. The efficiency of the formula is presented in the graph 3.27 below.

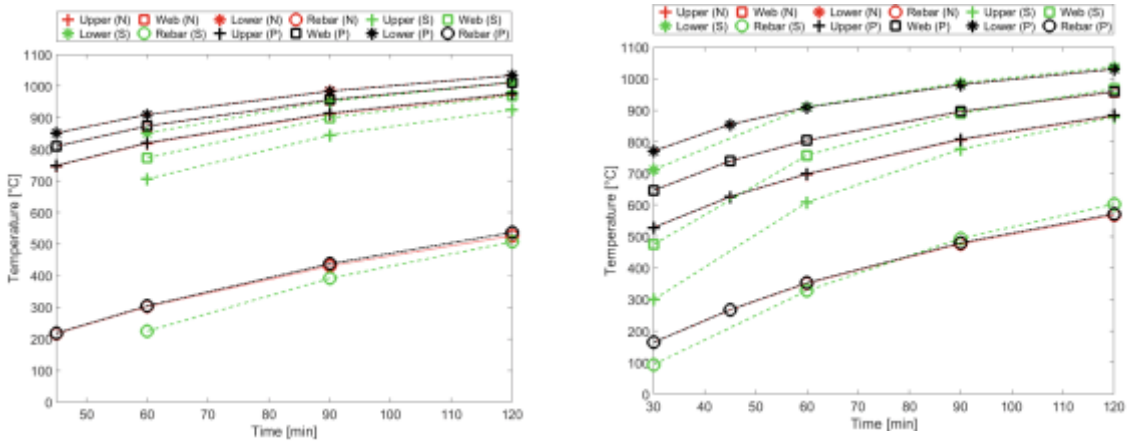

(a) Results for Polydeck 59S with NWC.

(b) Results for Multideck 50 with LWC.

Figure 3.27: Temperature corresponding to different fire rating times [46].

3.4. Experimental and numerical research

In 2012, S. Guo [47] carried out and experimental and numerical investigation on, restrained composite slabs during heating and cooling phase. Using in total six composite slabs tested under different load rations and different fire scenarios. The equipment used for the experiment was located on the Manchester's University and the FE model was developed using ABAQUS software. An over view, the Scheme of the setup and the FE model are represented in Figure 3.28 Below

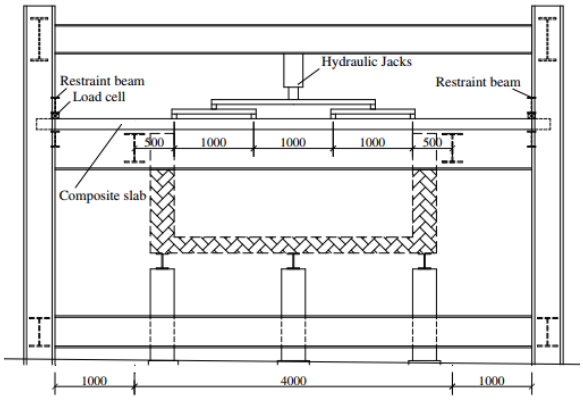

(a) Scheme of the setup.

(b) real view of the slab before the experiment.

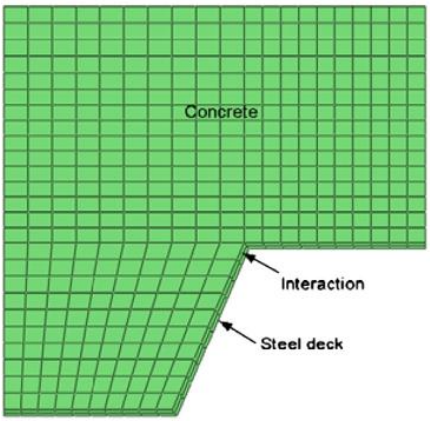

(C) Numerical model with the boundary conditions.

Figure 3.28: Furnace and the proposed model for the parametric studies [47].

From his study, he could point out the following conclusions: the fire scenario has a significant effect on the behaviour of the composite slabs during both phases heating and cooling. And it is also showed that the reaction force is related greatly to the heating and the cooling. Additionally, the FE results were near to the test measurement.

In 2018, M-P Nguyen et al. [48] presented both experimental and numerical results on the fire resistance time of composite slabs. Using three different types of profiled steel sheeting flat, re-entrant and trapezoidal. The main goal of their study is to demonstrate the effectiveness of embedded component and to determine post-fire residual strength of the composite slabs. The slabs were subjected to an ISO834 fire [49] applied by an electrical heating furnace (see Figure 3.29).

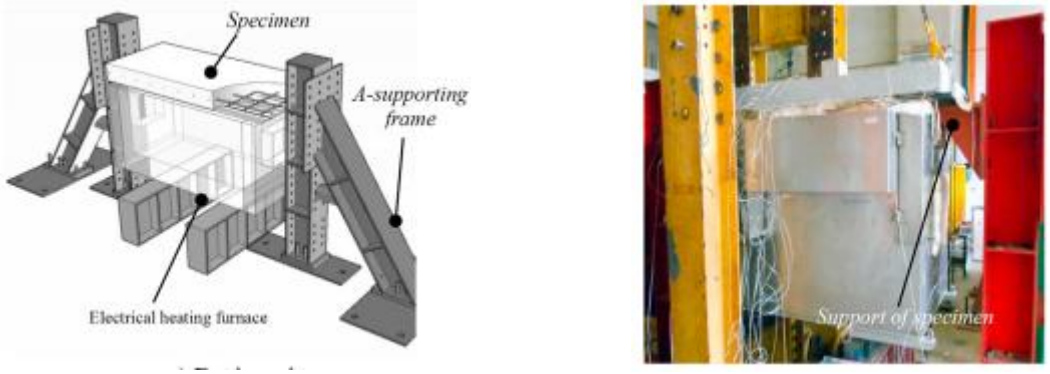

(a) Design view of the setup. (b) real view of the setup.

Figure 3.29: Proposed model for the parametric studies [48].

Concerning data input of the finite element heat transfer model presented in figure 3.30 is conformed to the Eurocode 1 part 1-2 [21].

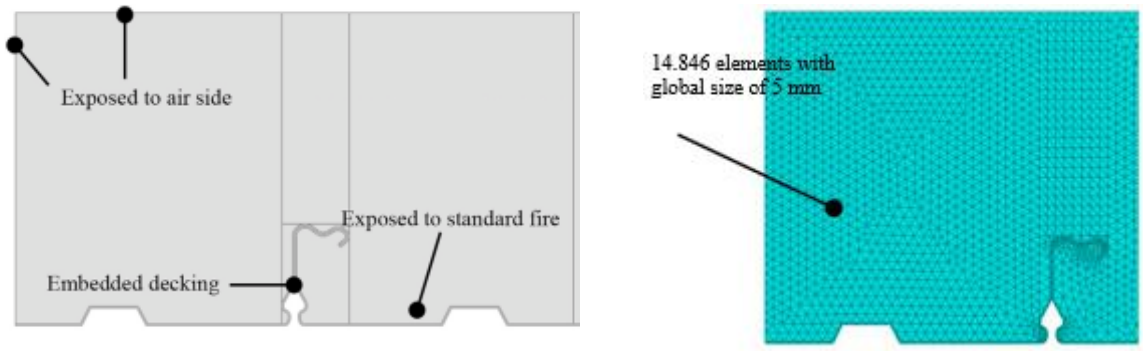

(a) Finite element modelling. (b) Finite element Meshing.

Figure 3.30: Proposed model for the parametric studies [48].

Out of there study, they established the following results: A total of 4 hour of resistance regarding to the integrity and insulation criteria was reached by embedding the web and top flange of flat decking. The proposed numerical models were able to predict accurately the thermal and thermal-mechanical behaviour of the flat decking composite slabs. A simplified assessment approach was presented to evaluate the post.

In 2021, F. Bolina et al. [50] indicated a thermal analysis composite slabs subjected to fire conditions. Using three different methods numerical, experimental and analytical. For that they prepared eight specimens with varying the position of the rebars their diameters. Using different tools to conduct their study such as ABAQUS for Numerical simulation, the simple method presented in Eurocodes 4 part 1-2 for the analytical method, and lastly a horizontal furnace was used for the experiment (see Figure 3.31).

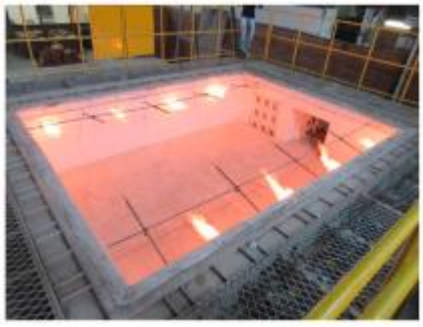

(a) Horizontal furnace.

(b) real view of the slab before the experiment.

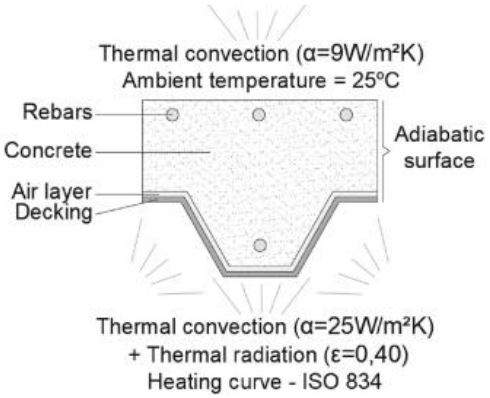

(C) Numerical model with the boundary conditions.

Figure 3.31: Furnace and the proposed model for the parametric studies [50].

From this investigation, the following points should be stretched: an early detachment occurs within the first five minutes of exposure, this detachment in a loss of the composite concept of the system. For the steel deck temperature all the three methods showed a convergence between them as shown in Figure 3.31. For the cases where the thickness of topping concrete is less than 70 mm the anti-crack mech rebars could attend a temperature of 500 °C. Lastly, the position of the rebars and the cover concrete had a large influence on the temperature evolution.

(a) Detachment of the steel decking during test.

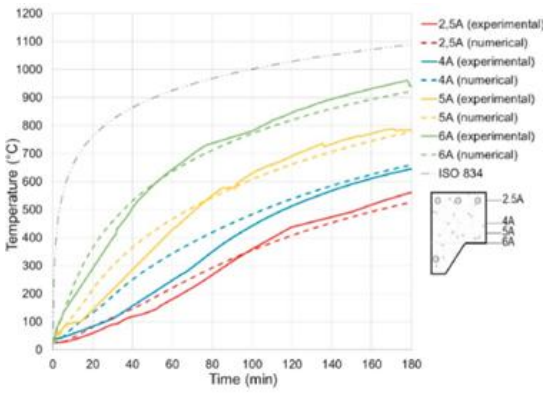

(b) Numerical and experimental temperatures

Figure 3.32: Proposed model for the parametric studies [48].

In 2022, Zhao et al. [51] performed four full-scale fire tests for a duration of 90 min on composite slabs including closed profiles steel decking and recycled aggregate concrete (RAC) using a horizontal furnace which runs on gas (see Figure 33), aligned with a numerical investigation using ABAQUS software for the development of the numerical model (see Figure 33). Taking into account the airgap and the effect of the moisture content, they concluded that the RAC releases more vapour than NWC. Also, After the 90 min of the fire exposure of the slab, they noticed that more vapour was released from the specimen of the RAC rather than the NWC and now spalling of the concrete was observed (See Figure 34). The temperature distribution inside the specimen made from RAC is lower due to the better thermal conductivity (see Figure 34). Therefore, for the numerical model the thermal convection at the rib location and the thermal resistance at the steel-concrete interface in the model were recommended to be 1 W/m²·K and 0.01 (m²K)/W, respectively

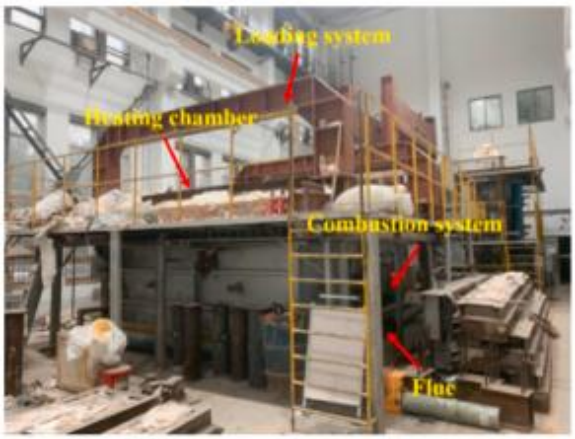

(a) Horizontal furnace.

(b) real view of the slab before the experiment.

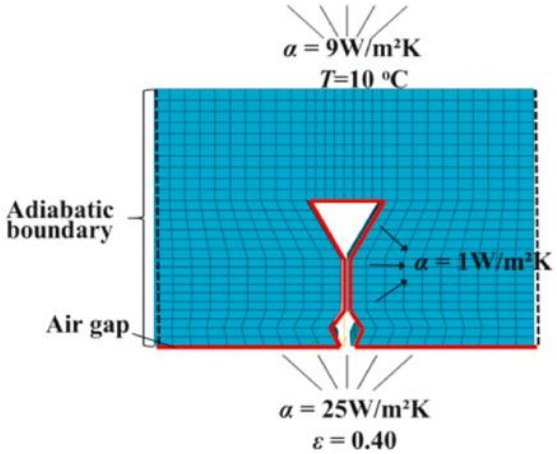

(C) Numerical model with the boundary conditions.

Figure 3.33: Furnace and the proposed model for the parametric studies [51].

(a) Free water evaporation. (b) Slab specimen after testing.

(C) fire resistance comparison.

Figure 3.34: Observations and results comparison [51].

Below in Table 3.3, is a summary of the main conclusions from previous experimental and numerical studies, providing an overview to highlight the novelty of the present work in comparison to past research.

Table 3.3: Summary of the conclusions.

Authors	Nature of the work	
	Experimental work results	**Numerical work results**
S. Guo et al (2012)	the fire scenario has a significant effect on the behaviour of the composite slabs during both phases heating and cooling. And it is also showed that the reaction force is related greatly to the heating and the colling.	the FE results were near to the test measurement.
Yu-Cheng Kan et al (2013)	Both NWC and LWC had the same mechanical behaviour and debonding had place, which leaded to a peak of load.	/
D. Waldmann et al (2017)	dead load reduction up to 50% was measured while using the renewable concrete instead of the NWC, and loss of 20% in load bearing capacity was estimated.	/

G.Q. Li et al (2017)	Highest temperatures of reinforcement and steel deck occurred during the cooling phase and the location of the reinforcement had a significant influence on its temperature.	/
Jian Jiang et al. (2017)	/	The temperature distribution on the composite slab is highly non-uniform due to the presense of the ribs, and the heat transfer analysis was particularly affected by the mesh size.
Jian Jiang et al. (2018)	/	parameters influencing the fire resistance of the slab were: the thickness of topping concrete, the emissivity of the steel deck, the view factor of the upper flange and the moisture concrete of the concrete. The convective heat transfer coefficient had little effect on the temperature distribution of composite slabs.
M-P Nguyen et al (2018)	A total of 4 hour of resistance regarding to the integrity and insulation criteria was reached by embedding the web and top flange of flat decking.	The proposed numerical models were able to predict accurately the thermal and thermal-mechanical behaviour of the flat decking composite slabs. A simplified assessment approach was presented to evaluate the post.
Piloto et al. (2018)	/	The simulation method gives a lower fire resistance compared to the Annex D method in most cases.
Arrayago et al (2019)	For the simple supported duck the current standards for carbon steel provided safe results and it might be used for the ferric steel, contrary for the two span.	/
Jiang et al. (2019)	/	EC4 was unconservative up to 35% and overconservative up to 46% predictions of fire resistance of composite slabs.
Piloto et al. (2019)	/	new proposals for the calculation of both thermal insulation criteria I were provided, and load bearing resistance criteria R, these proposals provide better results for the evaluation of the fire resistance.
S. Sharma et al (2019)	/	a new formula to predict the concrete bottom surface temperature for a given slab was established.
Del Coz-Díaz et al. (2020)	The heat transfer phenomenon is influenced by moisture content and permeability of concrete.	/
Piloto et al. (2020)	/	the fire resistance according the insulation criterion I was under estimated by the numerical model with perfect contact and better agreement were obtained with the airgap model.
Piloto et al. (2020)	/	they proposed a new methodology to evaluate these temperatures of the slab

		component. They noticed that the results obtained for the steel contents were unsafe for most of the analysis.
Balsa et al. (2021)	/	LWC moisture and the mechanical effect of the airgap is recommended to be include for future studies.
F. Bolina et al (2021)	an early detachment accrued within the first five minutes of exposure, this detachment losses the composite concept of the system. For the steel deck temperature all the three methods showed a convergence between them.	the position of the rebars and the cover concrete had a large influence on the temperature evolution.
Balsa et al. (2022)	/	The new coefficients for determining the temperature in the steel deck components and the rebars based on the numerical results was presented.
Zhao et al (2022)	The RAC releases more vapor than NWC.	the thermal convection at the rib location and the thermal resistance at the steel-concrete interface in the model were recommended to be 1 $W/m^2 \cdot K$ and 0.01 $(m^2K)/W$, respectively.

3.5. Conclusion

The behaviour of the composite slabs subjected to fire conditions has been numerically and experimentally investigated by several authors, particularly in this decade. The main works have been divided into three categories, the first focused solely on the thermal behaviour, the second on the thermal mechanical behaviour and the third on mechanical behaviour through analysis and experiments. According to the state of art presented in this chapter 3, it is notified that most of the published works were conducted on the NWC and only few of them are carried out on the LWC without considering the effect of the moisture content like Jiang et al in 2018 considered the LWC but without the airgap with the TRPZ steel deck only; also Piloto et al considered the airgap but without the LWC without the Re-entrant steel deck in 2022 Balsa considered the LWC and NWC with two geometries but without the MC of LWC. This chapter is ending by a summary of the main conclusions from previous experimental and numerical studies, providing an overview to highlight the novelty of the present work which is related to the collection of multiple parameters and consider them in one parametric study to determine the effect of each parameter with the regard to the others to compare them also with the past research. In the next chapter, the different analysis methods of composite slabs were explored.

Analysis Methods for the behaviour of composite slabs

4.1. Introduction

Nowadays, different methods of analysis can be used to assess the thermal behaviour of composite slabs exposed to fire, namely the analytical method called simplified calculation methods defined in standard and numerical simulations known as advanced calculation models. In this chapter, we have tackled the thermal and the mechanical analytical method, in addition to the thermal and thermal mechanical finite elements methods. This chapter ends by suggesting a hybrid method.

4.2. Eurocode 4 part 1-2 analytic method

The calculation methods provided in Annexe D has its own application field, in which it is limited with the geometrical characteristics of the composite slab as show in Figure 4.1.

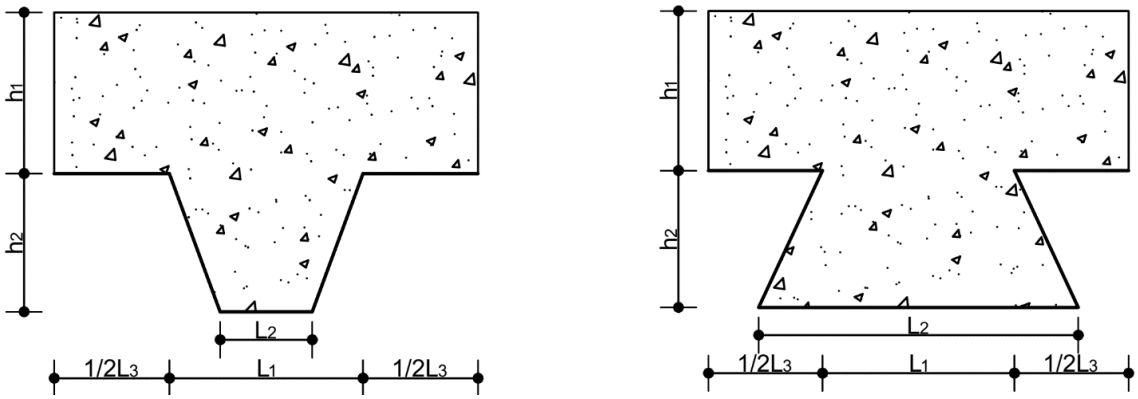

(a) Trapezoidal profile. (b) Re-entrant profile.

Figure 4.1: Composite slab geometry.

The limitations conditions are represented in Table 4.1 below :

Table 4.1: Application Field.

For re-entrant composite slabs			For trapezoidal composite slabs		
77	≤ L1 ≤	135	80	≤ L1 ≤	155
110	≤ L2 ≤	150	32	≤ L2 ≤	132
38,5	≤ L3 ≤	97,5	40	≤ L3 ≤	115
50	≤ h1 ≤	130	50	≤ h1 ≤	125
30	≤ h2 ≤	60	50	≤ h2 ≤	100

4.2.1. Thermal analysis of the slab

EC4 part 1-2 annex D, requires the verification of the insolation criteria "I" which prevents fire propagation on the unexposed surface of the element. The rise of temperature must not exceed an average of 140 °C (T_{int}+140°C) on the unexposed surface above the initial temperature, or a maximum of 180 °C (T_{int}+180°C) above the initial temperature at any point of the unexposed surface.

The verification is done upon time using the equation (4.1) below:

$$t_i = a_0 + a_1 h_1 + a_2 \phi + a_3 \frac{A}{L_r} + a_4 \frac{1}{l_3} + a_5 \frac{A}{L_r}\frac{1}{l_3} \tag{4.1}$$

$$\frac{A}{L_r} = \frac{h_2\left(\frac{l_1 + l_2}{2}\right)}{l_2 + 2\sqrt{{h_2}^2 + \left(\frac{l_1 - l_2}{2}\right)^2}} \tag{4.2}$$

$$\phi = \frac{\left[\sqrt{{h_2}^2 + \left(l_3 + \frac{l_1 - l_2}{2}\right)^2} - \sqrt{{h_2}^2 + \left(\frac{l_1 - l_2}{2}\right)^2}\right]}{l_3} \tag{4.3}$$

With h1 representing the thickness of the continuous upper portion of the slab, ϕ is the view factor of the upper flange of the steel decking, A/Lr demonstrates the rib geometry factor A the area of the rib and Lr the length of the rib (see Figure 4.1). Lastly, the coefficients a_0 to a_5 are specified in EC4 for both NWC and LWC (see Table 4.2).

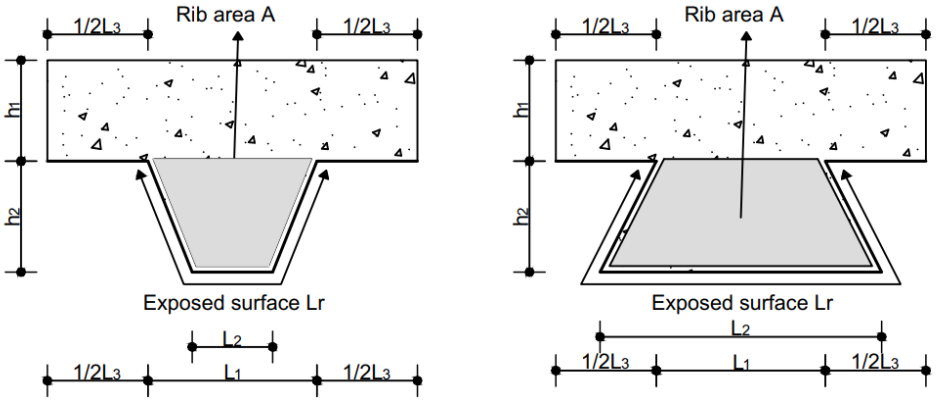

Figure 4.2: Definition of the rib geometry factor

Table 4.2 below regroups the coefficient a_i for both NWC and LWC. These coefficients, related to the type of concrete, are used to determine the fire resistance of the composite slabs according to the thermal insulation criterion.

Table 4.2: Coefficients for the determination of fire resistance according to thermal insulation criterion [11].

Concrete type	a0 [min]	a1 [min/mm]	a2 [min]	a3 [min/mm]	a4 [min.mm]	a5 [min]
NWC	-28,8	1,55	-12,6	0,33	-735	48
LWC	-79,2	2,18	-2,44	0,56	-542	52,3

According to the building code EC4 part 1-2, "t_i" must be superior than the fire rating periods R30, R60 R90 and R120.

4.2.2. Mechanical-Thermal analysis of the slab

4.2.2.1. Evolution of the temperature of the component of the composite slab

Specific periods of fire resistance can be calculated by the annex D can be used for the determination if the temperature of the principal component of the composite slab such as the steel deck (lower and upper flanges and the web), the concrete and the reinforcement rebars in the rib, it is noticed that the analytical method does not provide the temperature for the anti-crack mech.

a) Temperature of the steel deck components

The calculation of the temperature of the steel deck components θ_a may be given by the following equation (4.4):

$$\theta_a = b_0 + b_1 \frac{1}{l_3} + b_2 \frac{A}{L_r} + b_3 \phi + b_4 \phi^2 \qquad (4.4)$$

Where bi is coefficients for the determination of the temperatures of the parts of the steel decking which are represented in Table 4.3.

Table 4.3: Coefficients for the determination of the temperatures of the parts of the steel deck [11].

Concrete type	Fire resistance class	Part of the steel deck	b0 °c	b1 °c.mm	b2 °c/mm	b3 °c	b4 °c
NWC	R60	Upper flange	340	-3269	-2,62	1148,4	-679,8
	R90	Upper flange	618	-2786	-1,79	767,9	-472
	R120	Upper flange	770	-2460	-1,67	592,6	-379
	R60	Web	661	-833	-2,96	537,7	-351,9
	R90	Web	816	-959	-2,21	464,9	-340,2
	R120	Web	925	-949	-1,82	344,2	-267,4
	R60	Lower flange	951	-1197	-2,32	86,4	-150,7

	R90	Lower flange	1018	-839	-1,55	65,1	-108,1
	R120	Lower flange	1063	-679	-1,13	46,7	-82,8
LWC	R30	Upper flange	331	-2284	-1,54	488,8	-131,7
	R60	Upper flange	607	-2261	-1,02	664,5	-410
	R90	Upper flange	789	-1847	-0,99	469,5	-313
	R120	Upper flange	903	-1561	-0,92	305,2	-197,2
	R30	Web	483	-286	-2,26	439,6	-244
	R60	Web	761	-558	-1,67	426,5	-303
	R90	Web	906	-654	-1,36	287,8	-230,3
	R120	Web	989	-629	-1,07	186,1	-152,6
	R30	Lower flange	800	-1326	-2,65	114,5	-181,2
	R60	Lower flange	955	-622	-1,32	47,7	-81,1
	R90	Lower flange	1019	-478	-0,91	32,7	-60,8
	R120	Lower flange	1062	-399	-0,65	19,8	-43,7

b) Temperature of the reinforcement rebars

The calculation of the temperature of the steel deck components θ_a may be given by the following equation (4.5) :

$$\theta_{ai} = c_0 + c_1 \frac{u_3}{h_2} + c_2 z + c_3 \frac{A}{L_r} + c_4 \alpha + c_5 \frac{1}{l3} \quad (4.5)$$

$$\frac{1}{z} = \frac{1}{\sqrt{u_1}} + \frac{1}{\sqrt{u_2}} + \frac{1}{\sqrt{u_3}} \quad \text{With approximation} \quad u_1 = u_2 = \frac{l_2}{2}, \; u_3 = h_2 + d \quad (4.6)$$

Where u_1, u_2 and u_3 are geometrical distances represented in Figure 4.3, Z symbolised the position of the rebar inside the rib, α indicates the angle of the rib, and Ci are Coefficients for the determination of the temperatures of the reinforcement rebars temperatures which are given in Table 4.4.

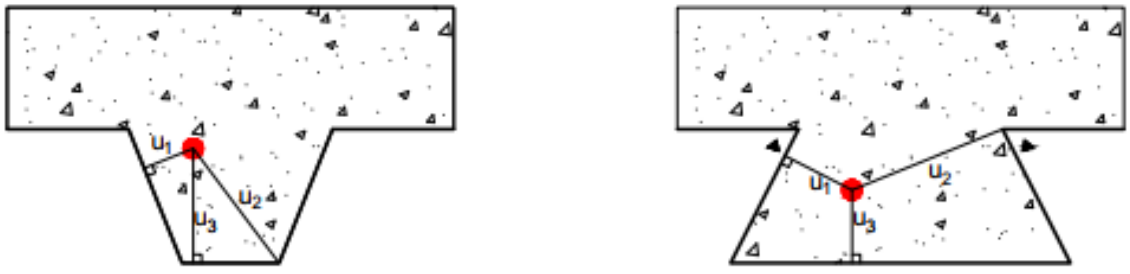

Figure 4.3: Parameters for the position of the reinforcement bars.

Table 4.4: Coefficients for the determination of the temperatures of the reinforcement bars in the rib [11].

Concrete type	Fire resistance class	c0 °c	c1 °c	c2 °c.mm$^{0.25}$	c3 °c.mm	c4 °c	c5 °c.mm
NWC	R60	1191	-250	-240	-5,01	1,04	-925
	R90	1342	-256	-235	-5,3	1,39	-1267
	R120	1387	-238	-227	-4,79	1,68	-1326
LWC	R30	809	-135	-243	-0,7	0,48	-315
	R60	1336	-242	-292	-6,11	1,63	-900
	R90	1381	-240	-269	-5,46	2,24	-918
	R120	1397	-230	-253	-4,44	2,47	-906

4.2.2.2. Evaluation of the bending moment of the slab

The bending moment of the slab is evaluated by using the equation (4.7) below:

$$M_{fi,Rd} = \sum A_i z_i k_{y,\theta,i} \left(\frac{f_{y,i}}{\gamma_{M,fi}}\right) + \alpha_{slab} \sum A_j z_j k_{y,\theta,j} \left(\frac{f_{c,j}}{\gamma_{M,fi,c}}\right) \quad (4.7)$$

Where:

α_{slab} : a slab coefficient equal to 0.85.

$f_{y,i}$: yeild stress for steel.

$f_{c,j}$: mechanical resistance of the concrete.

$k_{y,\theta,i}$ $k_{c,\theta,j}$: Reduction coefficient defined by table 4.6.

A_i A_j : Area of the components.

z_i z_j : distance between the natural axis of the components and natural plastique axis of the rib.

4.2.2.3. Position of the neutral plastic axis of the rib

The natural plastic axis of the rib is determent by the equilibrium of the horizontal forces and it is given by the following equation (4.8):

$$z_{pl} = \frac{\sum Z_i}{\alpha_{rib} \cdot w_{rib} \cdot f_{ck}} \quad (4.8)$$

$$w_{rib} = l_1 + l_3 \quad (4.9)$$

4.2.2.4. Load bearing verification

The load bearing capacity is evaluated by using the equation (4.10) bellow:

$$\frac{M_{fi,d}}{M_{fi,Rd}} = \frac{M_{fi,d}}{\frac{M_{pl,web}}{w_{rib}}} \leq 1 \tag{4.10}$$

Note that the following table 4.5 might be used to facilitate the calculation of $M_{fi,Rd}$.

Table 4.5: Steps for the calculation of $M_{fi,Rd}$.

Compo	θa | θc °C	Ky,θ | Kc,θ -	Ai mm²	fy | fc N/mm²	Zi kN	zi m	Mi kN.m
Lower flange	$\Theta_{a,l}$	$k_{y,\theta}$	$l_2 \cdot t$	fy	$A \cdot k_{y,\theta} \cdot f_y$	$h_T - t/2$	$Z_i \cdot z_{pl}$
Web	$\Theta_{a,w}$	$k_{y,\theta}$	$2\left(\frac{h_2}{sin(\alpha)}\right)t$	fy	$A \cdot k_{y,\theta} \cdot f_y$	$h_T - h_2/2$	$Z_i \cdot z_{pl}$
Upper flange	$\Theta_{a,u}$	$k_{y,\theta}$	$l_3 \cdot t$	fy	$A \cdot k_{y,\theta} \cdot f_y$	$h_T - h_2 + t/2$	$Z_i \cdot z_{pl}$
Rebar	Θ_s	$k_{y,\theta}$	$\frac{\pi \cdot \phi^2}{4}$	fy	$A \cdot k_{y,\theta} \cdot f_y$	$h_T - u_3$	$Z_i \cdot z_{pl}$
Concrete	Θ_c	$k_{c,\theta}$	$w_{rib} \cdot Z_{pl}$	fc	$A \cdot k_{c,\theta} \cdot f_c$	$z_{pl}/2$	$Z_i \cdot z_{pl}$
						$M_{fi,Rd}$	$\sum M_i$

The following table regroups the values of the reduction factors for the material steel, NWC and LWC according to Eurocodes.

Table 4.6: Reduction factors for Steel and concrete [19].

Steel temperature θa	reduction factor Ky,θ
20	1
100	1
200	1
300	1
400	1
500	0.78
600	0.47
700	0.23
800	0.11
900	0.06
1000	0.04
1100	0.02

Concrete temperature θc	NWC reduction factor Kc,θ	LWC reduction factor Kc,θ
20	1	1
100	1	1
200	0.95	1
300	0.85	1
400	0.75	0.88
500	0.6	0.76
600	0.45	0.64
700	0.3	0.52
800	0.15	0.4
900	0.08	0.28
1000	0.04	0.16

1200	0	1100	0.01	0.04
		1200	0	0

4.3. Finite element numerical simulation

For the advanced calculation, different models were devolved by the use of ANSYS to predicted the fire behaviour of the composite slabs under thermal loads only and under thermal-mechanical loads.

ANSYS mechanical APDL abbreviation of Ansys parametric design language (APDL) is a powerful software applied in the engineering fields to solve complex problems for both linear and nonlinear problems such as the thermal conditions in transient regime and steady-state regime. It is used for two-dimensional or three-dimensional geometries. This analysis is performed taking into consideration boundary conditions, steel deck geometries and mesh convergence.

4.3.1. Thermal finite element study

For the thermal analysis parametric study, a reduced and multi-ribs models were devolved to conduct this study. The finite element method requires the solution of the heat diffusion equation (4.11) below:

$$\frac{\partial^2 T}{\partial x^2}+\frac{\partial^2 T}{\partial y^2}+\frac{\partial^2 T}{\partial z^2}+\frac{\dot{q}}{\lambda}=\frac{\rho c}{\lambda}\frac{\partial T}{\partial t} \qquad (4.11)$$

With, λ is the thermal conductivity, T is the temperature of the element, c is the specific heat of the material, and ρ is the material's density.

To solve equations (4.11), the heat transfer boundaries conditions should be given in the equation (4.12) below:

$$\dot{h}_{net,d}=\dot{h}_{net,r}+\dot{h}_{net,c}=\sigma\phi\varepsilon_m\varepsilon_f\left[\left(T_g+273\right)^4-(T_m+273)^4\right]+\alpha_c\left(T_g-T\right) \qquad (4.12)$$

In equation (4.12), $\dot{h}_{net,r}$and $\dot{h}_{net,c}$ represent the heat flux from radiation and convection correspondingly,σ is Stefan-Boltzmann's constant, ε_f is the fire emissivity equal to 1, ε_m is the emissivity of the materials which is equal to 0.7, θ_g symbolizes the gas temperature, θ_m represents the materials temperature, α_c defines the convection coefficient. Finally, the view factor ϕ is purely a geometrical parameter. It represents the portion of the radiative heat flux, which leaves the surface that strikes another surface [52], for the lower flange it is equal to 1, and for the upper flange which is calculated referring to equation (4.14) and for the web which is also calculated according to the following equation (4.13):

$$\phi_{web} = \frac{ad + cb - ad - cd}{2ab} = \frac{\left[\sqrt{{h_2}^2 + \left(\frac{l_1 - l_2}{2}\right)^2} + (l_3 + l_1 - l_2) - \sqrt{{h_2}^2 + \left(l_3 + \frac{l_1 - l_2}{2}\right)^2}\right]}{2\sqrt{{h_2}^2 + \left(\frac{l_1 - l_2}{2}\right)^2}} \quad (4.13)$$

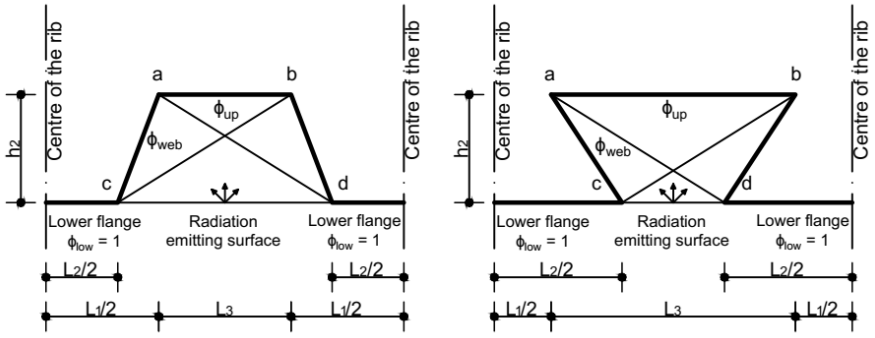

Figure 4.4: Schematic for the calculation of view factor [6].

4.3.1.1. Numerical model boundary conditions (calculation hypothesis)

The lower edge of the slab is assumed to be submitted to standard fire condition for a considerable time to satisfy the insolation criterion, where the time step is 60 s and maybe reduced to 1 s. An initial temperature of 20 °C is applied on all nodes. The heat transfer by convection on the exposed side is represented by the coefficient α_c=25 W/m²K [21]. Regarding to the unexposed side, upper edge of the slab, a coefficient of heat transfer by convection equal to α_c=9 W/m² is taken to include the radiation effect as well [21]. The interface between steel and concrete is modeled as a perfect thermal contact, assuming no thermal resistance or friction. Mechanical interaction effects such as slip or friction were not considered in this thermal analysis. A transient thermal analysis was performed to simulate the time-dependent temperature distribution throughout the composite section under fire exposure.

The geometry of the composite slab is defined with five parameters h1, h2, L1, L2, L3 (shown in Figure 4.5), they represent respectively: the height of the concrete above the steel deck, the depth of the steel deck, the length of the lower flange, the width of the rib measured from the top (between two upper flanges) and the length of the upper flange.

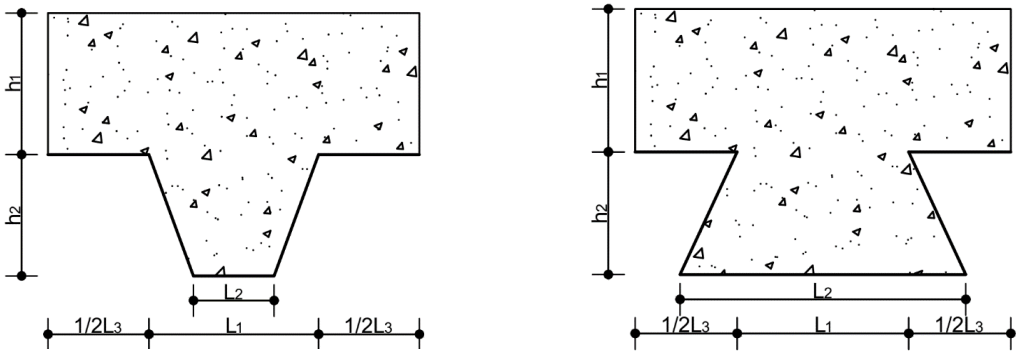

(a) Trapezoidal profile (b) Re-entrant profile

Figure 4.5: Composite slab geometry.

For the parametric study, four different deck geometries were used, two of them were re-entrant Multideck 50 and Cofrastar 40 and the other two trapezoidal geometries are Polydeck 59S , Hi-bond 55, these steel decks are represented bellow in Figure 4.6:

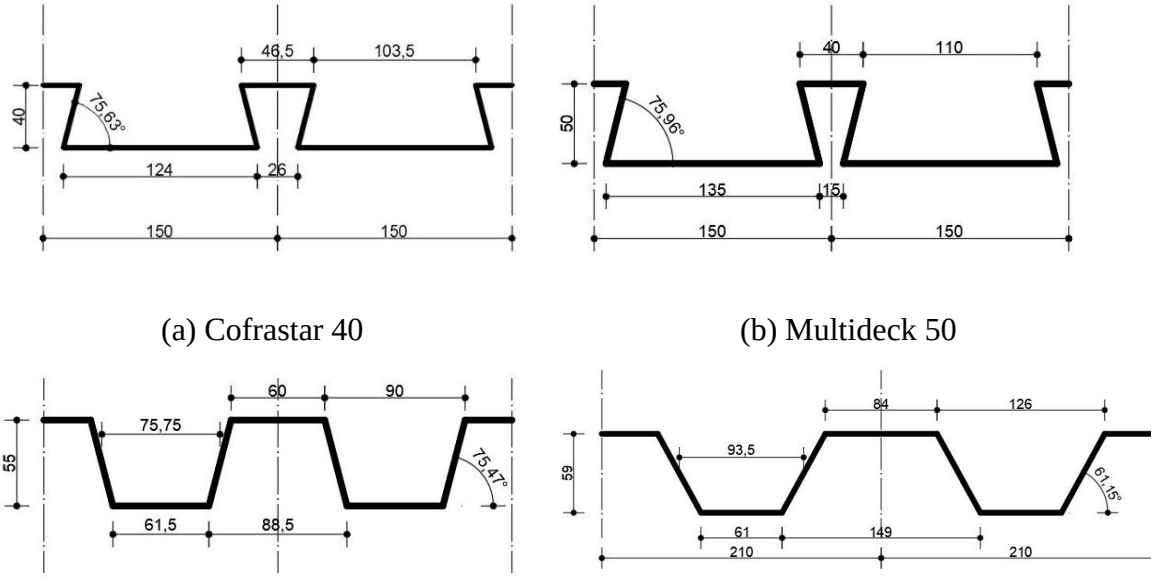

(a) Cofrastar 40 (b) Multideck 50

(c) Hi-bond 55 (d) Polydeck 59S

Figure 4.6: Steel decks geometric characteristics and dimensions [mm].

4.3.1.2. Model type

Before selecting the model type, a comparison between multi ribs and one rib model was done and the results are shown below in Figure 4.7.

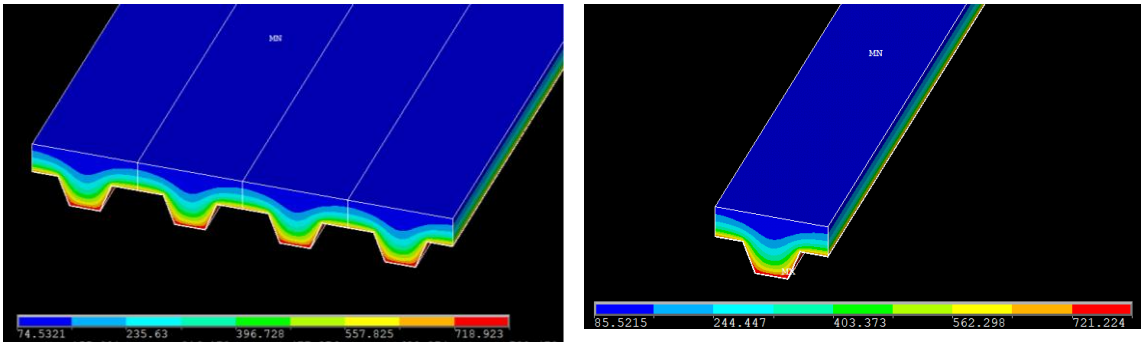

(a) Temperature distribution while using multi-ribs

(b) Temperature distribution while using one ribs.

Figure 4.7: Temperature distribution on both models.

After 1860 s of fire exposing on the lower side of both slabs, the thermal simulation gives the temperature of 800.68 °C and 799.47 °C for one rib model and multi-ribs model respectively. The results found are similar. Then, the work can be done relying on the reduced scale model to gain time and computational efforts.

4.3.1.3. Mesh convergence study

The model presented in Figure 4.8 was made using one finite element SOLID70 to simulate each part: steel deck, concrete and the airgap. SOLID70 is a three-dimensional finite element with 8 nodes and a single freedom degree which is temperature[53].

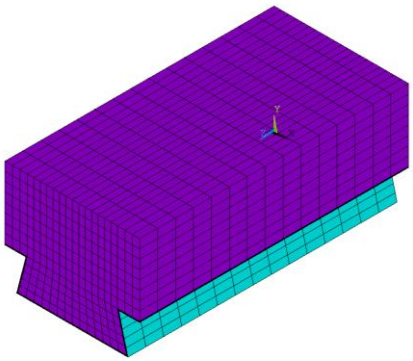

Figure 4.8: Finite element meshes.

The meshes convergence study was performed using several element lengths to determine when the model converges to a constant value. The results represented in Figure 4.9 are for a transient regime, the fill material is NWC using a time step of 60 s which can be reduced to 1 s.

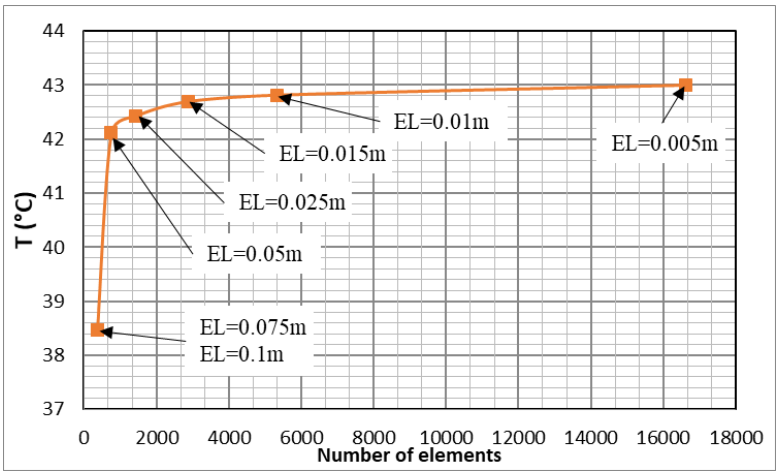

Figure 4.9: Mesh convergence study.

From the results above, it can be seen that the use of greater element length, leads to inaccurate results (EL>0.05 m). The results became more appreciable when decreasing the element lengths, smaller elements length led to a dense number of elements. Thus, the solution requires more time, computational effort, and considerable memory consumption. To make the mesh convergence study more efficient, we assume that EL=0.01 m satisfies both the criterion of computational effort and convergence value. It is to be noted that the number of elements used in this study reaches around 5500 elements, this demonstrates the accuracy of the model as shown in Figure 4.9.

4.3.2. Thermal-mechanical finite element study

The thermal-mechanical simulation for the standard fire behaviour is presented in this section, for this study another two finite element models is presented to carry on the parametric study related to this section this model contains in addition to the previous model steel rebars for the lower reinforcement and anti-crack mesh. This method is based on time step incrementation and iterations, due to the non-linear behaviour of the material and the variable geometry. The slab is subjected to additional live and dead loads which are constant under fire conditions. These forces must be balanced the stress according to the following equation (4.14):

$$\nabla[\sigma] + \{F\} = 0 \tag{4.14}$$

Where F represents the external forces and σ defines the stress. The load bearing capacity of the slab can be determined using the equation bellow for the positive sagging moment resistance:

$$M_{p,Rd} = N_{p,pl}\left(d_p - \frac{x_{pl}}{2}\right) + N_{s,pl}\left(d_s - \frac{x_{pl}}{2}\right) \tag{4.15}$$

Where $N_{p,pl}$, $N_{s,pl}$ represent the plastic tensile force for the effective section and steel rebars respectively, d_p, d_s symbolised the position of the plat and the position of the rebars and both are measured from top of the slab, lastly x_{pl} defines the plastic centroid of the effective section.

4.3.2.1. Numerical model boundary conditions

The thermal mechanical study is based on the use the combination of the result of two models, one model for the thermal analysis only and the second one for the thermal mechanical results. First file which contains the result of the thermal analysis of the slab only. In which will be switched to mechanical analysis, this late will be run through the same amount of time and the same time step with the first model and for each iteration it takes the temperature results of the first model and apply it into the second model. This section uses the same boundary condition for the thermal part.

4.3.2.2. Mesh convergence study

This section relies in the simulation of composite slab with bond width of one sheet. The simulation is done by the use of a three-dimensional models as represented in Figure 4.10 bellow, as mentioned on the upper paragraph a switch between two models was need (thermal model analysis converted to thermal mechanical analysis), the thermal model was created using two different element types namely the SOLIDE70 for the simulation of Concrete (NWC and LWC) also steel deck and the airgap, and LINK33 for simulation of the rebars. These elements were switched to SOLIDE65 to simulate the mechanical behaviour of the slab and LINK180 for the mechanical behaviour of the steel rebars. The models use an element length of 0.01 m which his accuracy was demonstrated perilously.

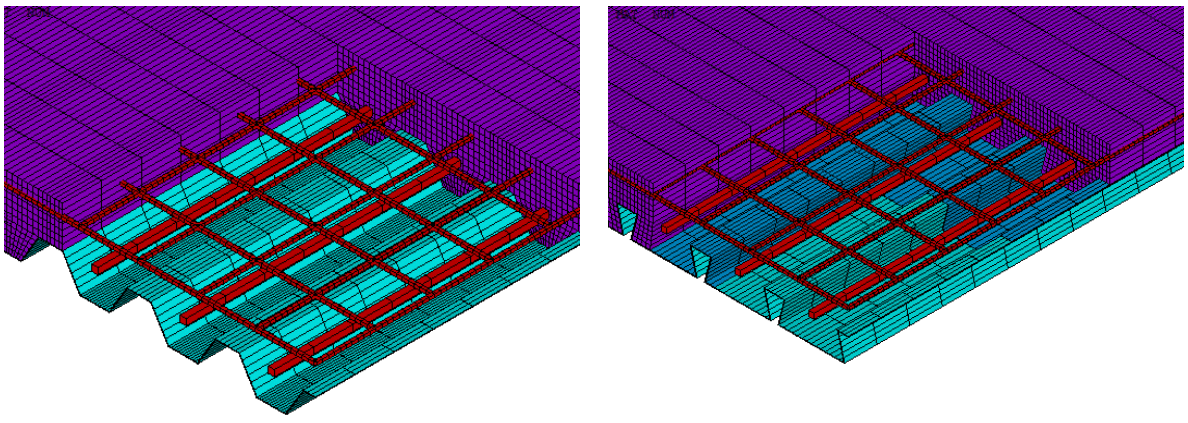

(a) Trapezoidal model with perfect contact. (b) re-entrant model with airgap.

Figure 4.10: Proposed model for the parametric studies.

SOLIDE65 is used for 3-D modelling of solids with or without reinforcing bars (rebar). The solid is capable of cracking in tension and crushing in compression. In concrete applications, for example,

the solid capability of the element may be used to model the concrete while the rebar capability is available for modelling reinforcement behaviour. Other cases for which the element is also applicable would-be reinforced composites (such as fiberglass), and geological materials (such as rock). The element is defined by eight nodes having three degrees of freedom at each node: translations in the nodal x, y, and z directions. Up to three different rebar specifications may be defined [54].

LINK33 is a uniaxial element with the ability to conduct heat between its nodes. The element has a single degree of freedom, temperature, at each node point. The conducting bar is applicable to a steady-state or transient thermal analysis [55].

LINK180 is a 3-D spar that is useful in a variety of engineering applications. The element can be used to model trusses, sagging cables, links, springs, and so on. The element is a uniaxial tension-compression element with three degrees of freedom at each node: translations in the nodal x, y, and z directions. Tension-only (cable) and compression-only (gap) options are supported. As in a pin-jointed structure, no bending of the element is considered. Plasticity, creep, rotation, large deflection, and large strain capabilities are included [56].

4.4. Hybrid thermal-mechanical analysis

The proposed method for the thermal-mechanical analysis is a hybrid method based on both analytical equations and the Finite element thermal results. The concept of the method is the use of the equations mentioned above with the thermal results of the finite elements method, by passing the tables of the EC4 part 1-2 for the calculation of the temperature for each competent of the slab. This combination allows to calculate both the resisting moment and the deflection of the slabs step by step. For each time step the mechanical properties of the materials was calculated by the multiplication of the reduction factors on the initial values of the properties and both are dependent on the temperature at the time step. Thus, the Mrd and δ was calculated and plotted into figures.

The resisting moment is calculated with the equation 4.16 bellow:

$$M_{fi,Rd} = \sum A_i z_i k_{y,\theta,i} \left(\frac{f_{y,i}}{\gamma_{M,fi}}\right) + \alpha_{slab} \sum A_j z_j k_{y,\theta,j} \left(\frac{f_{c,j}}{\gamma_{M,fi,c}}\right) \qquad (4.16)$$

Where:

α_{slab} : a slab coefficient equal to 0.85.
$f_{y,i}$: yeild stress for steel.
$f_{c,j}$: mechanical resistance of the concrete.
$k_{y,\theta,i}$ $k_{c,\theta,j}$: Reduction coefficient defined by tables 4.6.

A_i A_j : Area of the components.

z_i z_j : distance between the natural axis of the components and natural plastique axis of the rib.

Regarding to the deflection of the slab is calculated based on the following (4.17):

$$\delta_1 = \frac{5}{384}\frac{(b \cdot q) \cdot L^4}{E \cdot I_c} \tag{4.17}$$

Where:

b: bond width of the loads.
q: the applied load on the slab.
L: Span of the slab between the supports.
E: Young modulus of the material.
Ic: Second moment of area for the section.

The second moment of area Ic of the section is the mean value of both the second moment of area of the cracked and the uncracked section, they can be determent as follows:

a) The second moment of area of the cracked section Icc

The value of Icc can be determined according to the following figures:

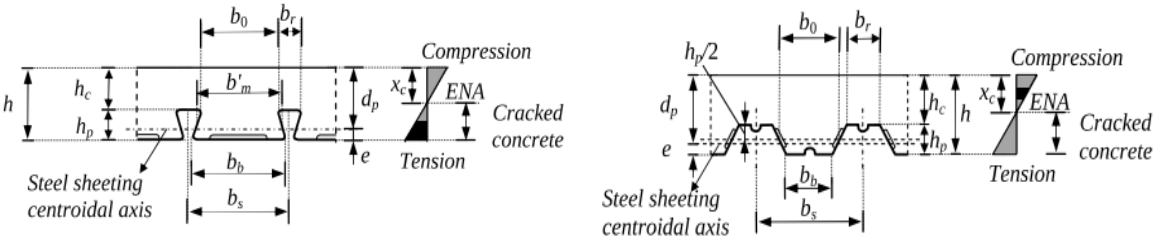

Re-entrant profile. Trapezoidal profile.

Figure 4.11: Second moment of area calculation for the cracked cross section, Icc [4].

The second moment of area for the cracked section and the slab width b is calculated as:

$$I_{cc} = \frac{b \cdot {x_c}^3}{3 \cdot n} + A_p \cdot \left(d_p - x_c\right)^2 + I_p + A_s \cdot (h - e_s - x_c)^2 \tag{4.18}$$

Where xc is the position of the elastic neutral axis relative to the upper side of the slab.

$$x_c = \frac{n \cdot \left(A_p + A_s\right)}{b} + \sqrt{\left[\frac{n \cdot \left(A_p + A_s\right)}{b}\right]^2 + \frac{2 \cdot n \cdot \left[A_p \cdot d_p + A_s(h - e_s)\right]}{b}} \tag{4.19}$$

n: is the equivalent coefficient for long and short terms.

$$n = \frac{E_a}{E'_{cm}} = \frac{E_a}{\frac{2}{3}E_{cm}} \tag{4.20}$$

b) The second moment of area of the uncracked section Icu

The value of Icu can be determined according to the following figures:

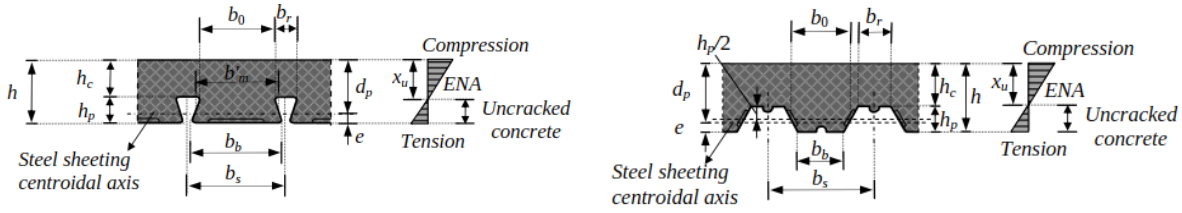

Re-entrant profile. Trapezoidal profile.

Figure 4.12: Second moment of area calculation for the cracked cross section, Icu [4].

The second moment of area for the cracked section and the slab width b is calculated as:

$$I_{cu} = \frac{b \cdot {h_c}^3}{12 \cdot n} + \frac{b \cdot h_c}{n} \cdot \left(x_u - \frac{h_c}{2}\right)^2 + \frac{b_m \cdot {h_p}^3}{12 \cdot n} + \frac{b_m \cdot h_p}{n} \cdot \left(h - x_u - \frac{h_p}{2}\right)^2 + A_p \cdot \left(d_p - x_u\right)^2 + I_p + A_s \cdot (h - e_s - x_u)^2 \tag{4.21}$$

Where xc is the position of the elastic neutral axis relative to the upper side of the slab

$$x_u = \frac{b \cdot \frac{{h_c}^2}{2} + b_m \cdot h_p \cdot \left(h - \frac{h_p}{2}\right) + n \cdot A_p \cdot d_p + n \cdot A_s \cdot (h - e_s)}{b \cdot h_c + b_m \cdot h_p + n \cdot A_p + n \cdot A_s} \tag{4.22}$$

The values of bm are determined in function of the shape of the section as follows:

For the re-entrant slabs $b_m = \frac{b}{b_s} b'_m \quad and \quad b'_m = \frac{(b_b - 2 \cdot t) + b_0}{2}$

(4.23)

For the trapezoidal slabs $b_m = \frac{b}{b_s} b_0$

(4.24)

4.5. Conclusion

This chapter has addressed three calculations methods for evaluating the fire resistance of composite slabs. The first method is an analytical approach, which relies on simplified calculation rules and formulas provided from Eurocode 4 1-2 [11]. This method focuses on determining the coefficient for the calculation of both temperature of the elements constituting the slab and the resisting mechanical moment. The second method is an advanced calculation approach, using the finite element method

(FEM) through ANSYS software to evaluate ~~also~~ both thermal and mechanical performance of composite structures. The third method is the new proposed hybrid method, which combines the analytical equations and the finite element thermal results to determine the deflection and the resisting moment for the composite slabs under fire conditions. This chapter is followed by the thermal analysis of the composite slabs.

Thermal analysis of the behaviour of the composite slabs

5. Thermal analysis of the behaviour of the composite slabs

5.1. Introduction

Chapter five presents a parametric study of the thermal analysis of the slab made with LWC. It includes the effect of the steel deck geometry, airgap between steel deck and concrete, moisture content, concrete density and thermal conductivity. The last subsection deals with the equivalent section in fire resistance time.

5.2. Thermal insulation results

The maximum temperature is the highest value of the temperature measured on the unexposed side of the slab whereas the average temperature is the mean of the given temperatures measured on the unexposed side of the slab on the points presented in Figure 5.1.

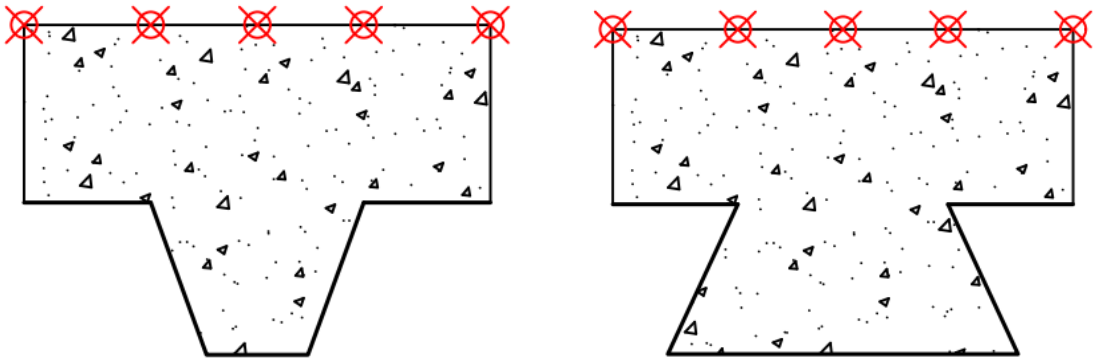

(a) Trapezoidal profile (b) Re-entrant profile

Figure 5.1: Measuring points.

Figure 5.2 (a) represents the evolution of the average and the maximum temperatures of the re-entrant composite slab (Cofrastar 40) for the different slab thicknesses made by LWC. However, Figure 5.2 (b) shows the temperature distribution inside the slab, with h_1 the depth of the concrete on top of the steel deck equal to 80 mm. One can see that the temperature increases with the decrease of the concrete thickness because of the reduction of the thermal mass The maximum temperature and the average temperature for all slab thicknesses considered in this study exceeds the temperature limited by the insulation criterion [11]. It is to be noted that the moisture content and the airgap are neglected in this case (the airgap thickness δa is equal to 0).

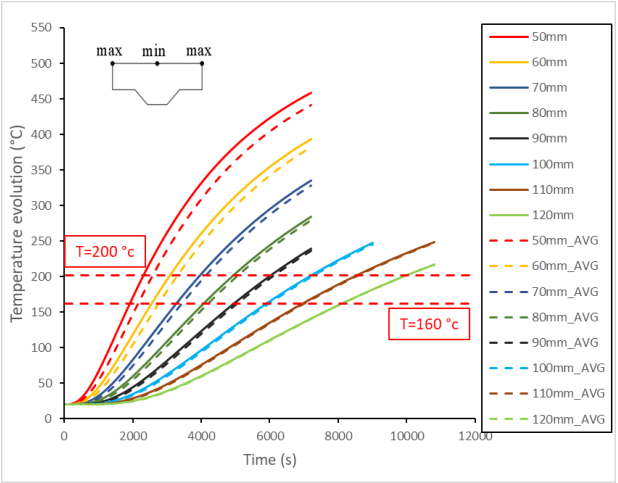

(a) Average and maximum temperatures evolution for different slab thicknesses.

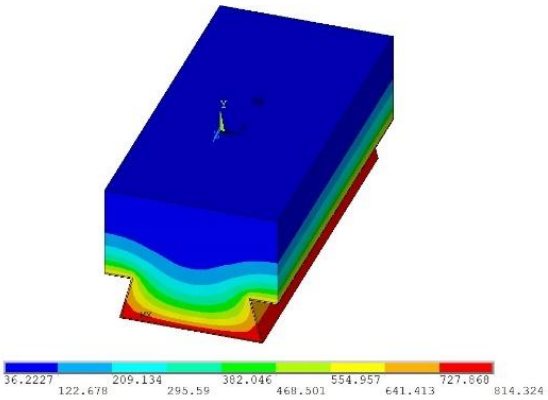

(b) Temperature distribution on the slab.

Figure 5.2: Results of the Cofrastar40 made with LWC, M.C=0% and δa=0mm.

Figure 5.3 (b) illustrates the temperature distribution inside the slab made by NWC, the depth of the concrete on the top of the steel deck h_1=80 mm taking the same conditions as in the section above. Also, Figure 5.3 (a) shows the same tendency as in Figure 5.2 (a). It is observed that the maximum temperature and the average temperature for all slab thicknesses exceeds the temperature limited by the insulation criterion on the considered points [11]. Since the results of the temperature distribution are approximately similar in both composite sections with different steel decks, it seems that this temperature distribution is independent of the geometrical form of the slab regarding the considered points [11].

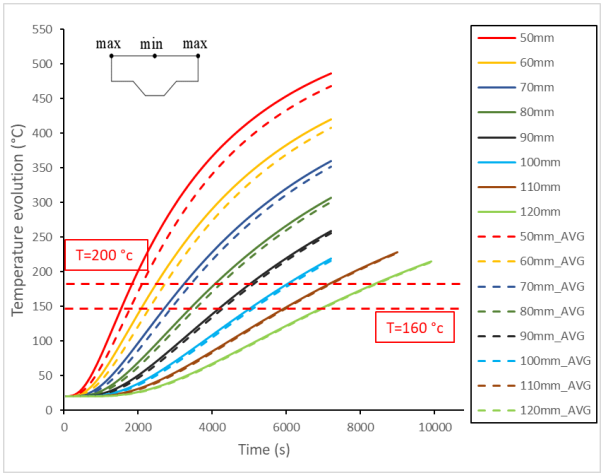

(a) Average and maximum temperatures evolution for all slab thicknesses.

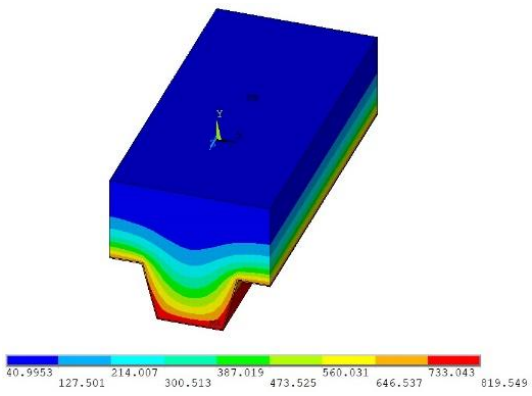

(b) Temperature distribution at the end of simulation (h_1=80mm).

Figure 5.3: Results of the Hi-Bond55 made with NWC, M.C=0% and δa=0mm.

5.3. Effect of the steel deck geometry

The fire resistance time of the composite slabs is evaluated regarding to the effect of the steel deck geometry. A set of 64 numerical simulations were carried out varying the value of the topping concrete (h_1) from 50 mm to 120 mm for both trapezoidal and re-entrant composite slabs (two different sections for each profile) and carrying alsi the type of the concrete from NWC to LWC. The effect of the airgap, moisture content, thermal conductivity and density of concrete are not considered in this case.

Figure 5.4 shows the fire resistance time evolution for all composite slabs with different steel decks made with LWC and NWC as a function of the topping concrete thickness. According to this figure, the time resistance of the re-entrant steel deck is better than the trapezoidal steel deck for both concretes.

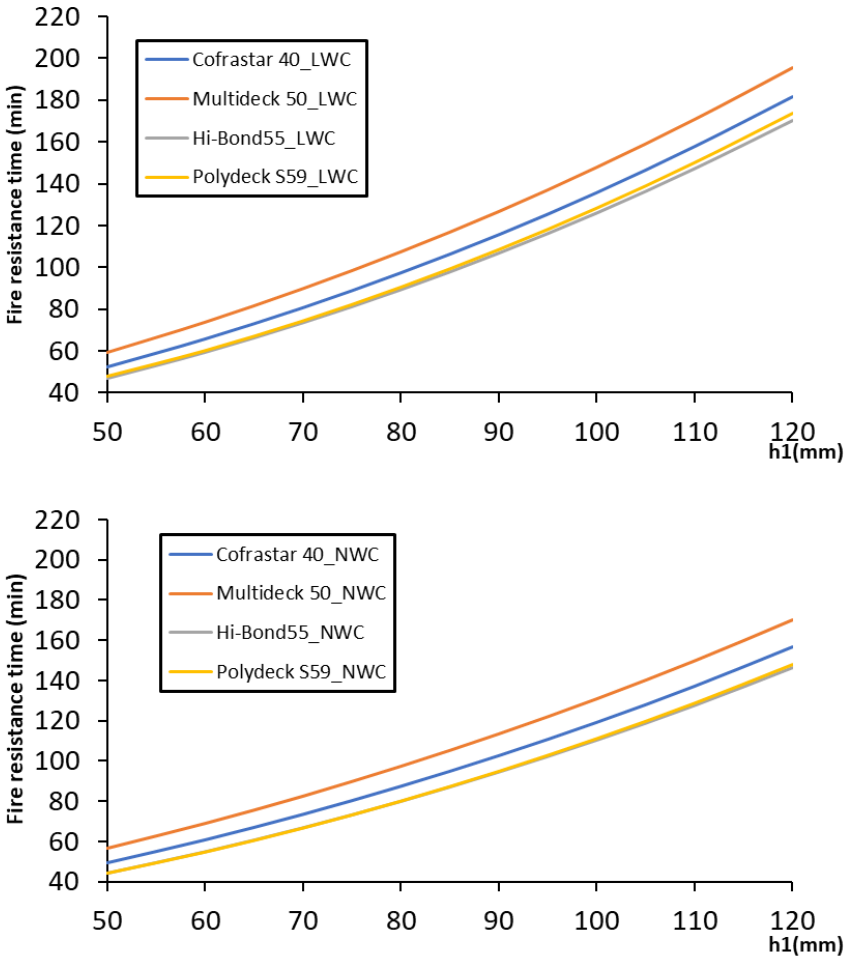

Figure 5.4: Resistance time comparison between trapezoidal and re-entrant steel decks made with LWC and NWC.

5.4. Effect of the airgap

To show the influence of the airgap on the fire resistance time, the characteristics of the lightweight concrete of the composite slab namely the moisture content, the density and the thermal conductivity are kept constant and the airgap between the steel deck profile and the LWC varies from 0 mm to 1 mm. In the literature, 0.5 mm is commonly used for the airgap [46].

The evolution of the fire resistance time of the composite slab as a function of the thickness of the slab for the airgap values is plotted in Figure 5.5. It is observed that the fire resistance time of the composite slab increases with the increase of the airgap. At a given airgap, the fire resistance time increases with the increase of the slab thickness.

The fire resistance time results obtained by the EC4 method are greater than that of the simulation method (the present work). This difference may be attributed to the initial boundary conditions taken at the beginning of the calculation[6].

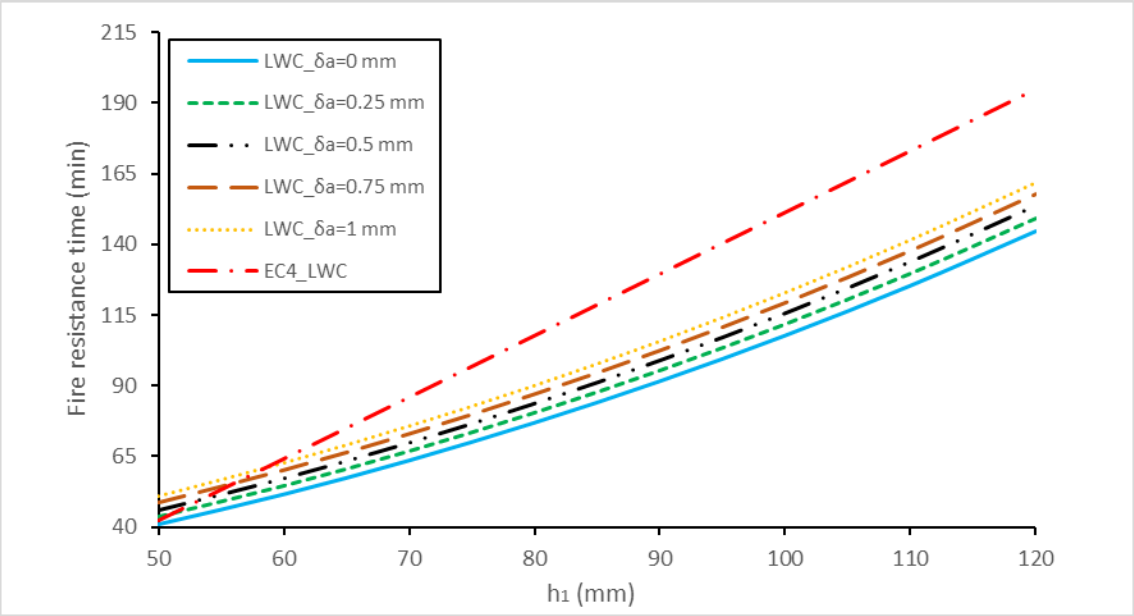

Figure 5.5: Fire resistance time of the composite slab versus the thickness of the slab with different airgap values.

To clarify the effect of the airgap on the fire resistance time of the composite slab, Figure 5.6 is plotted. An increase of approximately 10 min of the fire resistance time is reached when the airgap is taken equal to 1 mm for 50 mm of slab thickness. However, for the thickness of 100 mm, an airgap

of 0.5 mm and 1 mm is needed to have an increase of the fire resistance time of 8 min and 15 min respectively. It is evident that the increase of the void between the steel deck profile and the topping concrete leads to the increased fire resistance time of the composite slab.

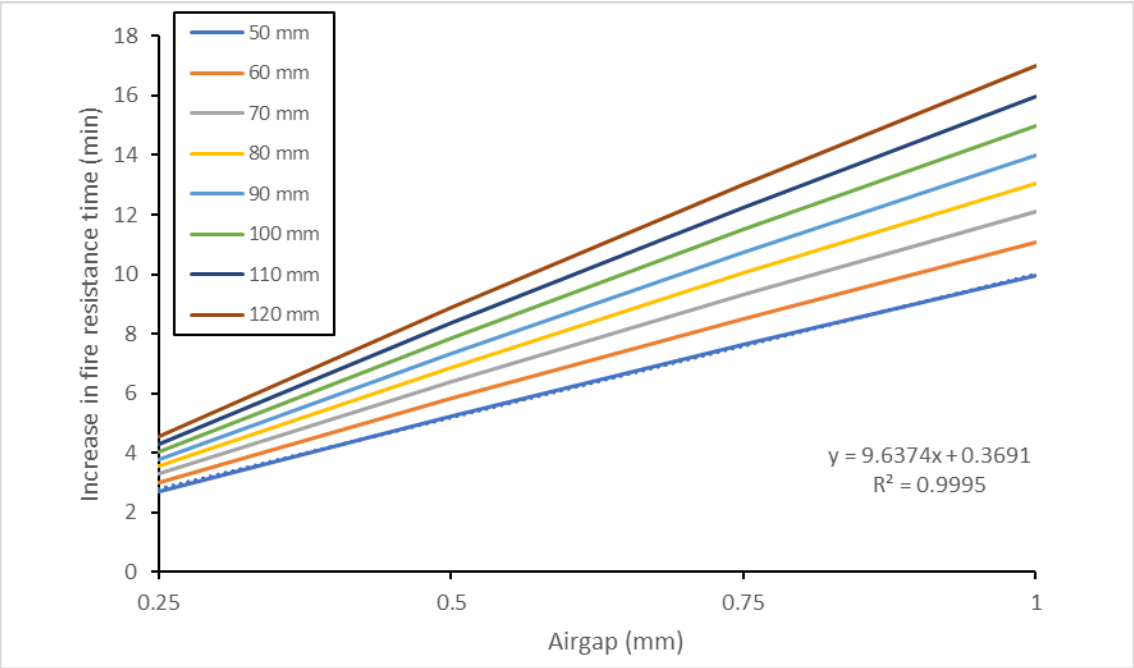

Figure 5.6: The increase in fire resistance time on function of the airgap.

5.5. Moisture content effect

According to Figure 5.7, the specific heat of lightweight concrete shows no peak, indicating the absence of moisture content. In this study, we varied the moisture content percentage to compare it with normal weight concrete (NWC).

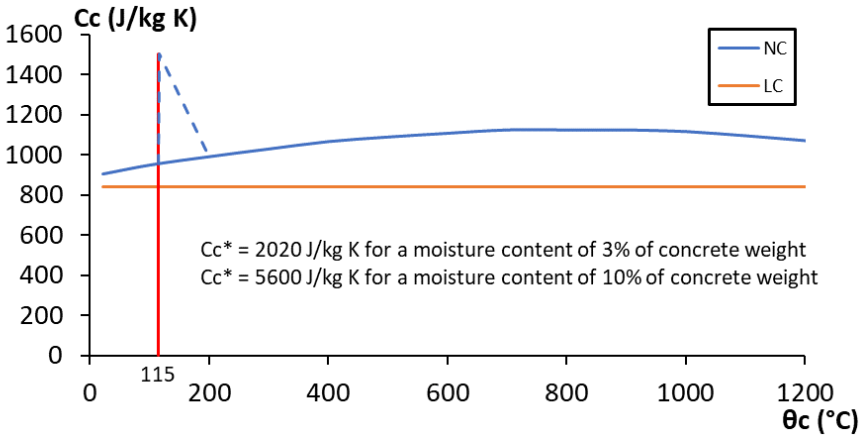

Figure 5.7: Specific heat of normal weight concrete (NC) and lightweight concrete (LC) as a function of the temperature (Eurocode 4 2005).

5.5.1. Comparison between LWC and NWC

A set of 64 numerical simulations were carried out, with varying the value of h1 from 50 mm to 120mm for both trapezoidal and re-entrant composite slabs, all the simulations were done for LWC and NWC. This part was done regarding two cases, in which the parameters influencing the studies are represented in table 5.1 as follows:

Table 5.1: Parameters of the studies.

Parameter	First case	Second case
	Concrete	
Moisture content	LWC: 0% NWC: 2%	LWC: 3% NWC: 3%
Density	LWC: 1800 KN/m^3 NWC: 2300 KN/m^3	LWC: 1800 KN/m^3 NWC: 2300 KN/m^3
	Air	
Presence of the airgap	None	None

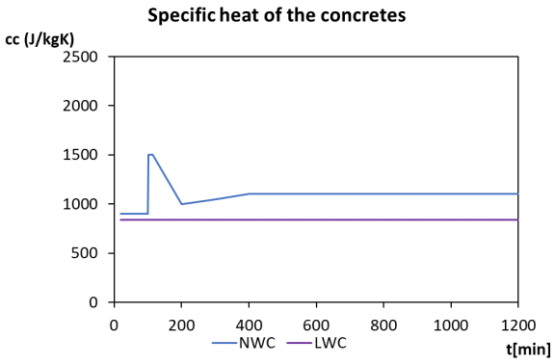

First case specific heat diagram

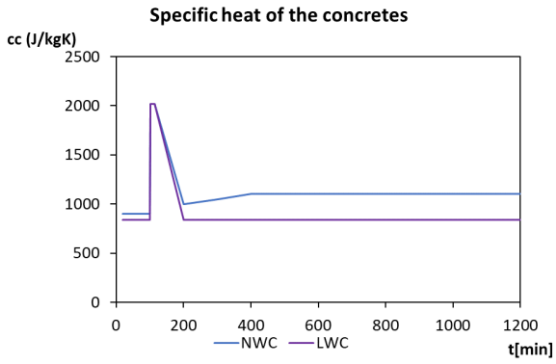

Second case specific heat diagram

Figure 5.8: specific heat of the concretes for the two cases**.**

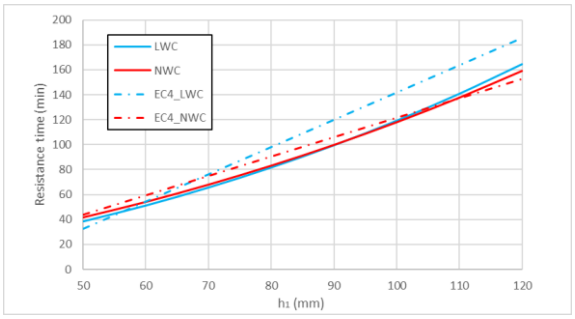

(a) Cofrastar 40.

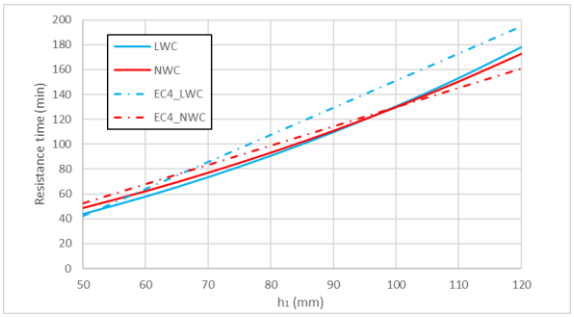

(b) Multideck 50.

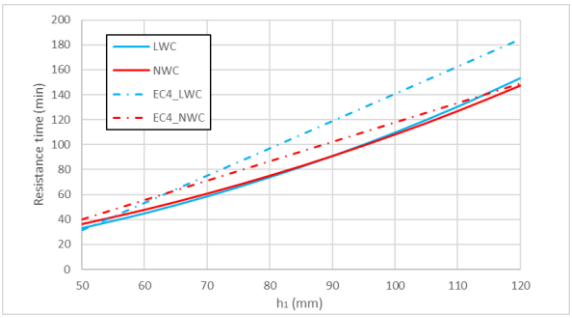

(c) Hi-Bond 55.

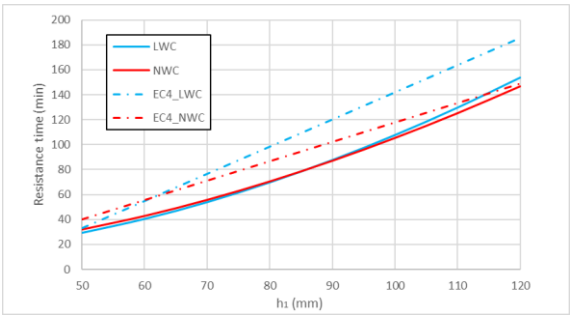

(d) Polydeck 59S.

Figure 5.9: Simulation results for all composite slabs in the first case.

Figure 5.9 represents the resistance time as function of the topping concrete thickness, the relationship between these two parameters is directly proportional and the graphs are uphill and it illustrates that for the depths approximately under 100 mm for the re-entrant slabs and 90 mm for trapezoidal ones, the fire resistance of the NWC is better than that of the LWC, due to the effect of the presence of the moisture content in the NWC which delays the heating process [10], after this the phenomenon is reversed and fire resistance of LWC becomes better than that of the NWC. It is thought that the effect of the moisture content is finished and only the effect of the porosity is influencing.

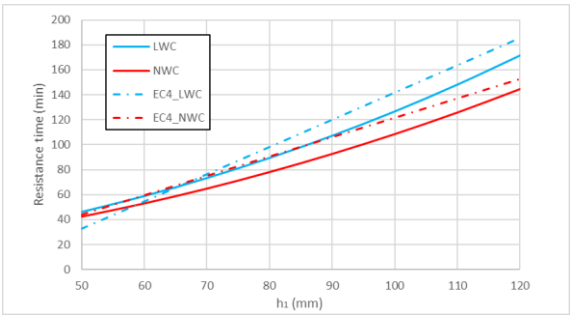

(a) Cofrastar 40.

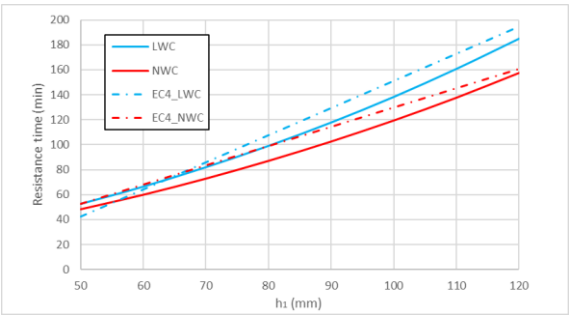

(b) Multideck 50.

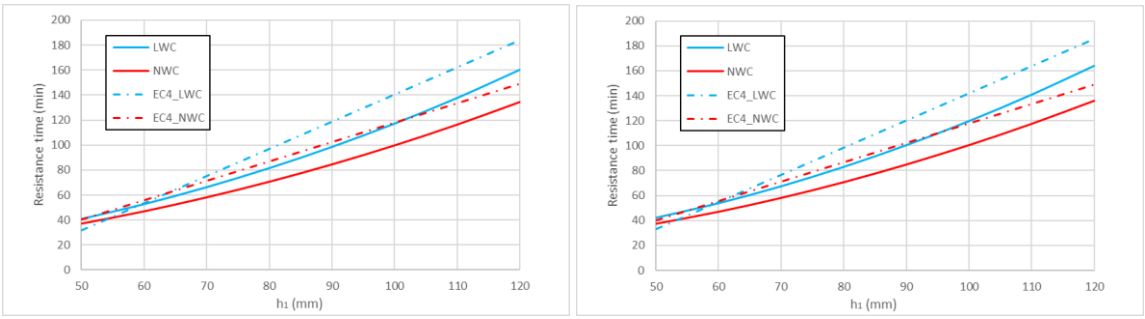

(a) Hi-Bond 55. (d) Polydeck 59S.

Figure 5.10: Simulation results for all composite slabs in the second case.

Figure 5.10 demonstrates the results of the second case. For all slab thickness and slab shapes the LWC fire resistance time is better than that of NWC, the LWC curve is always above the NWC curve. This may be explained by the evaporation process which occurs slowly in LWC slabs regarding the NWC slabs. This is attributed to the higher permeability of the LWC, which enhances the moisture content. As a result, the LWC heat transfer is lower than for NWC under fire conditions [10].

5.5.2. Moisture content effect on the LWC

In this section, all the parameters are kept constant except the moisture content, which varies from 0 to 6%. It is noted that beyond the 6% of the moisture performing the ANSYS software doesn't work properly, one can conclude that the numerical simulation of the thermal analysis does not converge.

The effect of the variation of the moisture content (MC) of the LWC on the evolution of fire resistance time is illustrated in Figure 5.11. For a given slab thickness, it is noticed a great increase of the fire resistance with the increase of the moisture content. This improvement of the fire resistance is associated with the peak that appeared in the specific heat curve (see Figure 5.7). It is reported in the literature [57], that the free water inside the LWC evaporates during the heating. This phenomenon leads to a delay of the heating process. It can be seen that the results of the EC4 method are comparable to the results of the numerical simulation starting from 75 mm when taking 3% of MC and 0.5 mm airgap.

According to the results found, with 6% of MC, the fire resistance time can reach the value of four hours, which is sufficient for the evacuation and fire safety services to intervene.

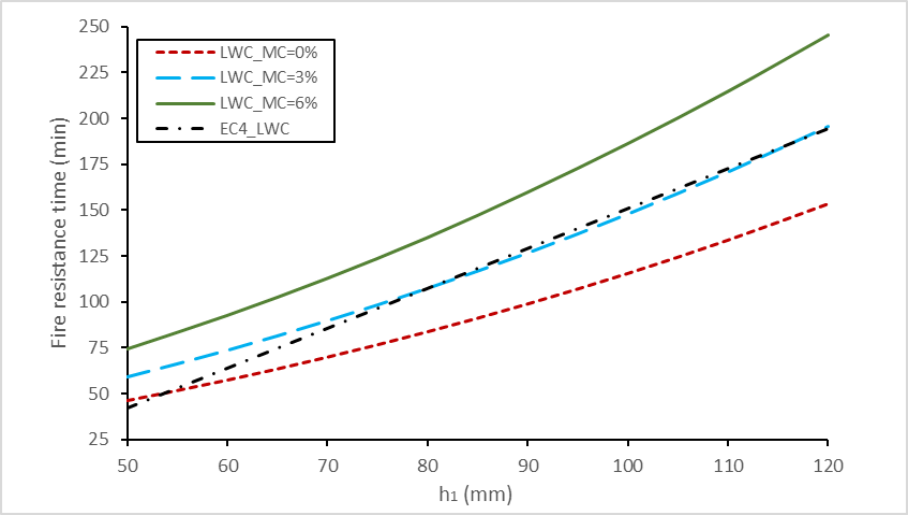

Figure 5.11: Resistance time comparison between three LWC made with different moisture contents.

5.6. Effect of the thermal conductivity

This section investigates the effect of the variation of the thermal conductivity. However, the other parameters influencing are kept constant. Table 5.2 below regroups the values of the thermal properties.

Table 5.2: Parameters for the thermal conductivity effect study.

Parameter	LWC-1	LWC-2	LWC-3
Moisture content	LWC: 3%	LWC: 3%	LWC: 3%
Density (Function of Temp)	*LWC: 1920 kN/m^3	**LWC: 1822 kN/m^3	*LWC: 1600 kN/m^3
Thermal conductivity (Function of Temp)	*0.9 to 1.3 W/m.K (1.1 was taken)	**0.92 W/m.K	*0.68 to 0.89 W/m.K (0.79 was taken)
Airgap	0.5 mm	0.5 mm	0.5 mm

* Cavalline et al 2017 [58] ** Punlert et al 2017 [59]

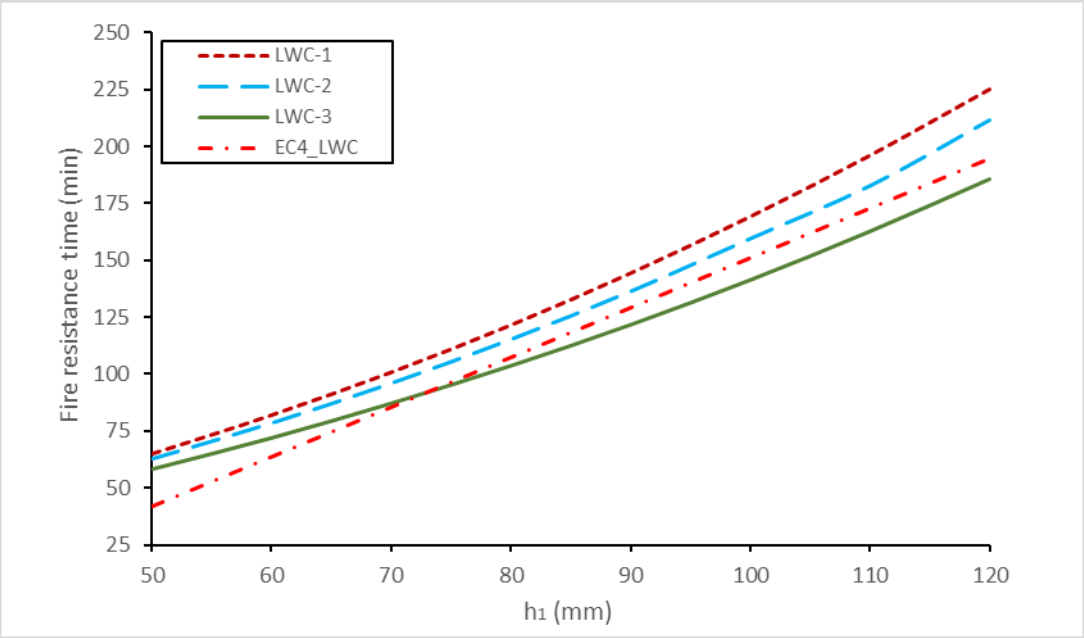

Figure 5.12: Resistance time comparison between three LWC made with different initial thermal conductivities.

Figure 5.12 shows the effect of the variation of the initial thermal conductivity of the LWC on the fire resistance time as a function of the topping concrete thickness. It can be seen that the lower density of the concrete (lower thermal conductivity) leads to higher fire resistance time. A decrease of the density of the concrete slab from 1922 kN/m^3 to 1822 kN/m^3, gives an enhancement of the fire resistance time up to 12% for a 100 mm thickness slab. The increase in the fire resistance time can be attributed to the porosity of the LWC, which makes the heat transfer inside the concrete not easy [57], The thermal conductivity of the LWC depends on the water-accessible porosity, the higher the LWC porosity, the lower the thermal conductivity [57].

When the slab is designed with a height of 120 mm of LWC, we have approximately four hours to reach the limited value of the insolation criteria (I).

For comparative reasons, LWC-2 and that of EC4 is selected. the results found show that the fire resistance time of the LWC-2 is slightly better than that of the EC4. This difference is associated with consideration or not of the airgap in the two materials. Also, it can be linked to the methodology used.

5.7. Equivalent section in fire resistance time

In this section, an attempt to quantify the effect of the presence of the LWC inside the composite slab with regard to the NWC at a given fire resistance class. We look to find a sufficient quantity of NWC,

which may replace the quantity of the LWC in order to get the same fire resistance. In this study, a set of 64 simulations was carried out on both concrete LWC and NWC using four different composite slabs, including the re-entrant and trapezoidal profiled steel deck. Eight different slab thicknesses were selected ranging from 50 mm to 120 mm with a constant step of 10 mm. The variation parameters were regrouped below in Table 5.3.

Table 5.3: Parameters for the equivalent section study.

Parameter	Concrete	
	LWC	NWC
Moisture content	3%	3%
Density (Function of Temp)	1800 kN/m3	2300 kN/m3
Thermal conductivity (Function of Temp)	1.00 W/m.K	1.95 W/m.K
Airgap	0.5 mm	0.5 mm

A calculation was performed separately on both concretes to find the necessary slab height for a given resistance time. The results are presented in Table 5.4.

Table 5.4: Fire resistance time for each concrete LWC and NWC with different fire resistance classes.

Fire resistance class	Steel deck	h_1 (mm)		Δh_1		Ac (cm²/ml)		Δ Ac	
		LWC	NWC	(mm)	%	LWC	NWC	(cm²)	%
R=60 min	Cofrastar 40	56	59	3	6	862	896	34	4
	Multideck 50	51	53	2	5	913	937	24	3
	Hi-Bond55	61	64	4	6	883	920	37	4
	Polydeck S59	60	64	4	7	863	906	43	5
R=90 min	Cofrastar 40	76	82	6	7	1060	1120	60	5
	Multideck 50	70	75	5	7	1109	1160	50	4
	Hi-Bond55	80	87	6	7	1082	1146	64	6
	Polydeck S59	80	87	7	8	1060	1128	69	6
R=120 min	Cofrastar 40	92	100	8	8	1225	1307	82	6
	Multideck 50	87	94	7	8	1274	1346	73	5
	Hi-Bond55	97	106	9	8	1246	1333	87	6
	Polydeck S59	96	105	9	9	1220	1312	91	7

h_1 : represents the thickness of the topping concrete; Ac : represents the area of the concrete section

It can be seen from Table 5.4 that the difference in thicknesses between the two different concretes (represented by Δh_1) increase as the increases of the fire resistance class. For instance, the difference in the Polydeck S59 composite slabs (Δh_1) is 4 mm, 7 mm and 9 mm for R60, R90 and R120 respectively. It seems that the trapezoidal form; namely Hi-Bond55 and Polydeck S59 influences significantly the value of the difference in thicknesses. This may be attributed to the fire-exposed side, which is more open than the re-entrant form. when the NWC is replaced by the LWC, the thickness of the composite slab decreases by 9% for the Polydeck S59 form at R120. This value corresponds approximately to 7% when it is estimated as a surface (Δ Ac) for 1 m length. These results have great importance when considering the cost and the charges in construction buildings.

5.8. Conclusion

A numerical study was conducted to evaluate the advantages of using lightweight concrete (LWC) instead of normal weight concrete (NWC) in composite slabs under fire conditions. The parametric analysis considered factors such as airgaps, moisture content, thermal properties of LWC, and geometric aspects. The study found that for all slab thicknesses, both maximum and average temperatures exceeded the insulation criterion limit. Finite element method (FEM) results showed that re-entrant steel decks provide greater fire resistance times compared to trapezoidal steel decks.

Introducing a 1 mm airgap between the concrete and deck profile increased the fire resistance time by 15 minutes for a 100 mm thick composite slab. When moisture content exceeds 3%, the Eurocode method predicts lower fire resistance times compared to the simulation method. Reducing the concrete slab density from 1922 kg/m³ to 1822 kg/m³ improved fire resistance time by approximately 12% for a 100 mm slab. To achieve the same fire resistance time, normal weight concrete sections need to be 7% thicker than lightweight concrete sections. The proposed numerical model was validated for lightweight concrete as its results closely match experimental data. The model is shown to underpredict temperatures for normal weight concrete and merits future investigation. In the next chapter, we are going to study the thermal mechanical behaviour of the composite slabs.

Thermal mechanical analysis of the behaviour of the composite slabs

6.1. Introduction

This chapter portrays the results of thermal mechanical analysis of the composite slabs using the hybrid method under fire conditions. Specifically, the analysis focuses on four critical parameters: the type of concrete used (NWC, LWC), the thickness of the steel deck, the size of the reinforcement rebar, and the position of the rebar within the rib. Each of these factors plays a significant role in determining the fire resistance, load-bearing capacity, and overall stability of composite slabs. By examining these variables individually, this study aims to provide a comprehensive understanding of their impact on the structural performance of composite slabs in fire conditions.

The main parameters examined in this parametric study are summarized in Table 6.1.

Table 6.1: The key parameters of the thermal mechanical analysis.

Parameter / Steel deck geometry	Hibond55 (trapezoidal)	Multideck50 (re-entrant)
Type of the concrete	NWC, LWC	NWC, LWC
Height of the slab (mm)	130	130
Steel deck thickness (mm)	0.85, 1, 1.2	0.85, 1, 1.2
Diameter of the rebar (mm)	10, 12, 14	10, 12, 14
Position of the rebar	$h_2; \frac{2}{3} h_2 ; \frac{1}{3} h_2$	$h_2; \frac{2}{3} h_2 ; \frac{1}{3} h_2$
Anti-crack mesh (mm)	6	6

6.2. Effect of the type of the concrete

In this section, a range of numerical simulations were performed varying the type of the concrete for both slabs Hibond55 and Multideck50. The characteristics of the concrete used is presented below on the table 6.2:

Table 6.2: Properties of the materials used.

Concrete type	Density	Moisture content	Compressive strength	Young's modulus
	kN/m^3	%	MPa	MPa
LWC	1875	4.81	25.6	2.76E+4
NWC	2435	3.70	36.97	4.57E+4

The different characteristics of the materials were taken from an experimental work [10]. The other parameters of the slab are constant as follows: the anti-crack mesh size is 6 mm, the reinforcement rebars is 10 mm, the height of the section is 130 mm for both slabs, lastly the thickness of the steel deck is kept constant at 1 mm.

According to EC4 part 1-2 Annex D [11, p. 4] the insulation criterion "I" limits the temperature on the unexposed side of the slab at 160 °C and 200 °C for the average temperature and the maximal temperature respectively. Only the unexposed side of the slab is studied.

6.2.1. Unexposed Side temperature evolution

Using Finite element method (ANSYS), The maximal and average temperature evolution for both slabs plotted as a function of the time are represented in the Figures 6.1a and 6.1b. As it can be seen, the temperature is raising fast for the NWC slabs (red color) rather than LWC slabs (blue color). The difference of the temperature between NWC and LWC is more noticeable in the Re-entrant slab rather than the trapezoidal slab. For Example, at the end of each simulation for the Hibond55, the difference of the temperature is about 72 °C but for the multideck50 it is 97 °C. This result can be attributed to the shape of the steel deck profile (re-entrant section), which offers a large quantity of concrete with the regard to the other form (trapezoidal). As a consequence, the insulation property is high in the Multideck50 section. the presence of the LWC has decreased the temperature evolution by 22%, 41% for the Hibond55 and Multideck50 respectively. This can be beneficial in delaying the deterioration process of the concrete.

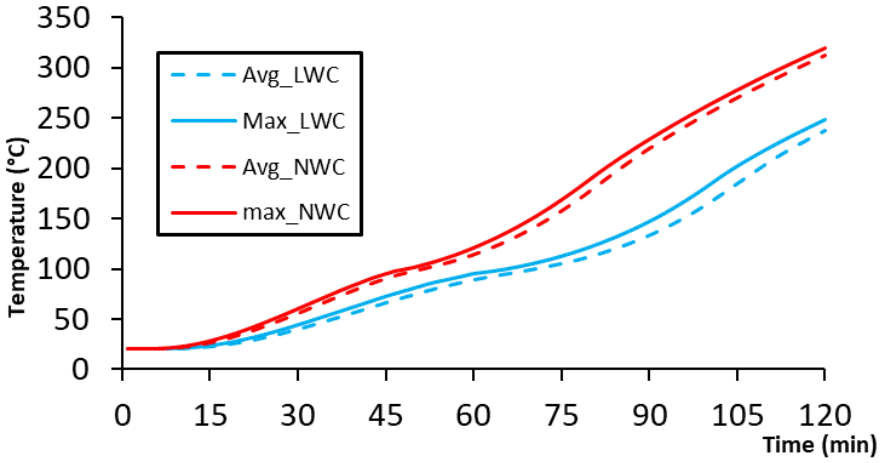

(a) Hibond55.

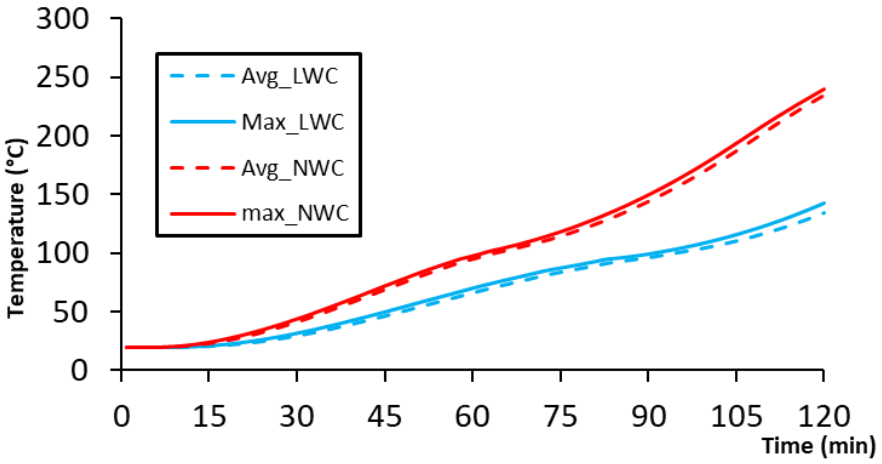

(b) Multideck50.

Figure 6.1: Unexposed Side temperature evolution for both slabs.

Table 6.3: Rate of the impact of the type of the concrete used on the unexposed side Temp.

Fire rates	Multideck50				Hibond55			
	NWC		LWC		NWC		LWC	
	°C	% Temp increase	°C	% Temp increase	°C	% Temp increase	°C	% Temp increase
1	20.00	0%	20.00	0%	20.00	0%	20.00	0%
15	23.40	17%	21.01	5%	26.12	31%	22.35	12%
30	41.65	108%	29.86	49%	55.34	177%	39.57	98%
45	69.18	246%	46.63	133%	89.96	350%	65.99	230%
60	95.29	376%	66.32	232%	113.95	470%	89.00	345%
90	144.36	622%	96.31	382%	219.78	999%	133.43	567%
120	234.89	1074%	134.36	572%	312.61	1463%	238.10	1090%

The results of the temperature evolution on the two different slabs made with different concretes are summarised in Table 6.3. After one hour under fire, the Multideck50 slab made with NWC heats more than three times regarding the initial temperature, however for the same section made with LWC, the increase temperature is only more than two times. If the sections are heated up two hours, the increase temperature in the LWC slab is six times more, but in the corresponding NWC, the temperature increase is more than ten times.

6.2.2. Temperature of the rebar

Figure 6.2 shows the influence of the type of the concrete on the temperature of the rebar for both trapezoidal and re-entrant slabs, represented in horizontal bars (the green bar represents the NWC

results and the blue bar represents the LWC results). It is shown that there is an offset between the bars for the two concretes, which represents the difference of the temperature. this difference is greater for low fire rates up to R60. At this stage, the concrete can protect more the rebars and the presence of the LWC is interesting. Beyond this fire rate, the difference in temperature is not significant. Around the 300 °C, the rebar characteristics are highly affected. So, it can be concluded that the type of the concrete has a limited effect on the temperature of the rebars.

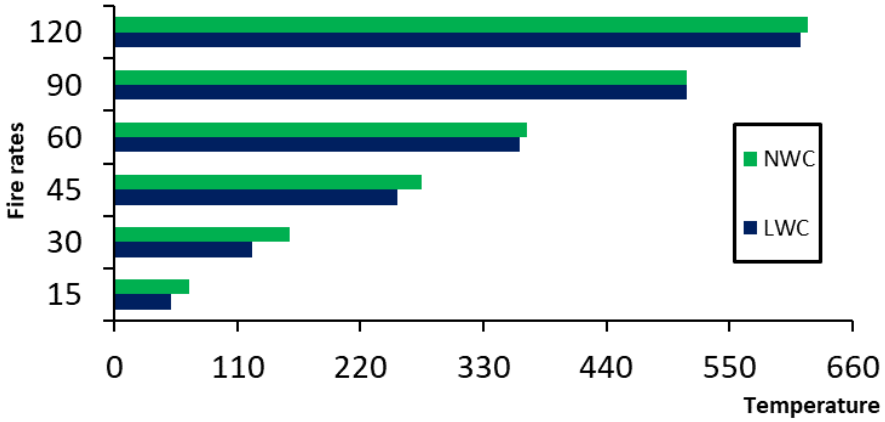

(a) Hibond55.

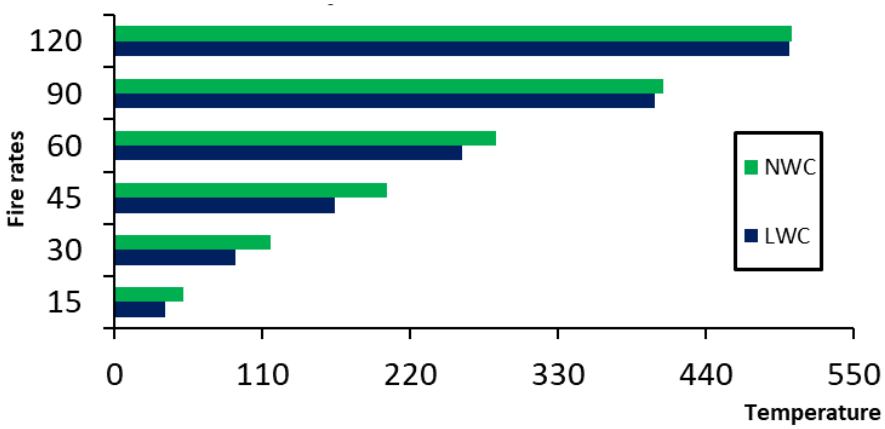

(b) Multideck50.

Figure 6.2: Rebars Temperature evolution for both slabs.

Table 6.4 regroups the results of the evolution temperature of the reinforcing rebars for the two sections made with different concretes. During half an hour of fire, the increase temperature in the reinforcing rebars is five times and three times and a half in the Hibond55 slab when the rebars are covered with NWC and LWC respectively. Here, LWC gives a good protection to the reinforcing rebars because of its low thermal conductivity.

Table 6.4: Rate of the impact of the type of the concrete used on the rebars temperature.

Fire rates	Multideck50				Hibond55			
	NWC		LWC		NWC		LWC	
	°C	% Temp increase	°C	% Temp increase	°C	% Temp increase	°C	% Temp increase
1	20.00	0%	20	0%	20.00	0%	20.00	0%
15	67.17	236%	51.10	156%	51.59	158%	37.62	88%
30	156.40	682%	123.23	516%	116.22	481%	90.42	352%
45	274.69	1273%	253.01	1165%	202.63	913%	164.24	721%
60	369.42	1747%	362.81	1714%	284.12	1321%	258.88	1194%
90	511.86	2459%	512.38	2462%	408.56	1943%	401.74	1909%
120	620.51	3003%	613.60	2968%	504.08	2420%	502.34	2412%

6.2.3. Load bearing capacity

The values of the moment resistance of the composite slab is plotted as a function of the exposure fire time for the two sections (trapezoidal and re-entrant sections) made with the different concretes in figure 6.3. The soliciting moment and the resisting moment are abbreviated by $M_{Ed}\ and\ M_{Rd}$ respectively and they are calculated according to the method mentioned in paragraph "3.3". Up to 15 min of fire exposure time (R15), the mechanical behaviour of the NWC (in red colour) is better than those of the LWC (in blue colour). Over this fire class, the resisting moment of the two concretes (taken in midspan) show a loss of the load bearing capacity. This loss of bearing capacity between the initial and final fire rate is estimated to be equal to $20.91\,kN.m$ and $11.94\,kN.m$ for the hibond55 slab made with NWC and LWC respectively. For the Multideck50 slab, the loss of the moment is found to be equal to $21.53\,kN.m$ and $12.33\,kN.m$ for the NWC and LWC respectively. For the Hibond55 slab, LWC shows a similar or slightly better mechanical behaviour compared to the NWC at high fire class (R120). These results may be attributed to the thermal performances of the concretes. Despite the deterioration of the mechanical performances of both concretes at high fire class, the residual resisting moment is higher than the soliciting moment. In this critical condition, the composite slab is steel safe and the structural stability is always ensured.

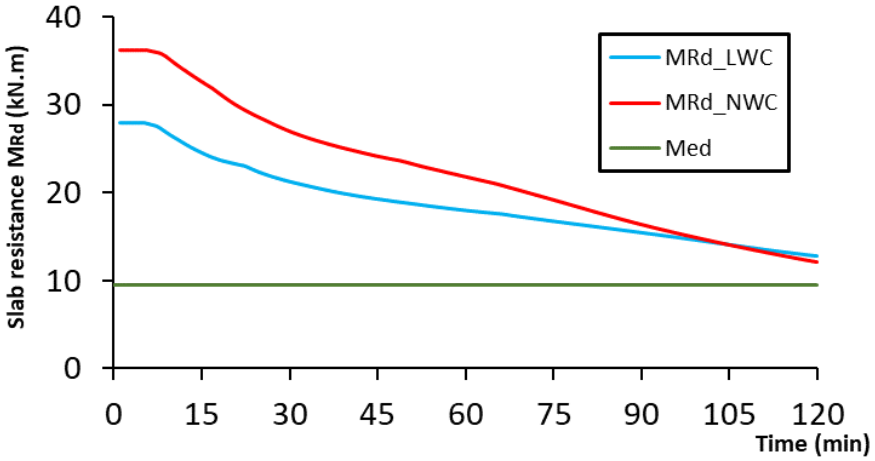

(a) Hibond55.

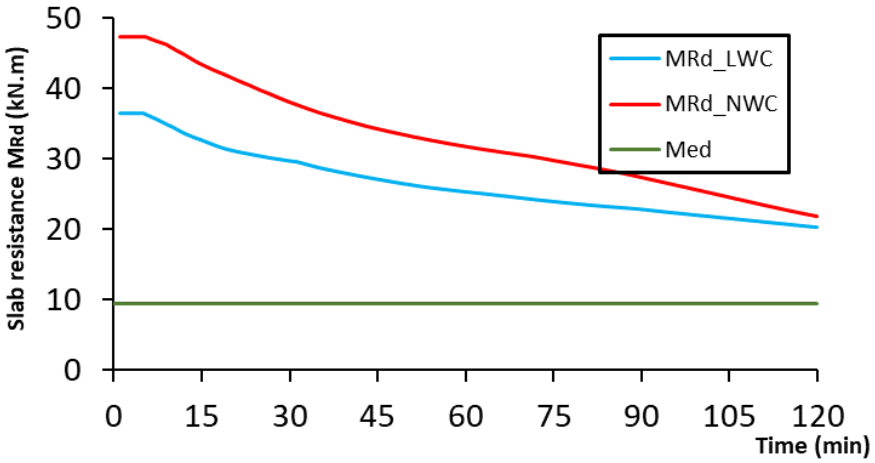

(b) Multideck50.

Figure 6.3: Load bearing evolution for both slabs.

Table 6.5: Rate of the impact of the type of the concrete used in the load bearing capacity.

Fire rates	Multideck50				Hibond55			
	NWC		LWC		NWC		LWC	
	M_{Rd}	% M_{Rd} loss	M_{Rd}	% M_{Rd} loss	M_{Rd}	% M_{Rd} loss	M_{Rd}	% M_{Rd} loss
1	47.39	0%	36.49	0%	36.25	0%	27.92	0%
15	43.62	8%	32.65	11%	32.63	10%	24.50	12%
30	38.41	19%	29.72	19%	26.98	26%	21.38	23%
45	34.50	27%	27.13	26%	24.13	33%	19.33	31%
60	31.96	33%	25.35	31%	21.80	40%	18.02	35%
90	27.63	42%	22.86	37%	16.36	55%	15.51	44%
120	21.93	54%	20.32	44%	12.07	67%	12.77	54%

It is recorded in Table 6.5 the results of the percentage of the moment loss in the two slabs. Up to one hour of fire, the percentage of moment loss is not significant between the two concretes for the Multideck50 slab. Beyond this fire rate, this difference becomes more important. After two hours, the resisting moment generally loses half its initial value for all the sections with the different concretes.

Piloto et al. [41] conducted a numerical work on the thermal mechanical behaviour of composite slab made with NWC (f_{ck} = 20 MPa) and trapezoidal steel deck. In their work, the composite slab was subjected to a bending moment of $4.64\ kN.m$. However, the resisting moment are found to be 11.27 $kN.m$, 8.3 $kN.m$ and 5.52 $kN.m$ at R60, R90and R120 respectively. A comparison between the results of the work of the Ref [41] and those of this study are illustrated in figure 6.4. Even the concrete properties are different in the two works, the same conclusion were deduced, it means the residuals moments were higher than the soliciting moment (see figure 6.4).

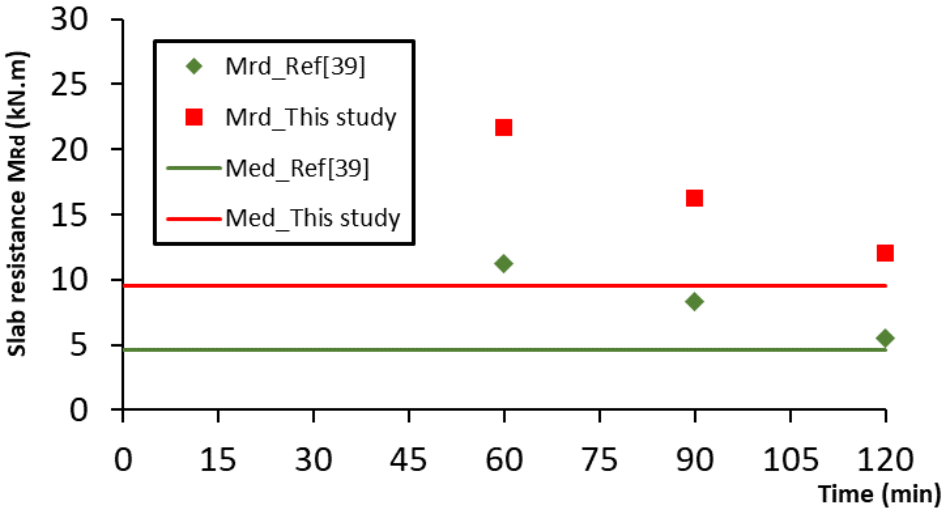

Figure 6.4: Residuals bending moments after heating.

6.2.4. Deflection of the slab

In order to check the structural stability of the composite slab it is useful to calculate the deflection of these elements. The deflection values were computed in the midspan of the composite slab according to the method expressed in paragraph "3.3". The obtained results were compared with the admissible values established by the EC4 [11, p. 4]. Figure 6.5 shows the deflections of both slabs sections Hibond55 and Multideck50 as function of the fire exposure time for the different concretes used. As expected, the defection in both slabs increases as the increase of the fire exposure time. Otherwise, this tendency is more pronounced in LWC than NWC. Beyond R90, the deflection of LWC exceeds the limited deflection mentioned in EC4 [11, p. 4] for Hibond55 slab. The deflection raises between the initial and the final rate (R15 to R120) is estimated to be equal to $6.73\ mm$ and

8.31 *mm* for the Hibond55 slab made with NWC and LWC respectively. For the Multideck50 slab, the raise is found to be equal to 3.55 *mm* and 5.43 *mm* for the NWC and LWC respectively.

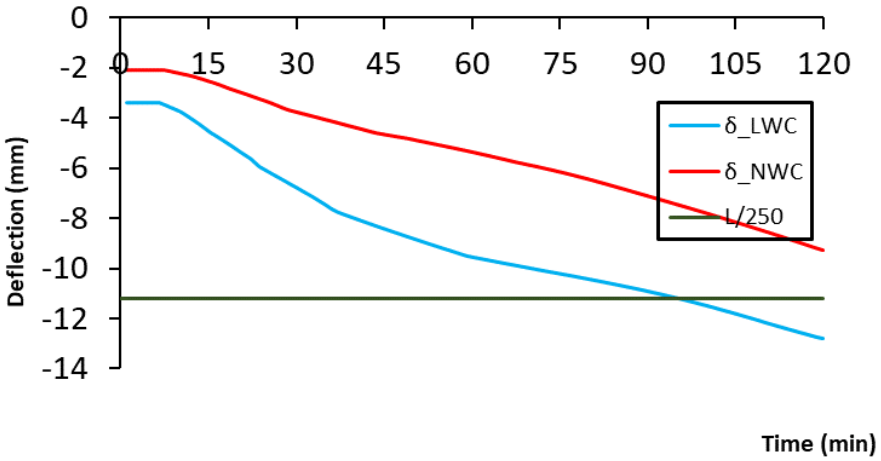

(a) Hibond55.

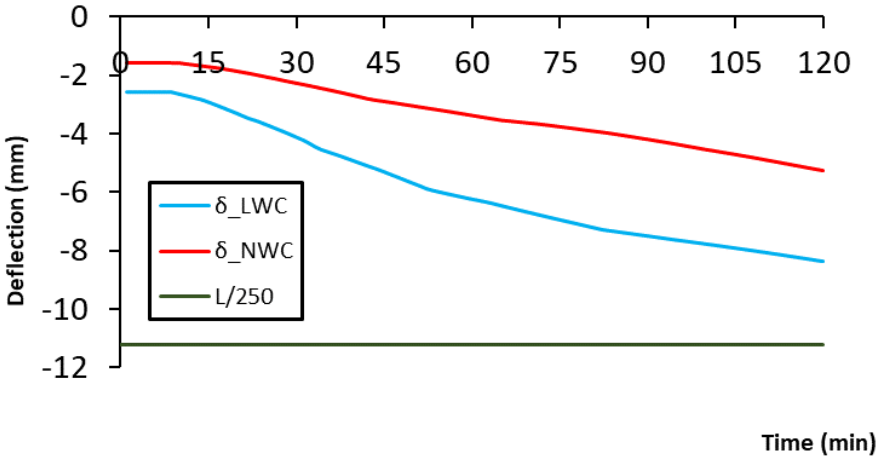

(b) Multideck50.

Figure 6.5: Deflection evolution for both slabs.

Table 6.6: Rate of the impact of the type of the concrete used on the deflection.

Fire rates	Multideck50				Hibond55			
	NWC		LWC		NWC		LWC	
	δ (mm)	% δ increase	δ (mm)	% δ increase	δ (mm)	% δ increase	δ (mm)	% δ increase
1	1.59	0%	2.57	0%	2.09	0%	3.37	0%
15	1.73	8%	2.92	14%	2.53	21%	4.51	34%
30	2.29	44%	4.11	60%	3.76	80%	6.77	101%
45	2.91	83%	5.30	106%	4.65	123%	8.42	150%
60	3.39	113%	6.23	143%	5.35	157%	9.55	183%
90	4.21	164%	7.48	192%	7.10	241%	10.92	224%

120	5.28	231%	8.35	225%	9.26	344%	12.82	280%

The results of the percentage of the deflection loss for the two sections with different concretes are gathered in Table 6.6. The deflection loss in the LWC shows a clear difference with the respect to the NWC for both sections. According to the values indicated in the table, the deterioration becomes too strong after 15 min of fire for all the sections. The maximum increase in deflection recorded here is 344% for the Hibond55 section made with NWC, the corresponding section in LWC indicates an increase of deflection of 280%. It is observed that the percentage of the deflection increase is more pronounced in the LWC slab up to 60 min, over this fire class the increase in deflection in the NWC becomes more important.

To show the contribution of each material on the mechanical properties (the resisting moment and deformation) of the two slabs, we have drawn the relative resisting moment and relative deflection in Figure 6.6.

For the Hibond55 section, it is observed that the contribution of LWC was less than NWC up to 60 min of fire exposure time. Over this fire class, this contribution becomes more noticeable and exceeds the unit after approximately 100 min. in this stage, the mechanical behaviour of LWC is better than that of NWC. Regarding the deformation, the NWC shows a better behaviour than the LWC during 120 min of fire exposure. It is noticed that this behaviour becomes less pronounced after 60 min for fire exposure time.

The high degradation noticed on the LWC deflection with the regard to the NWC can be explained by the weak microstructure of LWC compared with that of the NWC. A material which possesses a high resisting moment does not mean it has a good deformation.

It is concluded that the load bearing capacity of the composite element is less influenced when the element is made from LWC, however the deformation energy (ductility) of the structural element is less influenced when it is made from NWC.

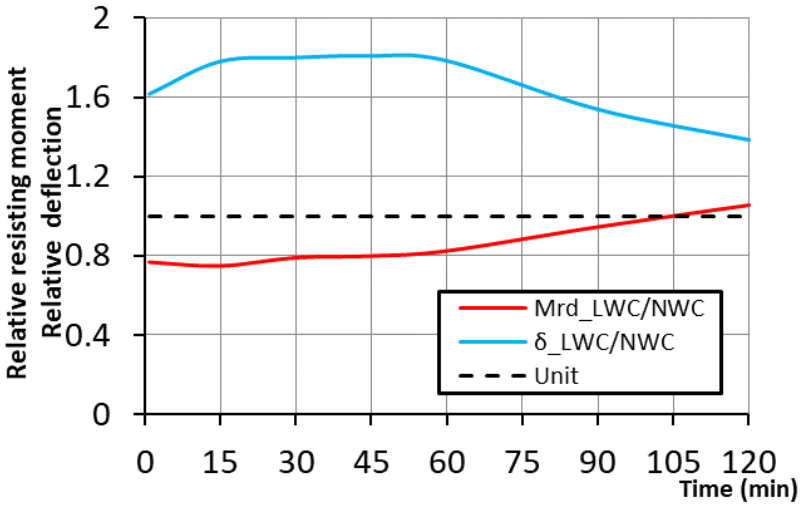

(a) Hibond55.

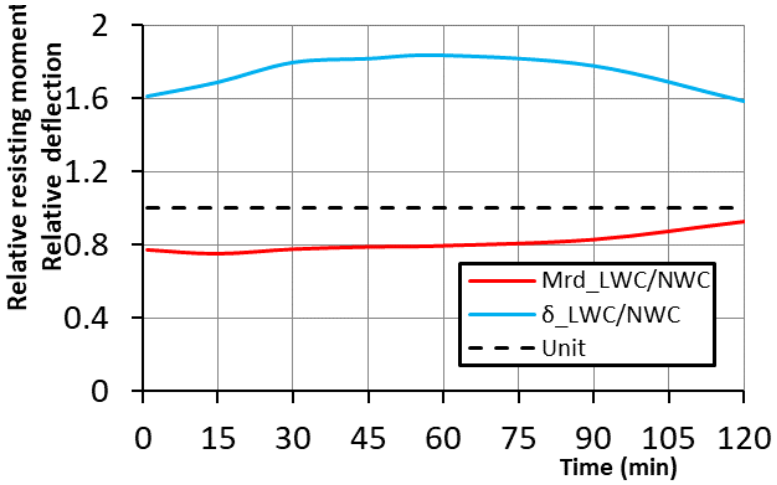

(b) Multideck50.

Figure 6.6: Relative resisting moment and relative deflection.

6.2.5. Limitation of the proposed method

In order to appreciate the results obtained here and to precise the limits of the conclusions deduced from this work, some data from EC4 [11], which uses different materials with low mechanical properties (shown in table 6.7), were used calculate the load bearing capacity and the deflection if the slab.

Table 6.7: Properties of the materials used.

Concrete type	Density	Moisture content	Compressive strength	Young's modulus
	kN/m^3	%	MPa	Mpa
LWC	1800	3	17	2.1E+4
NWC	2350	3	20	2.99E+4

The results found are as summarised in figure 6.7 and 6.8.

a) Load bearing

For the Hibond55 slab, the resisting moment in the NWC is less than the soliciting moment after 90 min of fire exposure time. However, the LWC behaves better and presents a resitting moment similar to the soliciting moment at around 120 min of fire exposure time. On the other side, for the Multideck50 slab, both concretes show a clear difference between the resisting moment and the soliciting moment (see figure 6.7b). The conclusion deduced earlier in section 5.1.3., i.e. The composite slab is safe and the structural stability is always ensured, is still valid for the Multideck50 slab, however we should pay attention when using the Hibond55 because in this case the conclusion mentioned previously is not right.

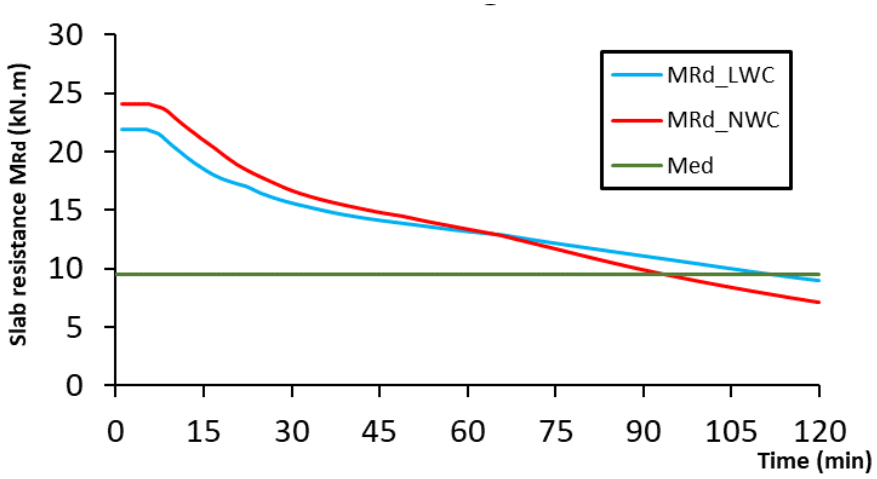

(a) Hibond55.

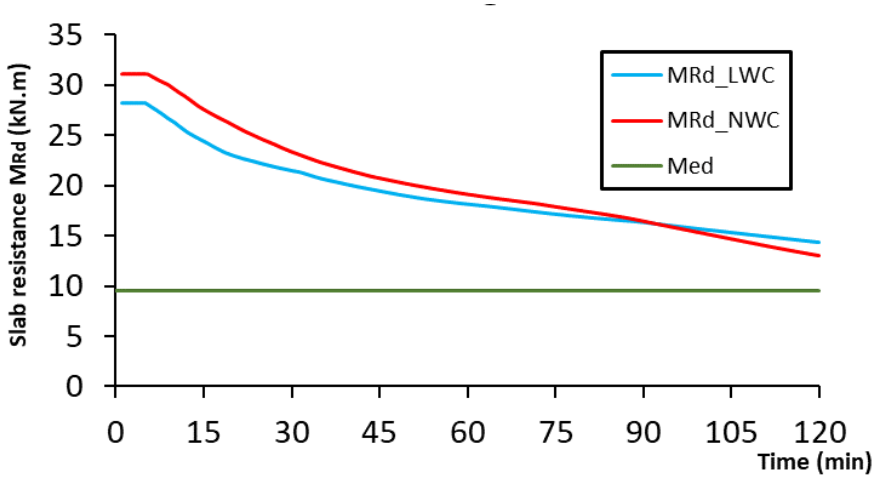

(b) Multideck50.

Figure 6.7: Load bearing evolution for both slabs.

b) Deflection

Considering the low mechanical characteristics of the concretes (details are given in table 6.7), the deflection of both slabs Hibond55 and Multideck50 are drawn in figure 6.8a and 6.8b. The same tendency is observed on the Hibond55 slab, in which the deflection achieves the limited value of the deflection after 100 min of fire exposure time. So, the structural stability of the slab is into question and the properties of the materials may be considered.

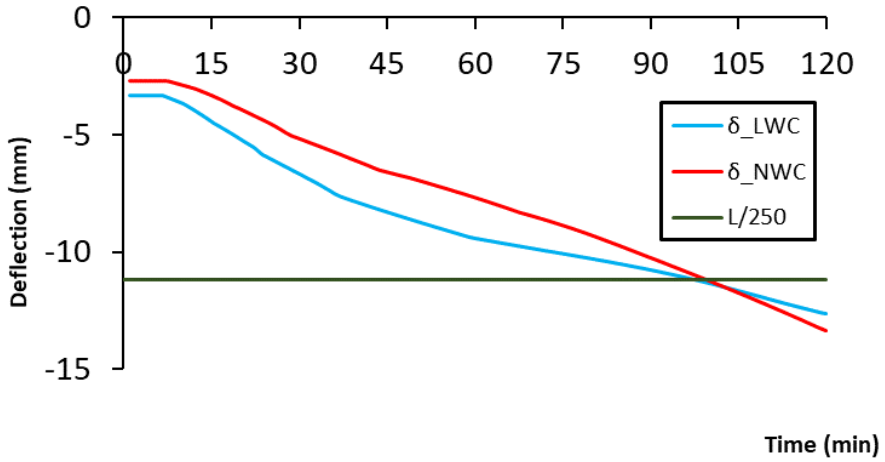

(a) Hibond55.

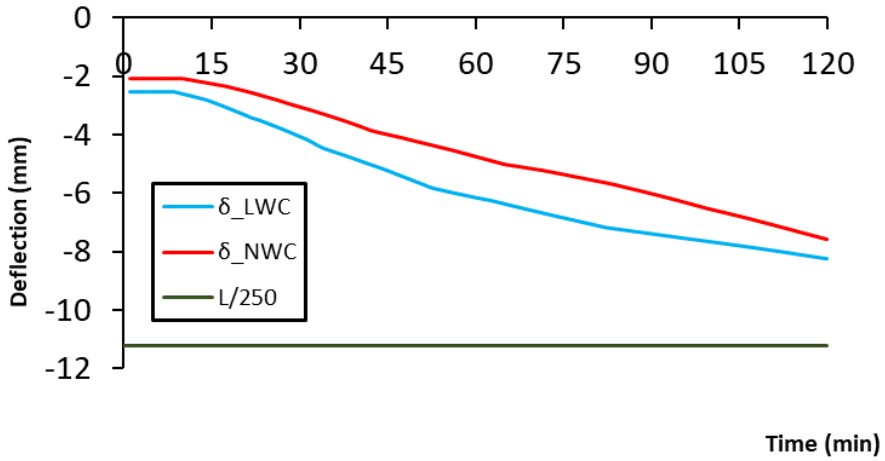

(b) Multideck50.

Figure 6.8: Deflection evolution for both slabs.

6.2.6. Comparison between the two different geometries of the slabs

In this section, the effect of the shape of the slab is taken into consideration regardless the type of the concrete and it is illustrated in figure 6.9, 6.10 and 6.11. The temperature evolution in the Multideck50 slab is lower than that of the Hibond55 slab. After one hour of fire exposure time, the difference in temperature between the two sections starts to be noticeable, it is recorded 22.68 $°C$ and 18.67$°C$ for

LWC and NWC respectively. These values reach 103.74 °C and 77.71 °C at the end (R120). These results highlight the effect of the slab geometry used. A good choice of the form of the slab can lead to improve to the thermal performances of the slab.

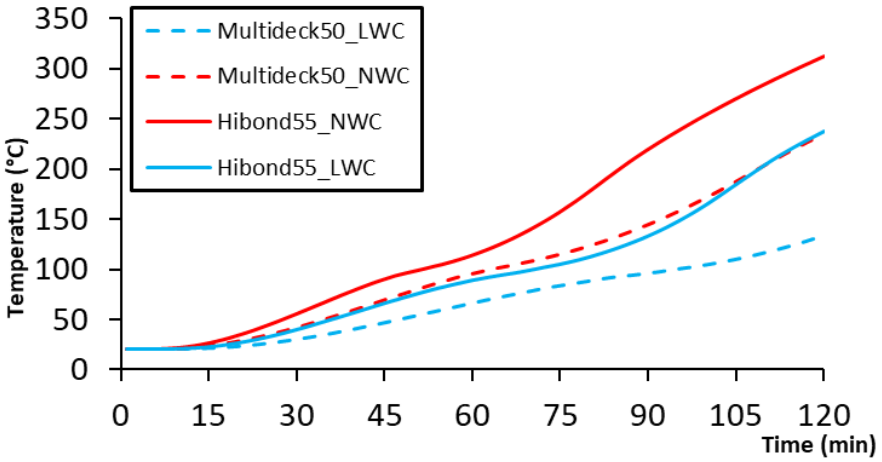

Figure 6.9: Comparison of the unexposed side temperature evolution for both slabs.

Referring to the results presented in table 6.3, it can be seen the percentage of temperature increase is in Hibond55 section is two times more than of the Multideck50 section for LWC. However, this increase is about one time and half for the corresponding NWC. The maximum temperature reached by the composite slabs is 312.61 °C, which is recorded for the hibond55 slab made with NWC. This high temperature corresponds to a percentage of temperature increase equal to more than 14 times the initial value.

Figure 6.10 represents the resisting moment of both slabs in function of fire exposure time. The loss of the load bearing capacity is 10.48 $kN.m$ and 9.86 $kN.m$ at R15 and R120 respectively for the NWC, however the loss for LWC is 7.94 $kN.m$ and 7.56 $kN.m$ at R15 and R120 respectively. During all the fire exposure time, the loss in the Multideck50 is higher than that of the Hibond55.The resisting moment for both sections exceeds the value of the soliciting moment. This difference can be attributed to the presence of the amount of concrete in each section. Also, LWC does not heat as NWC for the two different sections.

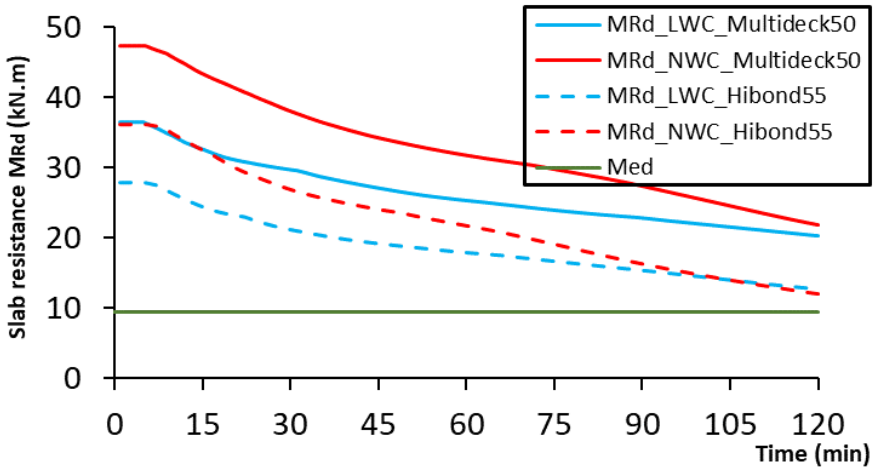

Figure 6.10: Comparison of the load bearing capacity evolution for both slabs.

According to the results presented in the table 6.5, it is useful to notice that the Hibond55 section made with NWC loses 67% of its initial resisting moment value, which leaves only a third of its resisting moment value (residual moment).

Figure 6.11 illustrates the deflection of both slabs made with both concrete in function of fire exposure time. It can be seen that the difference in the deflection between the two sections increases with the increase of the fire exposure time. This difference is equal to 0.81 mm and 3.99 mm at R15 and R120 respectively for NWC and for LWC, it is 1.6 mm and 4.5 mm at R15 and R120 respectively. These results can be explained by the geometry of the two sections, the Hibond55 (trapezoidal) promotes the deflection more than the Multideck50 (re-entrant).

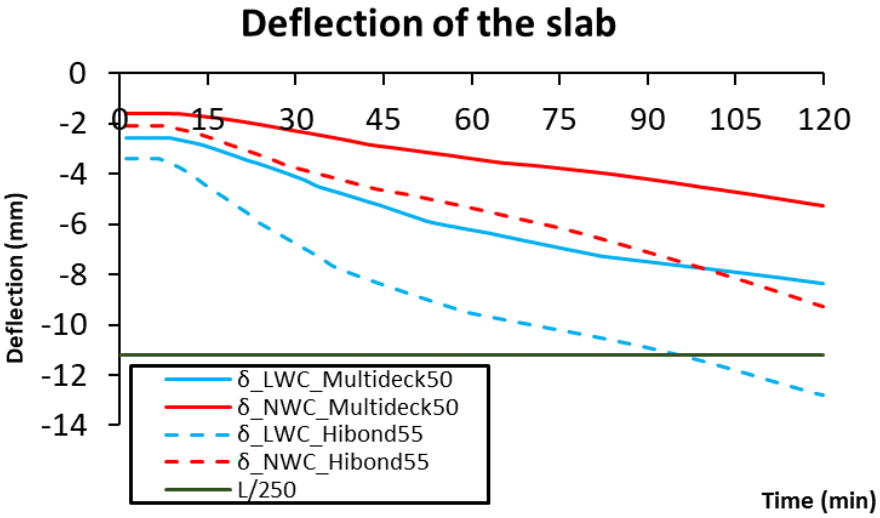

Figure 6.11: Comparison of the deflection evolution for both slabs

From the results of Table 6.6, it can be seen that the deflection increases in the Hibond55 section made with NWC is three times more than its initial deflection at R120, the corresponding percentage is only two times in the Multideck section.

6.3. Effect of the steel deck thickness

This section investigates the effect of steel deck thickness on the composite slab behaviour taking into account the steel deck thickness (SDT) as a variable and the other parameters are constant notably, the anti-crack mesh (6 mm), the reinforcement rebars(10 mm), the height of the section (130 mm) for both slab sections and the rebar cover distance is equal to h_2. firstly, only LWC was used as a fill material.

6.3.1. Unexposed Side temperature evolution

The average temperature evolution for both slabs sections for the different steel deck thicknesses plotted as a function of the temperature for several fire rates R15, R30, R45, R60, R90 and R120, are represented in horizontal bars (the green bar represents the SDT 1.00 mm results, the blue bar represents the 0.85 mm results and the red represents the SDT 1.20 mm) in Figure 6.12. It is shown that there is no effect or minor offset between the bars for the three SDT at all the fire rates for both slabs sections. Based on this observation, it can be concluded that the effect of the steel deck can be ignored for this parameter (temperature evolution) on the unexposed side of the slabs. This result is attributed to the high conductivity of the steel profile. Moreover, the limitation of the insulation criterion established in EC4 [11, p. 4] is not respected for the Hibond55 section at R120 because it exceeds the temperature 160 °C (average temperature). However, for the Multideck section, the temperature did not reach the limitation. For safety reasons, it is recommended to increase the concrete thickness.

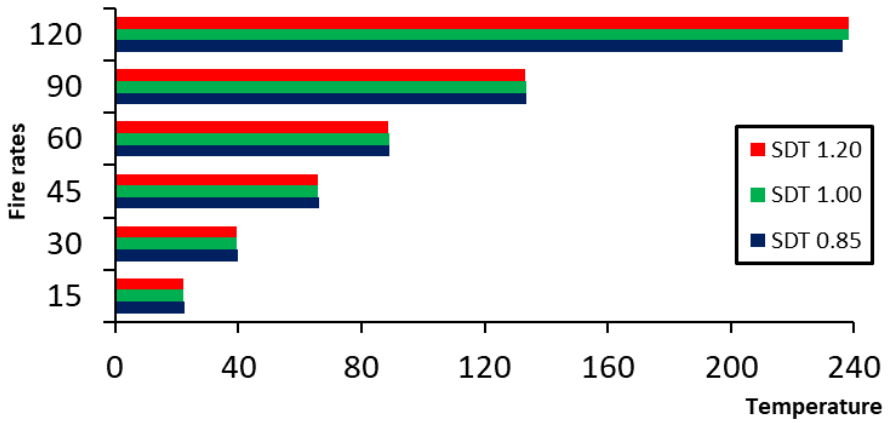

(a) Hibond55.

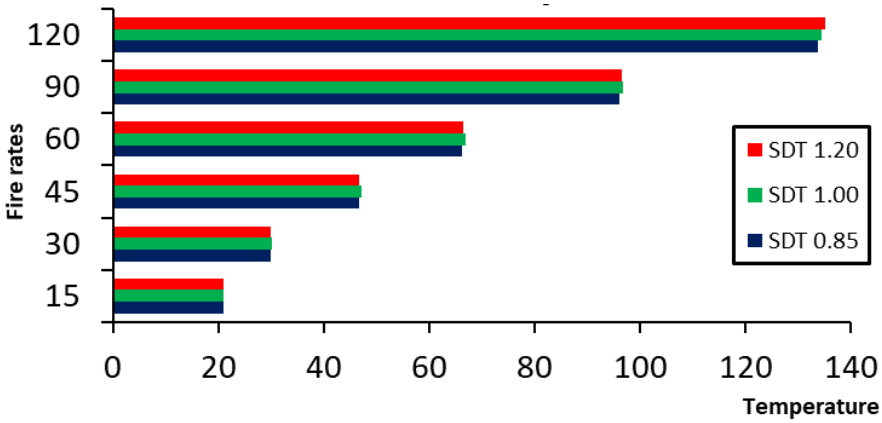

(b) Multideck50.

Figure 6.12: Unexposed Side temperature evolution for both slabs.

Table 6.8 regroups the results of the percentage of the temperature increase for both slabs with the different steel deck thickness. After one hour and a half of fire exposure, the Hibond55 slab heats up to five times and half regarding to its initial temperature value. However, varying the fire rate from R90 to R120, the slab temperature becomes double. It is important to mention also that the Hibond55 slab for all the SDT heats up two times more than the Multideck50 slab for the corresponding's SDT. The maximum temperature registered were 238.13 °C and 135.10 for the Hibond55 and the Multideck50 respectively.

Table 6.8: Rate of the impact of the SDT on the unexposed side temperature.

Resistance time	Multideck50						Hibond55					
	SDT 0.85	% Temp increase	*SDT 1.00*	% Temp increase	*SDT 1.20*	% Temp increase	*SDT 0.85*	% Temp increase	*SDT 1.00*	% Temp increase	*SDT 1.20*	% Temp increase
1	20.00	0%	20.00	0%	20.00	0%	20.00	0%	20.00	0%	20.00	0%
15	21.03	5%	21.01	5%	21.00	5%	22.38	12%	22.35	12%	22.27	11%
30	29.88	49%	30.23	51%	29.83	49%	39.72	99%	39.57	98%	39.37	97%
45	46.59	133%	47.19	136%	46.69	133%	66.19	231%	65.99	230%	65.79	229%
60	66.18	231%	66.91	235%	66.47	232%	89.07	345%	89.00	345%	88.87	344%
90	96.17	381%	96.66	383%	96.50	382%	133.56	568%	133.43	567%	133.29	566%
120	133.77	569%	134.47	572%	135.10	575%	236.32	1082%	238.10	1091%	238.13	1091%

6.3.2. Temperature of the rebar

Figure 6.13 represents the influence of the Steel deck thickness on the temperature of the rebar for both Hibond55 and multideck50 slabs, represented in horizontal bars keeping the same legend. It is shown that there is also no difference or small difference between the bars for the three SDT. So, it can be concluded that the SDT has no effect on the temperature of the rebars. It is noticeable that the maximum temperature measured was 614.32 °C and 503.90 °C for the Hibond55 and the Multideck50 respectively. It is useful to indicate that in the vicinity of these temperatures, the reduction factor of

the rebars reaches a critical low value. In this case, the presence of the rebars have no effect on the load bearing capacity.

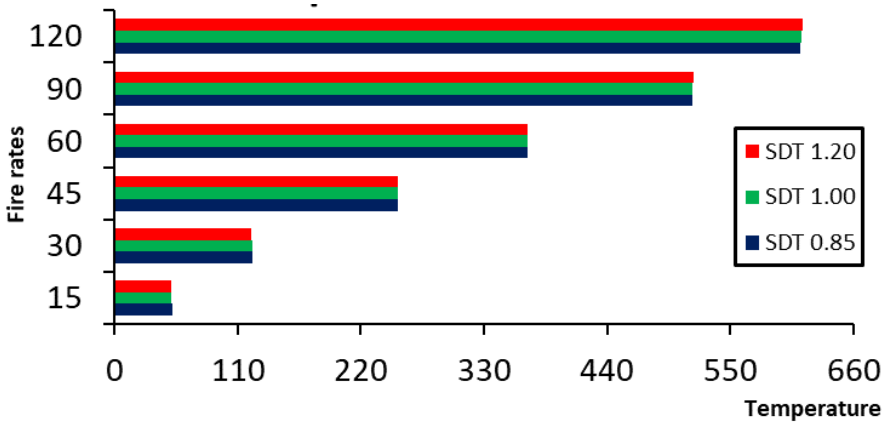

(a) Hibond55.

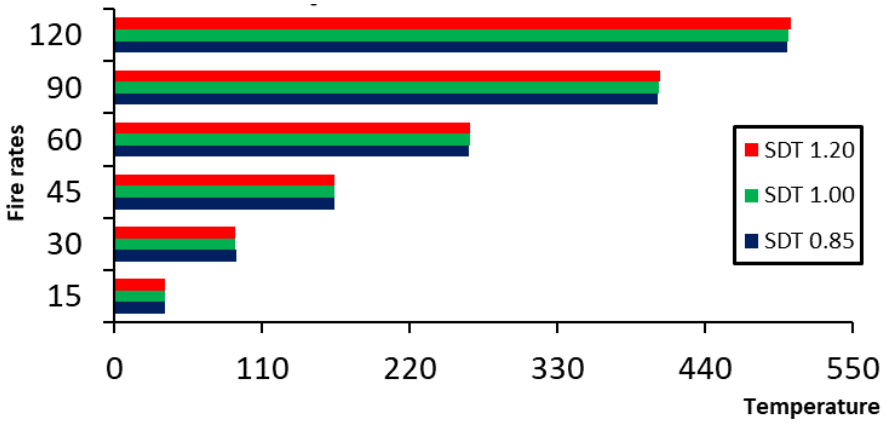

(b) Multideck50.

Figure 6.13: Rebars Temperature evolution for both slabs.

Table 6.9: Rate of the impact of the SDT on the rebars temperature.

Resistance time	Multideck50						Hibond55					
	SDT 0.85	% Temp increase	*SDT 1.00*	% Temp increase	*SDT 1.20*	% Temp increase	*SDT 0.85*	% Temp increase	*SDT 1.00*	% Temp increase	*SDT 1.20*	% Temp increase
1	20.00	0%	20.00	0%	20.00	0%	20.00	0%	20.00	0%	20.00	0%
15	37.85	89%	37.62	88%	37.60	88%	51.32	157%	51.10	156%	50.79	154%
30	90.55	353%	90.42	352%	90.38	352%	123.63	518%	123.23	516%	122.64	513%
45	164.09	720%	164.24	721%	164.40	722%	253.23	1166%	253.01	1165%	252.69	1163%
60	263.93	1220%	264.64	1223%	265.38	1227%	368.96	1745%	369.09	1745%	369.22	1746%
90	404.52	1923%	405.64	1928%	406.92	1935%	515.85	2479%	516.30	2481%	516.87	2484%
120	501.04	2405%	502.34	2412%	503.90	2419%	613.06	2965%	613.60	2968%	614.32	2972%

6.3.3. SDT temperature evolution

Figure 6.14 illustrates the influence of the thickness of the steel deck on the temperature evolution of the steel deck for both Hibond55 and multideck50 slabs, represented in horizontal bars with keeping the same legend. It is shown that there is a slight offset between the bars for the three SDT for the trapezoidal slab at low fire rates. For the Multideck50 slab, there isn't an influence between the different SDT. So, it can be concluded that the effect of the SDT is limited on its own temperature due to the small change on the steel deck thickness (variation of 0.15 mm and 0.2 mm). According to the table 6.10 At low fire rates (R15), the temperature in the steel deck reaches 596.61 °C and 515.47° C for Hibond55 and Multideck50 respectively for the thickness of 1.20 mm. it is observed that the temperature increase is almost linearly proportional to the fire rates in the steel deck.

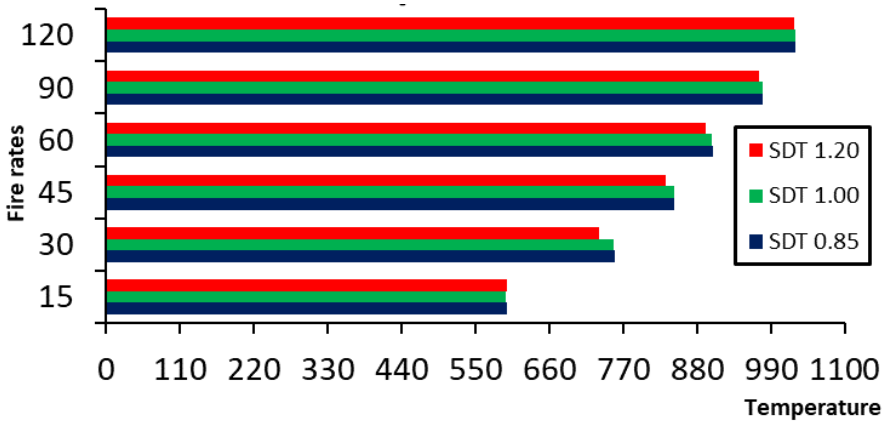

(a) Hibond55.

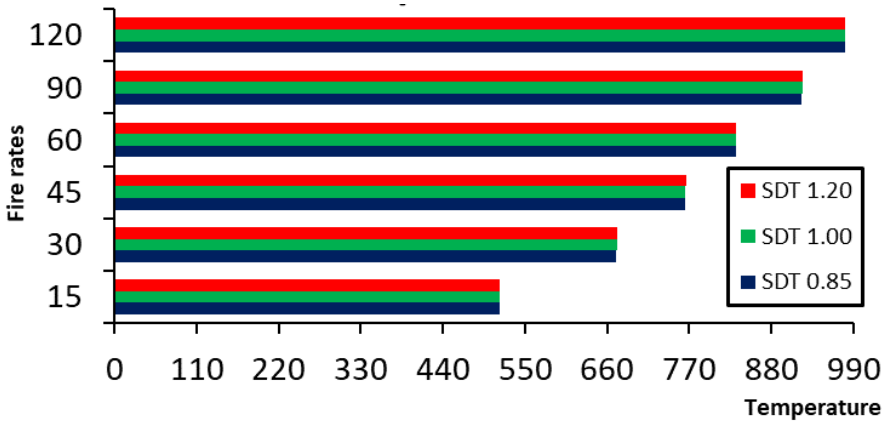

(b) Multideck50.

Figure 6.14: Steel deck Temperature evolution for both slabs.

Table 6.10: Rate of the impact of the SDT on the Its own temperature.

	Multideck50	Hibond55

Resistance time	*SDT 0.85*	% Temp increase	*SDT 1.00*	% Temp increase	*SDT 1.20*	% Temp increase	*SDT 0.85*	% Temp increase	*SDT 1.00*	% Temp increase	*SDT 1.20*	% Temp increase
1	110.47	0%	104.82	0%	98.31	0%	120.81	0%	114.40	0%	107.01	0%
15	516.06	367%	515.81	392%	515.47	424%	596.94	394%	594.65	420%	596.61	458%
30	672.55	509%	673.14	542%	673.76	585%	757.71	527%	756.54	561%	734.75	587%
45	764.72	592%	765.25	630%	765.91	679%	846.37	601%	845.89	639%	832.49	678%
60	832.08	653%	832.15	694%	832.25	747%	902.93	647%	902.66	689%	893.75	735%
90	921.23	734%	921.83	779%	922.65	839%	977.12	709%	976.97	754%	971.50	808%
120	978.13	785%	978.64	834%	979.51	896%	1026.5	750%	1026.2	797%	1024.2	857%

6.3.4. Load bearing capacity

The resisting moment of the two slabs in function of fire exposure time for the different SDT is plotted in figure 6.15. The resisting moment of the slabs made with SDT 0.85 is plotted in red colour for SDT1.00 is plotted by blue colour and lastly the yellow represents the SDT1.20. the graphs are falling, which means that the slabs are losing their own load bearing capacities. Despite this decrease, the Mrd of the slab with the three SDT is still higher than the Med during all the fire exposure time. It is thought that the mechanical performances of the different slabs are not strongly influenced with varying the thickness of the steel deck. According to Figure6.15, Mrd of SDT1.20 for the Hibond50 sections is higher than SDT1.00 and SDT0.85.

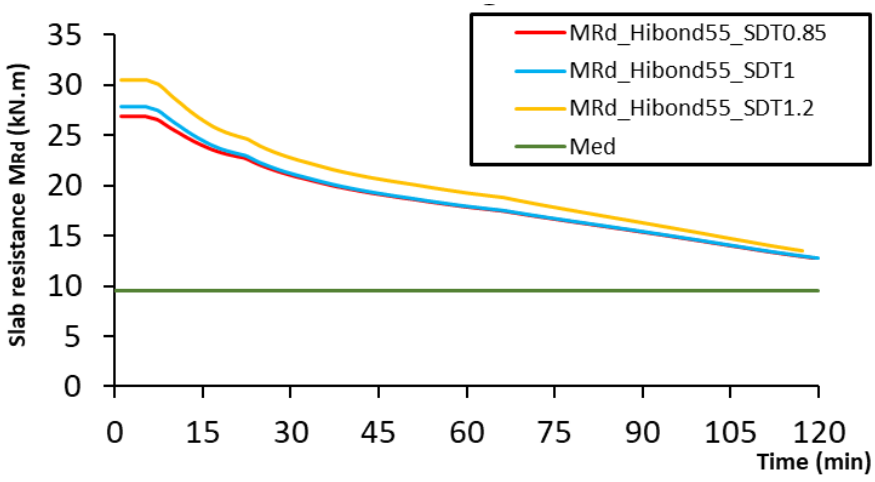

(a) Hibond55.

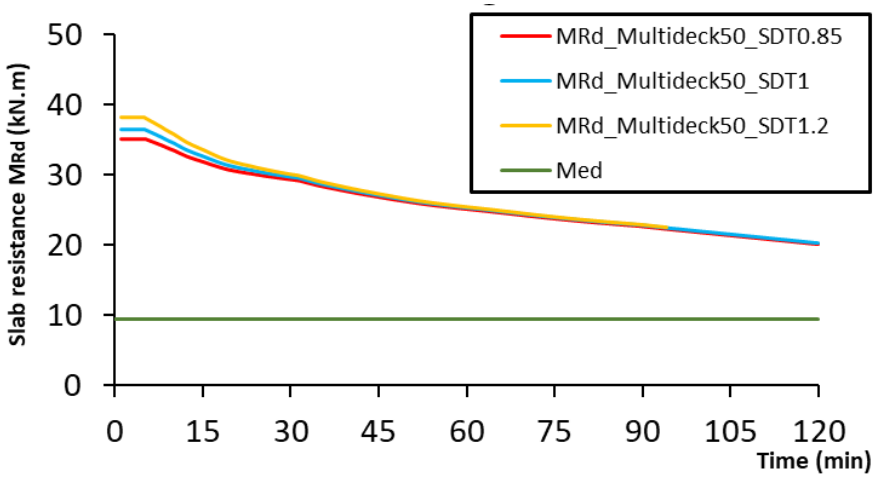

(b) Multideck50.

Figure 6.15: Load bearing evolution for both slabs.

It is recorded in Table 6.11 the results of the percentage of the moment loss in the two slabs. Up to one hour of fire, the percentage of moment loss is about 30% for both slabs with the different SDT. Beyond this fire rate, this percentage becomes more important. After two hours, the resisting moment loses approximately half of its initial value for all the sections with the different SDT. It is important also to mention that the Hibond55 section with all the SDT loses more load bearing capacity compared with those of the corresponding Multideck50. As a conclusion, the variation of the SDT has a small influence on the moment loss.

Table 6.11: Rate of the impact of the SDT on the load bearing capacity.

Resistance time	Multideck50						Hibond55					
	SDT 1.20	% MRd loss	*SDT 1.00*	% MRd loss	*SDT 0.85*	% MRd loss	*SDT 1.20*	% MRd loss	*SDT 1.00*	% MRd loss	*SDT 0.85*	% MRd loss
1	38.24	0%	36.49	0%	35.17	0%	30.54	0%	27.92	0%	26.92	0%
15	33.62	12%	32.65	11%	31.93	9%	26.50	11%	24.50	12%	23.98	13%
30	30.13	21%	29.72	19%	29.42	16%	22.77	22%	21.23	24%	21.04	25%
45	27.37	28%	27.13	26%	26.94	23%	20.67	29%	19.24	31%	19.15	32%
60	25.50	33%	25.35	31%	25.22	28%	19.29	34%	17.95	36%	17.89	37%
90	22.98	40%	22.86	37%	22.76	35%	16.31	43%	15.43	45%	15.38	47%
120	20.43	47%	20.32	44%	20.23	42%	13.43	53%	12.77	54%	12.74	56%

6.3.5. Deflection of the slab

Figure 6.16 illustrates the deflection of the slabs in function of the fire exposure time with keeping the same colour legend. The graphs are downhill which means the deflection of the slabs are increasing with the increase of the fire exposure time. As it is shown the deflection for SDT1.20 for

both sections is less than SDT1.00 and SDT0.85 respectively, so it is concluded that increasing the steel deck thickness leads to improving the deflection of the slab. Besides that the Hibond55 slab at around 90 min reaches the limited value L/250, regarding the Multideck50 over 120 min the slab didn't reach the limitation. It can be deduced that the Multideck50 section provide a better deflection.

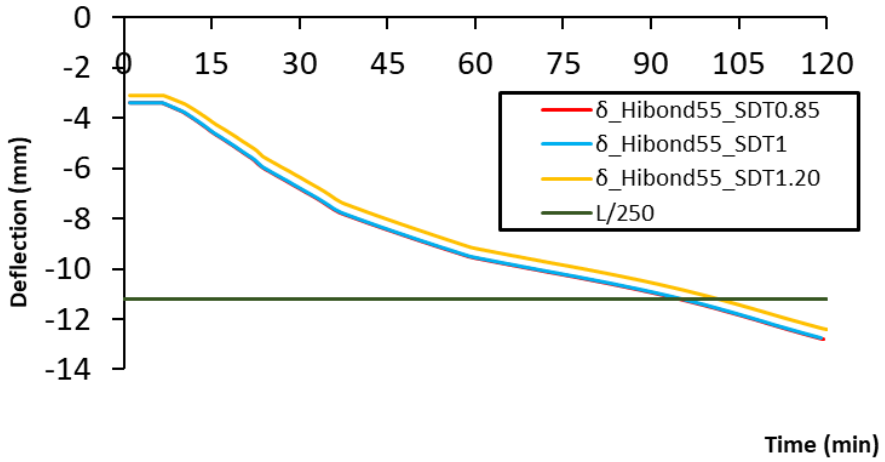

(a) Hibond55.

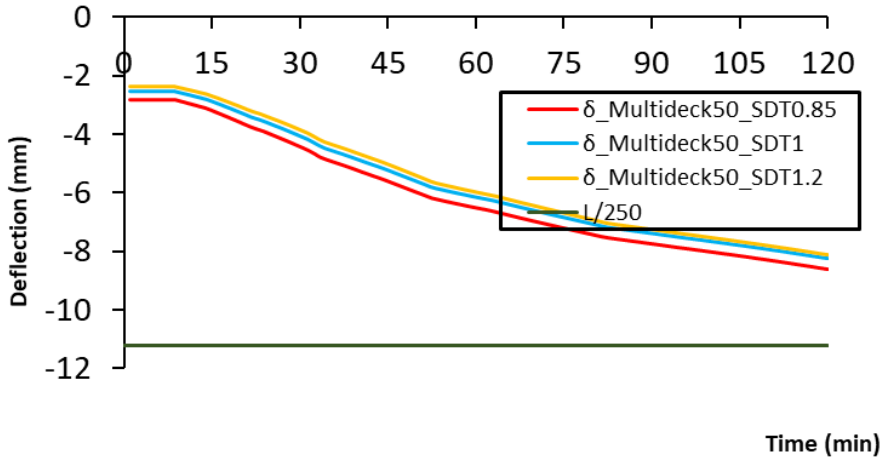

(b) Multideck50.

Figure 6.16: Deflection evolution for both slabs.

Table 6.12: Rate of the impact of the SDT on the deflection of the slab.

Resistance time	Multideck50						Hibond55					
	SDT 0.85	% δ increase	SDT 1.00	% δ increase	SDT 1.20	% δ increase	SDT 0.85	% δ increase	SDT 1.00	% δ increase	SDT 1.20	% δ increase
1	2.81	0%	2.54	0%	2.38	0%	3.34	0%	3.34	0%	3.08	0%
15	3.18	13%	2.89	14%	2.71	14%	4.49	34%	4.47	34%	4.12	34%
30	4.42	57%	4.07	60%	3.85	62%	6.72	101%	6.70	101%	6.30	104%
45	5.61	100%	5.24	106%	5.03	111%	8.34	149%	8.33	149%	7.96	158%
60	6.52	132%	6.16	142%	5.97	151%	9.45	183%	9.44	182%	9.10	195%
90	7.75	176%	7.39	191%	7.24	204%	10.79	223%	10.79	223%	10.44	239%

120	8.62	207%	8.25	224%	8.10	241%	12.66	279%	12.66	279%	12.18	295%

The results of the percentage of the deflection loss for the two sections with the different SDT are gathered in Table 12. According to the values indicated in the table, the deterioration becomes too strong after 15 min of fire for all the sections. The maximum increase in deflection recorded here is 295% for the Hibond55 section made with SDR1.2, the corresponding section in Multideck50 indicates an increase of deflection of 241%. It is concluded that the percentage and the deterioration in the hibond55 is higher than that of the multideck (12.18 mm against 8.1 mm).

6.4. Effect of the rebar size

In this section the rebar size effect on the behaviour of the slab is studied. For this section parameters of the slab are constant as follows: the anti-crack mesh size is 6 mm, the height of the section is 130 mm for both slabs lastly the thickness of the steel deck was constant at 1 mm. and the only parameter which is variable is the reinforcement rebars size from 10 mm to 14 mm with an increment of 2 mm.

6.4.1. Unexposed Side temperature evolution

Figure 6.17a and 6.17b represents the influence of the rebar size on the evolution of the temperature of the unexposed side. The data is plotted on horizontal bars the vertical axis represents the fire rates and the horizontal axis represents the temperature reached at each fire rates for three different rebar sizes (red for Ø14 mm, the green for Ø12 mm and Ø10 mm with blue). As it can be seen in these two figures there is no offset between the bars for the same fire rates with the exception for the fire rate 120 min where a small offset can be noticeable. Based on this interpretation it can be concluded that the rebar size had no important effect on the temperature of the exposed side of the slab. Furthermore, the temperature in the Hibond55 slabs at the R120 is bigger by Approximately 100°C.

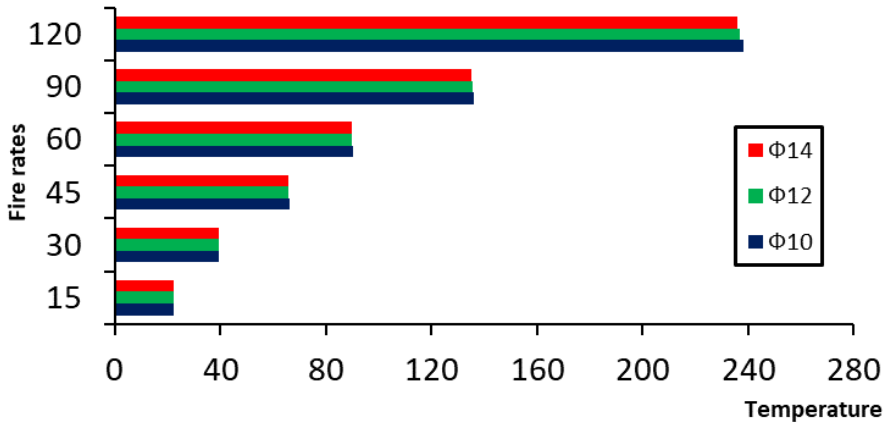

(a) Hibond55.

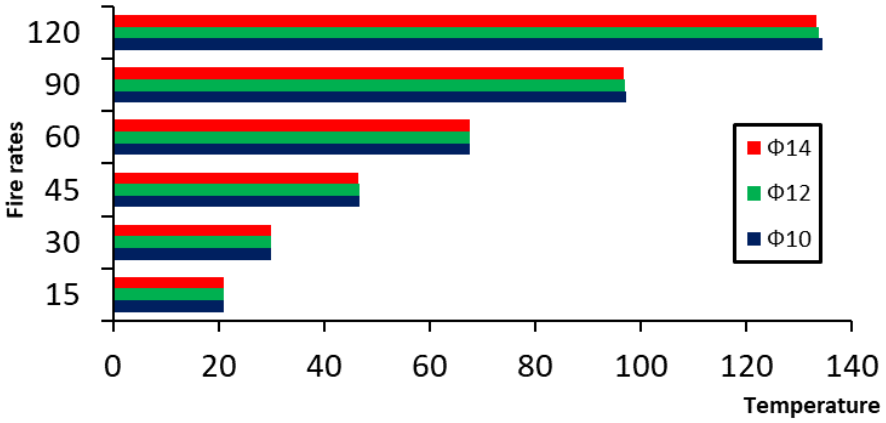

(b) Multideck50.

Figure 6.17: Unexposed Side temperature evolution for both slabs.

6.4.2. Temperature of the rebar

The influence of the rebars size on the evolution of their own temperature is plotted on figure 6.18a and 6.18b. When keeping the same legend and the same axis labels, as it can be seen, there is an offset between the three bars for all the fire rates and slabs. So, it can be concluded that the rebar size has a direct effect on its temperature. Diving into details for a fire rate of R30 the temperature is 123.23 min, 117,23 and 112.04 for Ø10 mm, Ø12 mm and Ø14 mm respectively for the Hibond55 slab. So, using a bigger rebars can reduce its temperature by 5.46°C (Ø10 mm to Ø12 mm) and by 11.20 °C (Ø10 mm to Ø14 mm) and for the multideck50 at R120 the temperature is 502.34 min, 493.11 and 482.51 for Ø10 mm, Ø12 mm and Ø14 mm respectively, for the higher fire rates it is logical to have grater temperature and to be notice that the effect of the rebar is higher also a reduce of 9.22 °C was measured while increasing the rebar size from Ø10 mm to Ø12 mm and a reduce of 19.82 °C was measured while increasing the rebar size from Ø10 mm to Ø14 mm. regarding the effect of changing of the rebar size, the slabs made Hibond55 at R120 exceeds 550 °C in which this temperature wasn't reached for the Multideck50.

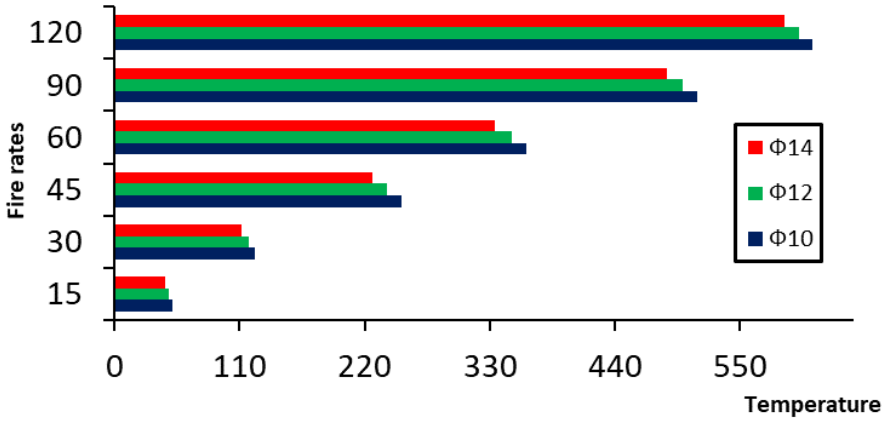

(a) Hibond55.

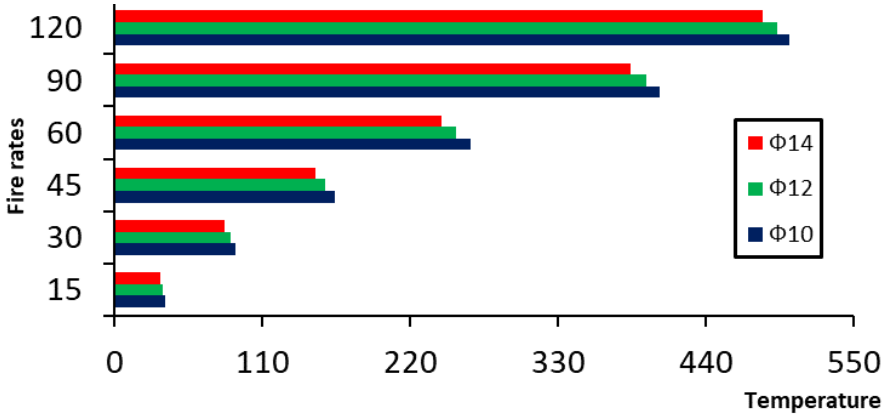

(b) Multideck50.

Figure 6.18: Rebars Temperature evolution for both slabs.

6.4.3. Load bearing capacity

Figure 6.19 plots the resisting moments of the two slabs for the various rebars sizes as a function of the fire exposure time. Plotting the resisting moment of slabs made with Ø10 mm is done in red, Ø12 mm is done in blue, and Ø14 mm is done in yellow. The graphs downward trend indicates that the slabs own load-bearing capacities are diminishing. Also, the gap between the curves for the Hibond55 is bigger than the curves of the Multideck50 illustrating that the effect of the rebar size is more pronounced in the Hibond55 than the Multideck50. Even with this reduction, the slab with the three different rebar sizes Mrd remains higher than the Med for the duration of the fire exposure.

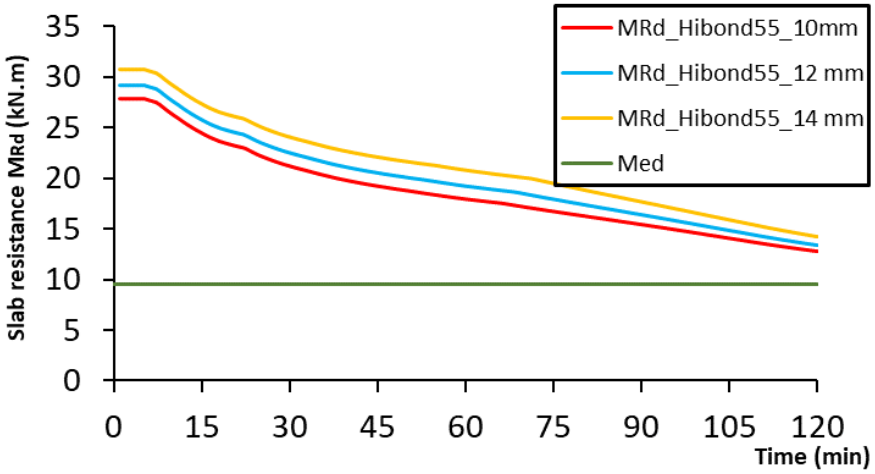

(a) Hibond55

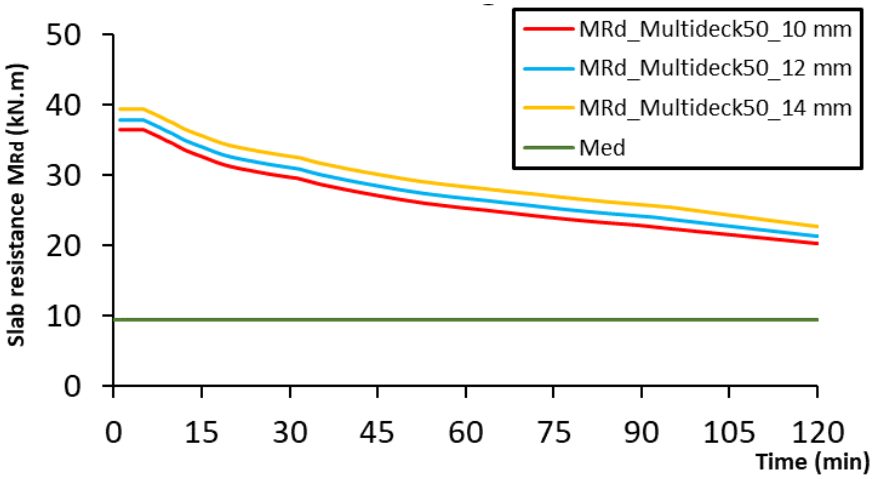

(b) Multideck50

Figure 6.19: Load bearing evolution for both slabs.

From the table 6.13, the slabs made with larger rebar sizes (Ø14 mm) maintain higher resisting moments for a longer duration compared to slabs with smaller rebar sizes (Ø10 mm). in terms of numbers at R60 for the Hibond55 slab made with the Ø10 lost approximately 36% of it load bearing capacity which is higher by 4% than the one made with Ø14 (32%). This indicates that larger rebars provide a better structural integrity and resistance to fire-induced degradation. Also, The rate of load-bearing loss is more pronounced in slabs with smaller rebars, suggesting that they lose their load-bearing capacity more quickly under fire conditions. Also, it is useful to mention that for all the fire rates the Hibond55 losses more load bearing capacity, the maximum value registered was 54% when it was made with 10Ø rebar equivalent to 44% for the Multideck made with the same rebar size.

Table 6.13: Rate of the impact of the rebars size on the load bearing capacity.

Resistance time	Multideck50						Hibond55					
	Ø10	% MRd loss	Ø12	% MRd loss	Ø14	% MRd loss	Ø10	% MRd loss	Ø12	% MRd loss	Ø14	% MRd loss

1	36.49	0%	37.87	0%	39.50	0%	27.92	0%	29.21	0%	30.74	0%
15	32.65	-11%	34.03	-10%	35.67	-10%	24.50	-12%	25.79	-12%	27.32	-11%
30	29.72	-19%	31.11	-18%	32.74	-17%	21.23	-24%	22.52	-23%	24.06	-22%
45	27.13	-26%	28.51	-25%	30.15	-24%	19.24	-31%	20.54	-30%	22.08	-28%
60	25.35	-31%	26.73	-29%	28.37	-28%	17.95	-36%	19.24	-34%	20.78	-32%
90	22.86	-37%	24.21	-36%	25.80	-35%	15.43	-45%	16.40	-44%	17.65	-43%
120	20.32	-44%	21.37	-44%	22.69	-43%	12.77	-54%	13.39	-54%	14.21	-54%

6.4.4. Deflection of the slab

Figure 6.20 shows the deflection of the slabs as a function of the fire exposure time, with the same colour legend. The graphs are downhill, indicating that the deflection of the slabs increases with increasing fire exposure duration.

As it is shown the graphs of the deflection for the three rebars sizes are much close to each other with a very small offset for both slabs, so it is concluded that increasing the reinforcing rebar size leads to a small improvement. Besides that, the Hibond55 slab at around 100 min reaches the limited value L/250, regarding the Multideck50 over 120 min the slab didn't reach the limitation. It can be deduced that the Multideck50 section provide a better deflection.

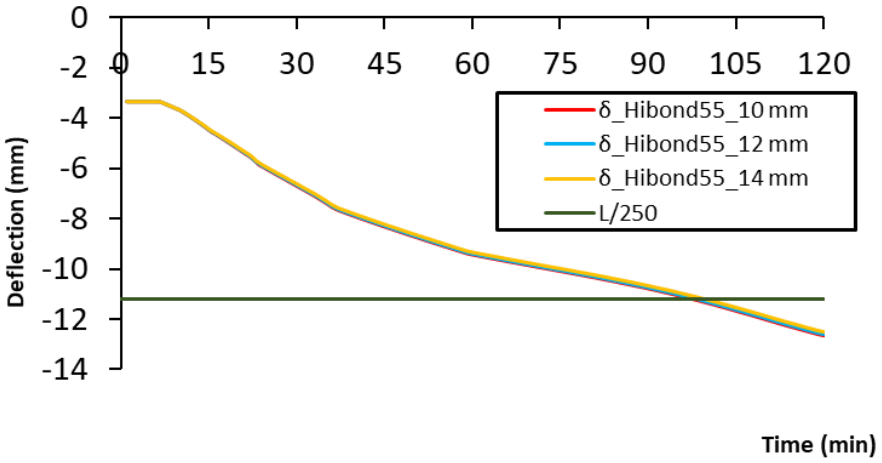

(a) Hibond55.

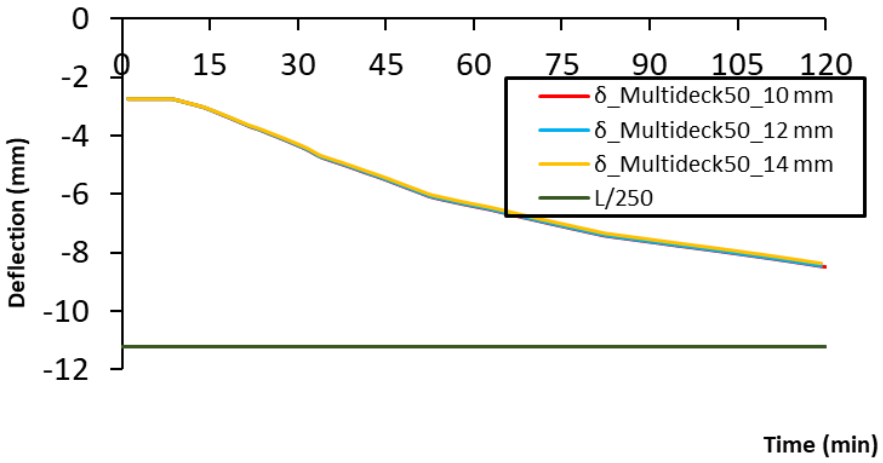

(b) Multideck50.

Figure 6.20: Deflection evolution for both slabs.

Table 6.14: Rate of the impact of the rebars size on the deflection of the slab.

Resistance time	Multideck50						Hibond55					
	SDT 0.85	% δ increase	*SDT 1.00*	% δ increase	*SDT 1.20*	% δ increase	*SDT 0.85*	% δ increase	*SDT 1.00*	% δ increase	*SDT 1.20*	% δ increase
1	-2.75	0%	-2.74	0%	-2.73	0%	-3.34	0%	-3.33	0%	-3.32	0%
15	-3.12	14%	-3.11	13%	-3.09	13%	-4.47	34%	-4.45	33%	-4.42	33%
30	-4.35	58%	-4.32	58%	-4.29	57%	-6.70	101%	-6.65	100%	-6.60	99%
45	-5.52	101%	-5.48	100%	-5.45	99%	-8.33	149%	-8.28	148%	-8.22	148%
60	-6.42	134%	-6.39	133%	-6.35	132%	-9.44	182%	-9.39	182%	-9.33	181%
90	-7.64	178%	-7.60	177%	-7.56	177%	-10.79	223%	-10.73	222%	-10.67	221%
120	-8.49	209%	-8.45	208%	-8.40	208%	-12.66	279%	-12.59	278%	-12.51	277%

Table 6.14 presents the results of the percentage of the deflection loss for the two sections with the different rebar sizes. According to the values in the table, the deterioration becomes too strong after 30 min of fire for all the sections. For the Multideck50 section, the deflection doubled compared to the initial value after 45 min of fire exposure, but for the Hibond55, it doubled around 30 min only. The maximum increase in deflection recorded here is 279% for the Hibond55 section made with 10Ø, the corresponding section in Multideck50 indicates an increase in deflection of 209%. It is concluded that the percentage and the deterioration in the hibond55 is higher than that of the multideck (12.66 mm against 8.49 mm).

6.5. Effect of the rebar position in the rib

This section investigates the effect of the rebar positions otherwise the thickness of the rebar cover on the overall behaviour if the slab. The parameters of the slab are constant as follows: the anticrack

mesh size is 6 mm, the reinforcement rebars is 10 mm, the height of the section is 130 mm for both slabs lastly the thickness of the steel deck is constant at 1 mm the only parameter which is changing is the rebar cover distance from h_2 to $2/3h_2$ and $1/3h_2$.

It is to be notice that the rebars for the three cases is located on the traction side of the cross section and the distances given are measured from the bottom of the slab.

6.5.1. Unexposed Side temperature evolution

The average temperature evolution for both slabs for the different rebar position is plotted as a function of the temperature for a fire rates R15, R30, R45, R60, R90 and R120 are represented in horizontal bars (the blue, green and red bars represent the results of h_2; $\frac{2}{3}$ h_2 ; $\frac{1}{3}$ h_2 respectively In the Figure 6.21. It is shown that there is no offset between the bars. It can be concluded that the effect of the steel deck can be ignored for the temperature evolution on the unexposed side of both slabs Hibond55 and the multideck50.

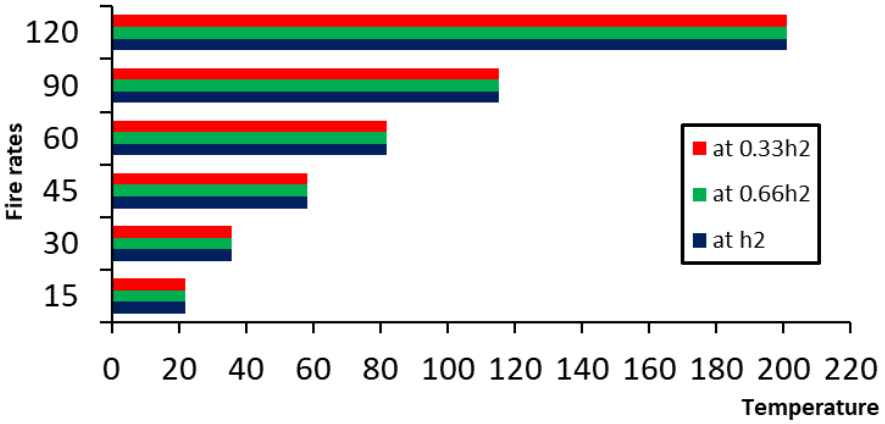

(a) Hibond55.

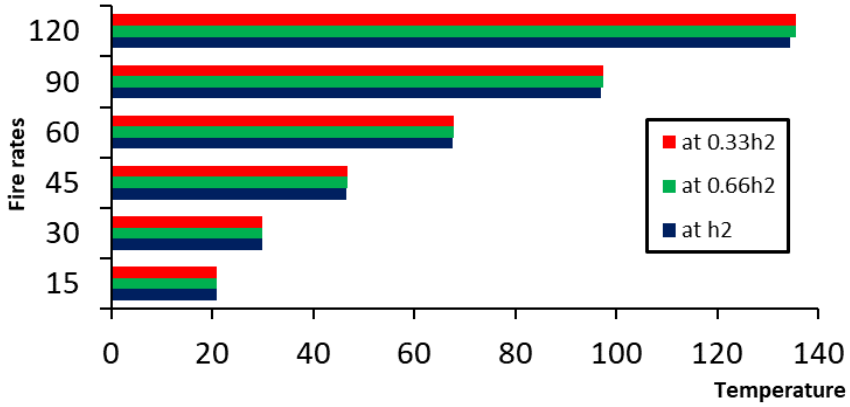

(b) Multideck50.

Figure 6.21: Unexposed Side temperature evolution for both slabs.

6.5.2. Temperature of the rebar

Figure 6.22 shows the influence of the rebar position on the temperature of the rebar for both trapezoidal and re-entrant slabs, represented in horizontal grading the same legend and labels. It is shown that there is a large offset between the bars for the three positions, which represents the difference of the temperature. this difference is greater for high fire rates. The results and the differences are illustrated on the figure and tables bellow So, it can be concluded that the position of the rebar has a large effect on its own temperature.

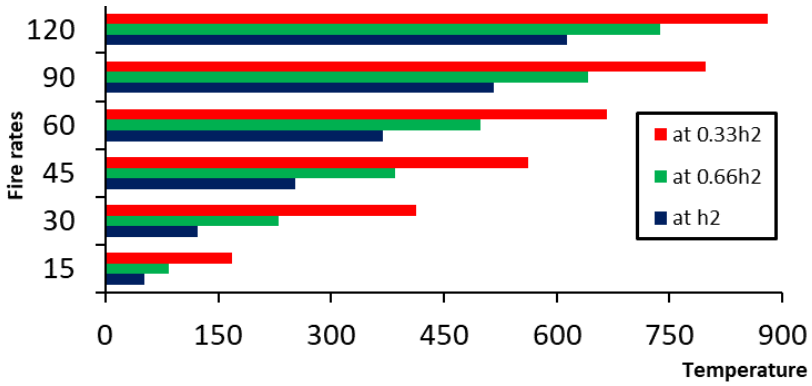

(a) Hibond55.

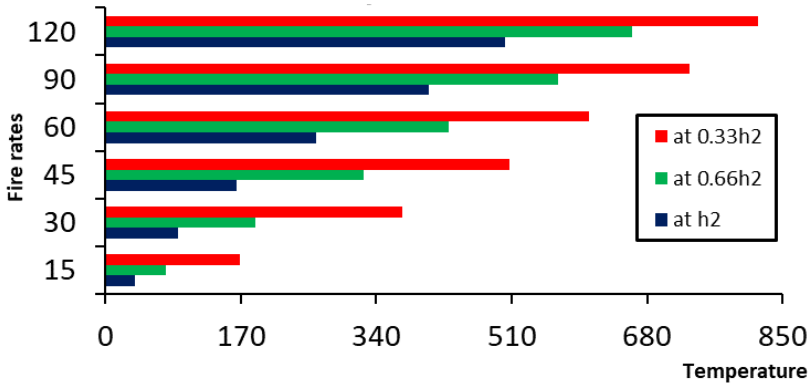

(b) Multideck50.

Figure 6.22: Rebars Temperature evolution for both slabs.

The table 6.15 presents fire resistance results for the two types of slabs Hibond55 and Multideck50. It compares rebar sizes temperature at different depths h2, 2/3h2, and 1/3h2 and evaluates the impact of changes in depth on fire resistance. Through a general observation we might say increasing the fire rate (time) results in a higher temperature values, and the temperature at the Hibond55 slabs raises more than the Multideck50, at the h2 position at R30 the temperature was 123.23°C for the Hibond55 versus 90.42°C for the Multideck50 a deference of 32.81°C equivalent for an raise of 36.28%, doing the same calculation at R120 the temperatures were as follow 613.60°C and 502.34°C for the Hibond55 and the Multideck50 respectively, a raise of 111.26°C was measured and which is

equivalent to 22.14%. It can be concluded that the rate of the raise is decreasing with the increase of the fire exposure time.

On another side, when placing the rebars at lower depths leads to a significant impact and the rebars heats more, at a given fire rates R60 the temperatures were 369.09°C, 498.64 °C and 666.48 °C respectively to h2 2/3h2 and 1/3 of h2. The maximum impact was measured in the Multideck50 at R30 a deference of 343.61 °C a raise similar to 3 times….. according to these results we can conclude that the differences in impact between heights indicate that the lower sections of the structure (closer to the base) may experience more stress or deformation compared to the upper sections.

Table 6.15: Rate of the impact of the rebars position on its own temperature.

Hibond55 results						
Fire rates	Rebar size			Difference of the impact		
	at h2	at 0.66h2	at 0.33h2	h2 to 0.66h2	0.66h2 to 0.33h2	h2 to 0.33h2
15	51.10	84.49	168.01	33.39	83.52	116.91
30	123.23	230.11	413.03	106.88	182.92	289.80
45	253.01	384.97	561.91	131.96	176.94	308.90
60	369.09	498.64	666.48	129.55	167.84	297.39
90	516.30	641.91	797.41	125.61	155.50	281.11
120	613.60	737.04	881.08	123.44	144.04	267.48
Multideck50 results						
Fire rates	Rebar size			Difference of the impact		
	at h_2	at 0.66h_2	at 0.33h_2	h_2 to 0.66h_2	0.66h_2 to 0.33h_2	h_2 to 0.33h_2
15	37.62	76.06	168.40	38.44	92.34	130.79
30	90.42	188.05	372.30	97.64	184.24	281.88
45	164.24	324.65	507.84	160.41	183.19	343.61
60	264.64	431.31	606.64	166.67	175.33	341.99
90	405.64	568.50	732.83	162.87	164.32	327.19
120	502.34	661.38	819.07	159.05	157.69	316.74

6.5.3. Load bearing loss

Figure 6.23 illustrate the load bearing capacity of the slabs (Hibond55 and multideck50) across the time. The curves are downhill suggesting that the slabs are losing their own load bearing capacities. For the Hibond55 the resisting moment of the 1/3position is higher than the other position which is

logical because of the distance between the natural axis of rebar and neutral plastic axis of the rib "z_i". But at approximately 50min the curve of the h2 position become on top of the 1/3h2 and 2/3h2 indicating that at high fire rates when the rebars are placed at lower depth losses their mechanical characteristics quickly and their contribution at the overall resistance of the slabs stopes. Beside the Hibond55 the Multideck50 show a similar result, but around 65min the curves of h2cross the 2/3h2 and it didn't cross the 1/3h2 even after 120min it can be concluded that the shape of the slabs also plays a role on protecting the rebars in low placement in the rib curve. As a conclusion the cover distance and the shape of the slab has a significant impact on the protection of the rebars on the long terms.

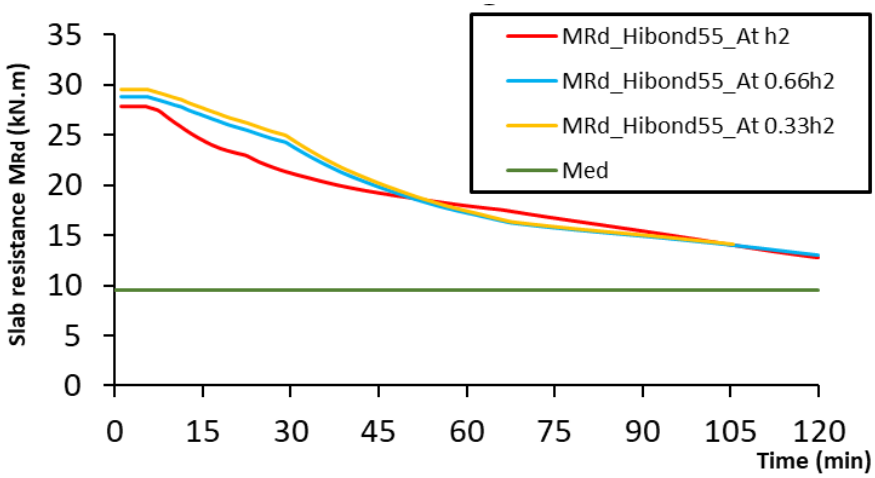

(a) Hibond55.

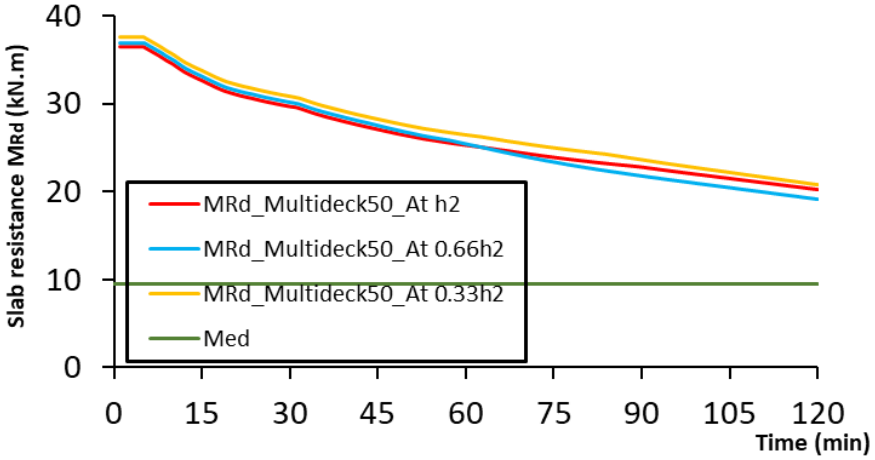

(b) Multideck50.

Figure 6.23: Load bearing evolution for both slabs.

6.6. Conclusion

This sixth chapter deals with the thermal mechanical behaviour of the composite slab. It was determined using a new proposed method based on the thermal results of the finite elements model and the analytical equations of the Eurocodes. After validating the results and considering the findings, the following conclusions can be drawn:

- The difference of the temperature between NWC and LWC is more noticeable in the Re-entrant slab rather than the trapezoidal slab.
- The presence of the LWC has decreased the temperature evolution by 22%, 41% for the trapezoidal and re-entrant slab respectively.
- The trapezoidal slabs heats more than the re-entrant slabs difference of approximately 100°C measured in the unexposed side of the slab.
- Regarding the type of the concrete, the trapezoidal slabs loss more load bearing capacity compared with re-entrant (67% and 54% for trapezoidal made with NWC and LWC respectively and 54% and 44% for re-entrant made with NWC and LWC respectively)
- Using concretes with higher mechanical resistance leads to a significant residual resisting moment after the heating (in this case the stability is still checked).
- Over 100 min of fire exposure the behaviour the trapezoidal slab made with LWC became slight better than of the NWC.
- The tendency of the development of the deflection is more pronounced in LWC than NWC.
- The trapezoidal slab deflects more than the re-entrant slab. the difference in the deflection between the two sections increases with the increase of the fire exposure time. This difference is equal to 0.81 mm and 3.99 mm at R15 and R120 respectively for NWC and for LWC it is 1.6 mm and 4.5 mm at R15 and R120 respectively.
- LWC may offer better performances in terms of limiting long-term deflection compared to NWC, particularly in trapezoidal section.
- Using concretes with low mechanical characteristics may lead to different results.
- Using a thicker steel deck enhances the load bearing capacity and reduces the deflection of the slab, however, the thickness of the steel deck has a limited effect on the fire insulation of the slab.
- The rebar size has a significant impact on its temperature evolution and the mechanical behaviour of the composite slab.

- The rebar position on the rib (cover distance) has a large effect on the temperature of the rebars and its effect is very pronounced on the thermal mechanical behaviour.

The following chapter concludes the present thesis and includes the validation of the proposed models.

7. Validation of the proposed models

7. Validation of the proposed models

7.1. Thermal models validations

To show that the proposed models in the present study are accurate, some of the experimental results from the literature [57] and [60] were examined to validate the obtained results. The data related to the materials including the geometrical form, collected from the experimental work mentioned above, were used in the numerical model of the present study.

The properties of these materials are regrouped in Table 7.1 below:

Table 7.1: Properties of the materials used for the validation [61]

Concrete type	Density	Moisture content	Thermal conductivity
	kN/m3	%	W/m.K
LWC	1875	4.81	1
NWC	2435	3.70	2.2

The results of the experimental work and the numerical model are illustrated in Figure 7.1.

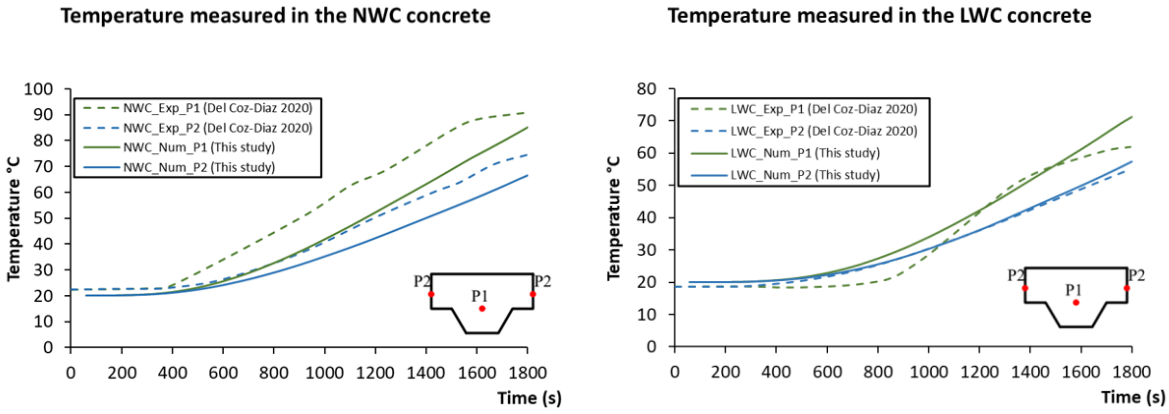

(a) NWC. (b) LWC.

Figure 7.1: Temperature evolution in the different concrete**s.**

The temperature represented by the plots was measured in points P_1 and P_2, situated at 100 mm and 40 mm from the top respectively as shown in Figure 7.1.

It is noticeable that both of the temperature curves for the experimental and numerical work in the same position and material look have similar tendencies and they are close to each other. this demonstrates that the results of this study are reasonable and very acceptable. Table 7 shows the difference between the experimental temperature readings and the temperatures predicted by the

numerical model at points P1 and P2. From this, it can be inferred that the numerical model is reliable and can be utilized to forecast fire resistance time for LWC.

Table 7.2: The difference between the experimental and the predicted temperature by the numerical model.

Time	Difference between EXP and NUM			
	P1 LWC	P2 LWC	P1 NWC	P2 NWC
60	1.6	1.3	2.7	2.4
300	1.7	1.4	2.2	2.3
400	2.2	1.3	2.9	2.1
600	4.1	0.6	6.9	2.3
800	7.0	0.1	10.7	3.8
1000	4.9	0.1	15.0	6.1
1200	0.0	0.2	14.6	8.2
1400	1.5	0.7	14.5	9.4
1600	2.3	1.0	13.6	8.1
1800	9.2	2.4	5.8	8.3

To assess the reliability of the numerical model outcomes, the differences between the experimental and the predicted temperature by the numerical model is calculated for each point and material, as detailed in Table 7.2. This difference values are close to zero for several pointes, indicating that the method employed is quite acceptable.

It is worthwhile to note that the results and the deduced conclusions obtained from this study are limited within the boundary conditions (mentioned previously), geometry slabs and the assumed materials properties. Furthermore, only the thermal insulation criterion is applied to determine the fire resistance time of the composite slabs. More accurate results could be found by using both thermal insulation criterion and structural resistance in other investigations.

7.2. Thermal Mechanical models validation

In order to check the efficiency of the models two validation checks were needed. the thermal mechanical parametric study is based on the thermal analysis which was switched into a mechanical analysis as mentioned before.

7.2.1. Thermal result validation

In order to check the efficiency of the model the experimental results of the test number six of Hamerlinck et al [7] were examined. And the information related to the form and geometrical

parameters of the slab along with the thermal properties in which were used. This information was collected and introduced into the numerical model.

The thermal characteristics used by Hamerlinck were taken from Eurocode 4 the version published in 1989 [62], the characteristics of the concrete and steel used is dependent on the temperature (ranged from 20 to 1200 °C) and given by the equations bellow:

Concrete

Density $$\rho_c = 2350 \quad {}^{kG}/_{m^3}$$

Conductivity $$\lambda_c = 2 - 0.24\left(\frac{T}{100}\right) + 0.012\left(\frac{T}{100}\right)^2 \quad {}^{W}/_{m.K}$$

Specific heat $$C_c = 900 + 80\left(\frac{T}{100}\right) - 4\left(\frac{T}{100}\right)^2 \quad {}^{J}/_{kG.K}$$

Steel

Density $$\rho_c = 7800 \quad {}^{kG}/_{m^3}$$

Conductivity $$\lambda_c = 54 - 3.33\left(\frac{T}{100}\right) \quad {}^{W}/_{m.K}$$

Specific heat $$C_c = 470 + 20\left(\frac{T}{100}\right) + 3.8\left(\frac{T}{100}\right)^2 \quad {}^{J}/_{kG.K}$$

The results of the experimental work and the numerical model are illustrated in Figure 7.2.

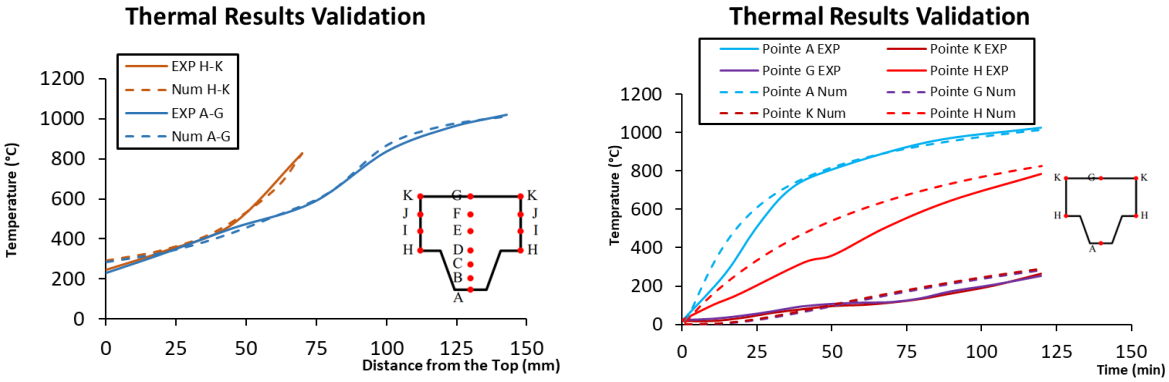

(a) Thermal result at 120 min of fire exposure on line A to G and H to K.

(b) Temperature evolution on points A,G,K and H.

Figure 7.2: Validation of the numerical results with Hamerlinck [7].

It can be seen that both of the temperature curves for the experimental and numerical work in the same measured points look have similar tendencies and they are close to each other. this demonstrates that the results of this model are reasonable and very acceptable.

7.2.2. Mechanical results

To check the accuracy of the results obtained was reliable, some of the experimental and numerical results was tested Hamerlinck et al [7] and Piloto et al [36] respectively, with taking into account the same materials and data used (the same data used in the subsection 6.2.2 for Hamerlinck study). These results are represented in the Figure bellow:

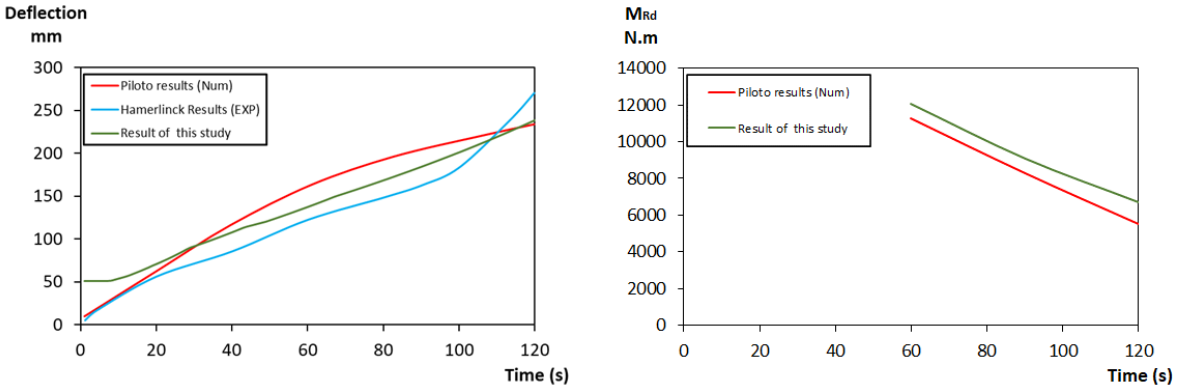

(a) Deflection. (b) Resisting moment.

Figure 7.3: Temperature evolution in the different concrete**s.**

Once again, the curves of this study results and the results from the EXP and NUM are close to each other and they have the same tendencies. This indicates that the study's results are plausible and excellent. Thus, it can be said that the proposed method is fairly reliable and may be applied to study the thermal mechanical behaviour of the composite slabs.

7.3 Conclusion

To ensure the significance and accuracy of the results obtained through the various methods presented in this work, a validation section has been included. The comparison shows that the differences between the experimental temperatures and those predicted by the numerical model are minimal for most of the studied positions, demonstrating the accuracy and reliability of the proposed models.

8. Conclusion

Conclusion

A numerical study was conducted to evaluate the thermal advantages of using lightweight concrete (LWC) instead of normal-weight concrete (NWC) in composite slabs under fire conditions. The parametric analysis considered factors such as airgap, moisture content, thermal properties of LWC, and geometric aspects. Also, the thermal mechanical behaviour of the composite slab was determined using a new proposed method based on the thermal results of the finite elements model and the analytical equations of the Eurocodes. After validating the results and considering the findings, the following conclusions can be drawn:

- The study found that for all slab thicknesses, both maximum and average temperatures exceeded the insulation criterion limit.
- Finite element method (FEM) results showed that re-entrant steel decks provide greater fire resistance times compared to trapezoidal steel decks.
- Introducing a 1 mm airgap between the concrete and deck profile increased the fire resistance time by 15 minutes for a 100 mm thick composite slab.
- When moisture content exceeds 3%, the Eurocode method predicts lower fire resistance times compared to the simulation method.
- Reducing the concrete slab density from 1922 kg/m³ to 1822 kg/m³ improved fire resistance time by approximately 12% for a 100 mm slab.
- To achieve the same fire resistance time, normal weight concrete sections need to be 7% thicker than lightweight concrete sections.
- The difference of the temperature between NWC and LWC is more noticeable in the Re-entrant slab rather than the trapezoidal slab.
- The presence of the LWC has decreased the temperature evolution by 22%, 41% for the trapezoidal and re-entrant slab respectively.
- The trapezoidal slabs heats more than the re-entrant slabs difference of approximately 100°C measured in the unexposed side of the slab.
- Regarding the type of the concrete, the trapezoidal slabs loss more load bearing capacity compared with re-entrant (67% and 54% for trapezoidal made with NWC and LWC respectively and 54% and 44% for re-entrant made with NWC and LWC respectively).
- Using concretes with higher mechanical resistance leads to a significant residual resisting moment after the heating (in this case the stability is still checked).

- Over 100 min of fire exposure the behaviour the trapezoidal slab made with LWC became slight better than of the NWC.
- The tendency of the development of the deflection is more pronounced in LWC than NWC.
- The trapezoidal slab deflects more than the re-entrant slab. the difference in the deflection between the two sections increases with the increase of the fire exposure time. This difference is equal to 0.81 mm and 3.99 mm at R15 and R120 respectively for NWC and for LWC it is 1.6 mm and 4.5 mm at R15 and R120 respectively.
- The LWC may offer better performance in terms of limiting long-term deflection compared to the NWC, particularly in the trapezoidal section.
- LWC may offer better performances in terms of limiting long-term deflection compared to NWC, particularly in trapezoidal section.
- Using concretes with low mechanical characteristics may lead to different results.
- Using a thicker steel deck enhances the load bearing capacity and reduces the deflection of the slab, however, the thickness of the steel deck has a limited effect on the fire insulation of the slab.
- The rebar size has a significant impact on its temperature evolution and the mechanical behaviour of the composite slab.
- The rebar position on the rib (cover distance) has a large effect on the temperature of the rebars and its effect is very pronounced on the thermal mechanical behaviour.
- Based on the results obtained from this analysis, the new proposed method gives close and interesting results and can help to better estimate the fire resistance time.

It is worthwhile to note that the results and the deduced conclusions obtained from this study are limited within the boundary conditions (mentioned previously), geometry slabs and the assumed materials properties. Furthermore, for future works the following points could be considered:

- The effect of the topping concrete thickness on the thermal mechanical study.
- the number of the spans could be considered.
- The mechanical effect of the ferritic steel deck may be a good alternative for the carbon steel decks.
- Refinement of the analytical model presented in the EC4.
- Studying the interface between rebars and the concrete.

- Studying the improvement of the adhesion between the concrete and the steel deck by a polymer glue.
- Studying the reinforcement lapping zone on the slab.
-

Bibliography

Bibliography

[1] Designing buildings, 'Concrete-steel composite structures'. [Online]. Available: https://www.designingbuildings.co.uk/wiki/Concrete-steel_composite_structures

[2] R. M. Lawson, 'Dalles mixtes pour bâtiments multi- étagés destinés à un usage commercial et résidentiel', 2006. [Online]. Available: https://www.cticm.com/centre-de-ressources/?fwp_taxonomy_first_line=librairie-documentation&fwp_taxonomy_second_line=doc-projet&fwp_projet=access-steel&fwp_category_projet=phase-avant-projet#woo-login-popup-sc-login

[3] S. J. Hicks, 'Composite slabs and beams using steel decking: best practice for design and construction', Metal Cladding & Roofing Manufacturers Association, Great Britain, 2009.

[4] D. Dujmović, B. Androić, I. Lukačević, and D. Dujmović, *Composite structures according to Eurocode 4: worked examples*. Berlin: Ernst/Wiley, 2015.

[5] NSC2, 'Safe working at height in the steelwork industry', newsteelconstruction.com. Accessed: Mar. 29, 2025. [Online]. Available: https://www.newsteelconstruction.com/wp/safe-working-at-height-in-the-steelwork-industry/

[6] J. Jiang, J. A. Main, F. H. Sadek, and J. M. Weigand, 'Numerical modeling and analysis of heat transfer in composite slabs with profiled steel decking', National Institute of Standards and Technology, Gaithersburg, MD, NIST TN 1958, Apr. 2017. doi: 10.6028/NIST.TN.1958.

[7] A. F. Hamerlinck, 'The behaviour of fire-exposed composite steel/concrete slabs', Phd Thesis 1 (Research TU/e / Graduation TU/e), Technische Universiteit Eindhoven, Eindhoven, 1991. doi: 10.6100/IR348360.

[8] C. G. Bailey, 'Efficient arrangement of reinforcement for membrane behaviour of composite floor slabs in fire conditions', *J. Constr. Steel Res.*, vol. 59, no. 7, pp. 931–949, Jul. 2003, doi: 10.1016/S0143-974X(02)00116-5.

[9] A. Fellouh, A. Bougara, P. A. G. Piloto, and N. Benlakehal, 'Non-linear buckling analysis of composite columns made from high and normal strength concrete under fire', *Asian J. Civ. Eng.*, vol. 21, no. 1, pp. 17–27, Feb. 2020, doi: 10.1007/s42107-019-00180-8.

[10] J. J. del Coz-Díaz, J. E. Martínez-Martínez, M. Alonso-Martínez, and F. P. Álvarez Rabanal, 'Comparative study of LightWeight and Normal Concrete composite slabs behaviour under fire conditions', *Eng. Struct.*, vol. 207, p. 110196, Mar. 2020, doi: 10.1016/j.engstruct.2020.110196.

[11] *Eurocode 4: Design of Composite Steel and Concrete Structures - Part 1-2: General Rules—Structural Fire Design*, EUROPEAN STANDARD, 2005.

[12] S. Hedjazi, 'Compressive Strength of Lightweight Concrete', in *Compressive Strength of Concrete*, P. Kryvenko, Ed., IntechOpen, 2020. doi: 10.5772/intechopen.88057.

[13] J. E. Martínez-Martínez, F. P. Álvarez Rabanal, M. Lázaro, M. Alonso-Martínez, D. Alvear, and J. J. Del Coz-Díaz, 'Assessment of Lightweight Concrete Thermal Properties at Elevated Temperatures', *Appl. Sci.*, vol. 11, no. 21, p. 10023, Oct. 2021, doi: 10.3390/app112110023.

[14] Y. A. Çengel and A. J. Ghajar, *Heat and mass transfer: fundamentals & applications*, Fifth edition. New York, NY: McGraw Hill Education, 2015.

[15] *Eurocode 3: Design of steel structures - Part 1-2: General rules - Structural fire design*, EUROPEAN STANDARD, 2005.

[16] *Eurocode 2: Design of concrete structures - Part 1-1 : General rules and rules for buildings*, EUROPEAN STANDARD, 2004.

[17] P. A. G. Piloto, 'Experimental and numerical analisys of metalic structures behaviour under fire conditions [in portuguese]',. University of Porto, 2000.

[18] *Eurocode 3: Design of steel structures - Part 1-1: General rules and rules for buildings*, EUROPEAN STANDARD, 2005.

[19] *Eurocode 2: Design of concrete structures - Part 1-2: General rules - Structural fire design*, EUROPEAN STANDARD, 2004.

[20] J.-M. Franssen, 'Analysis of the fire behaviour of composite steel-concrete structures [in french]', University of Liège.

[21] *Eurocode 1: Actions on structures - Part 1-2: General actions - Actions on structu res exposed to fire*, EUROPEAN STANDARD, 2002.

[22] A. H. Buchanan and A. K. Abu, *Structural Design for Fire Safety*, 1st ed. Wiley, 2016. doi: 10.1002/9781118700402.

[23] U. C. Ibáñez, 'Fire response analysis of circular concrete filled tubular columns and the effects of axial and rotational restraints', 2016.

[24] *American Society for Testing and Materials ASTM E119 - 00a: Standard test methods for fire tests of building construction and materials*, American Stadard, ASTM International,., 2000.

[25] M. Hurley and Society of Fire Protection Engineers, Eds., *SFPE handbook of fire protection engineering*, Fifth edition. New York Heidelberg Dordrecht: Springer, 2016.

[26] Y.-C. Kan, L.-H. Chen, and T. Yen, 'Mechanical behavior of lightweight concrete steel deck', *Constr. Build. Mater.*, vol. 42, pp. 78–86, May 2013, doi: 10.1016/j.conbuildmat.2013.01.007.

[27] D. Waldmann, A. May, and V. B. Thapa, 'Influence of the sheet profile design on the composite action of slabs made of lightweight woodchip concrete', *Constr. Build. Mater.*, vol. 148, pp. 887–899, Sep. 2017, doi: 10.1016/j.conbuildmat.2017.04.193.

[28] G.-Q. Li, N. Zhang, and J. Jiang, 'Experimental investigation on thermal and mechanical behaviour of composite floors exposed to standard fire', *Fire Saf. J.*, vol. 89, pp. 63–76, Apr. 2017, doi: 10.1016/j.firesaf.2017.02.009.

[29] *Eurocode 4: Design of composite steel and concrete structures – Part 1-1: General rules and rules for buildings*, EUROPEAN STANDARD, 2004.

[30] I. Arrayago, E. Real, E. Mirambell, F. Marimon, and M. Ferrer, 'Experimental study on ferritic stainless steel trapezoidal decks for composite slabs in construction stage', *Thin-Walled Struct.*, vol. 134, pp. 255–267, Jan. 2019, doi: 10.1016/j.tws.2018.10.012.

[31] J. Gozzi, 'structural Design of Cold Worked Austenitic Stainless Steel. WP3: Cold Formed Profiles and Sheeting Cold Formed Hat and Sheeting profiles', Division of Steel Structures, Luleå University of Technology, Technical rapport, 2004.

[32] P. A. G. Piloto, L. M.S. Prates, C. Balsa, and R. Rigobello, 'Numerical simulation of the fire resistance of composite slabs with steel deck', *Int. J. Eng. Technol.*, vol. 7, no. 2.23, p. 83, Apr. 2018, doi: 10.14419/ijet.v7i2.23.11889.

[33] *ANSYS,Academic Research*. [Online]. Available: ansys.com

[34] J. Jiang, J. A. Main, J. M. Weigand, and F. H. Sadek, 'Thermal performance of composite slabs with profiled steel decking exposed to fire effects', *Fire Saf. J.*, vol. 95, pp. 25–41, Jan. 2018, doi: 10.1016/j.firesaf.2017.10.003.

[35] J. Jiang, A. Pintar, J. M. Weigand, J. A. Main, and F. Sadek, 'Improved calculation method for insulation-based fire resistance of composite slabs', *Fire Saf. J.*, vol. 105, pp. 144–153, Apr. 2019, doi: 10.1016/j.firesaf.2019.02.013.

[36] P. A. G. Piloto, C. Balsa, F. Ribeiro, L. Santos, R. Rigobello, and E. Kimura, 'THREE-DIMENSIONAL NUMERICAL MODELLING OF FIRE EXPOSED COMPOSITE SLABS WITH STEEL DECK', *MATTER Int. J. Sci. Technol.*, vol. 5, no. 2, Art. no. 2, Aug. 2019, doi: 10.20319/mijst.2019.52.4867.

[37] I. ANSYS, *ANSYS Fluent*. (2025). [Online]. Available: https://www.ansys.com

[38] I. The MathWorks, *MATLAB*. (2025).

[39] S. Sharma, V. T. Vaddamani, and A. Agarwal, 'Insulation effect of the concrete slab-steel deck interface in fire conditions and its influence on the structural fire behavior of composite floor systems', *Fire Saf. J.*, vol. 105, pp. 79–91, Apr. 2019, doi: 10.1016/j.firesaf.2019.02.006.

[40] P. A. G. Piloto, C. Balsa, F. F. Ribeiro, and R. Rigobello, 'Three-Dimensional Numerical Analysis on the Fire Behaviour of Composite Slabs with Steel Deck', in *Advances in Fire Safety Engineering*, P. A. G. Piloto, J. P. Rodrigues, and V. P. Silva, Eds., in Lecture Notes in Civil Engineering. Cham: Springer International Publishing, 2020, pp. 12–30. doi: 10.1007/978-3-030-36240-9_2.

[41] P. A. Piloto, C. Balsa, L. M. Santos, and É. F. Kimura, 'Effect of the load level on the resistance of composite slabs with steel decking under fire conditions', *J. Fire Sci.*, vol. 38, no. 2, pp. 212–231, Mar. 2020, doi: 10.1177/0734904119892210.

[42] C. Balsa, M. B. Silveira, V. Mange, and P. A. G. Piloto, 'Computational Modeling of the Thermal Effects on Composite Slabs Under Fire Conditions', in *Advanced Research in Technologies, Information, Innovation and Sustainability*, T. Guarda, F. Portela, and M. F. Santos, Eds., in Communications in Computer and Information Science. Cham: Springer International Publishing, 2021, pp. 497–511. doi: 10.1007/978-3-030-90241-4_38.

[43] J. Jiang, W. Cai, W. Chen, J. Ye, and G.-Q. Li, 'An insight into eurocode 4 design rules for thermal behaviour of composite slabs', *Fire Saf. J.*, vol. 120, p. 103084, Mar. 2021, doi: 10.1016/j.firesaf.2020.103084.

[44] P. A. G. Piloto, C. Balsa, F. Ribeiro, and R. Rigobello, 'A new calculation method for the temperature of the components of composite slabs under fire', *J. Comput. Appl. Mech.*, vol. 52, no. 2, pp. 206–214, Jun. 2021, doi: 10.22059/jcamech.2021.316216.584.

[45] P. A. G. Piloto, C. Balsa, F. Ribeiro, and R. Rigobello, 'Computational Simulation of the Thermal Effects on Composite Slabs Under Fire Conditions', *Math. Comput. Sci.*, vol. 15, no. 1, pp. 155–171, Mar. 2021, doi: 10.1007/s11786-020-00466-0.

[46] C. Balsa, M. Silveira, V. Mange, and P. A. G. Piloto, 'Modelling the Thermal Effects on Structural Components of Composite Slabs under Fire Conditions', *Computation*, vol. 10, no. 6, p. 94, Jun. 2022, doi: 10.3390/computation10060094.

[47] S. Guo, ‘Experimental and numerical study on restrained composite slab during heating and cooling’, *J. Constr. Steel Res.*, vol. 69, no. 1, pp. 95–105, Feb. 2012, doi: 10.1016/j.jcsr.2011.08.009.

[48] Minh-Phuong, T.-T. Nguyen, and K.-H. Tan, ‘Temperature profile and resistance of flat decking composite slabs in- and post-fire’, *Fire Saf. J.*, vol. 98, pp. 109–119, Jun. 2018, doi: 10.1016/j.firesaf.2018.04.001.

[49] ‘ISO 834-11:2014’, ISO. Accessed: Mar. 30, 2025. [Online]. Available: https://www.iso.org/standard/57595.html

[50] F. Bolina, B. Tutikian, and J. P. C. Rodrigues, ‘Thermal analysis of steel decking concrete slabs in case of fire’, *Fire Saf. J.*, vol. 121, p. 103295, May 2021, doi: 10.1016/j.firesaf.2021.103295.

[51] H. Zhao, J. Zhao, R. Wang, W. Zhang, F. Liu, and S. Wu, ‘Thermal behavior of composite slabs with closed profiled steel decking and recycled aggregate concrete in fire’, *Fire Saf. J.*, vol. 132, p. 103637, Sep. 2022, doi: 10.1016/j.firesaf.2022.103637.

[52] ANSYS Innovation Courses, ‘View Factors — Lesson 2’.

[53] ‘SOLID70’. Accessed: Jan. 30, 2024. [Online]. Available: https://www.mm.bme.hu/~gyebro/files/ans_help_v182/ans_elem/Hlp_E_SOLID70.html

[54] ‘SOLID65’. Accessed: Jan. 30, 2024. [Online]. Available: https://www.mm.bme.hu/~gyebro/files/ans_help_v182/ans_elem/Hlp_E_SOLID65.html

[55] ‘LINK33’. Accessed: Jan. 30, 2024. [Online]. Available: https://www.mm.bme.hu/~gyebro/files/ans_help_v182/ans_elem/Hlp_E_LINK33.html

[56] ‘LINK180’. Accessed: Jan. 30, 2024. [Online]. Available: https://www.mm.bme.hu/~gyebro/files/ans_help_v182/ans_elem/Hlp_E_LINK180.html

[57] J. J. Del Coz-Díaz, J. E. Martínez-Martínez, M. Alonso-Martínez, and F. P. Álvarez Rabanal, ‘Comparative study of LightWeight and Normal Concrete composite slabs behaviour under fire conditions’, *Eng. Struct.*, vol. 207, p. 110196, Mar. 2020, doi: 10.1016/j.engstruct.2020.110196.

[58] T. Cavalline, R. Castrodale, C. Freeman, and J. Wall, ‘Impact of Lightweight Aggregate on Concrete Thermal Properties’, *ACI Mater. J.*, vol. 114, Nov. 2017, doi: 10.14359/51701003.

[59] S. Punlert, P. Laoratanakul, R. Kongdee, and R. Suntako, ‘Effect of lightweight aggregates prepared from fly ash on lightweight concrete performances’, *J. Phys. Conf. Ser.*, vol. 901, no. 1, p. 012086, Sep. 2017, doi: 10.1088/1742-6596/901/1/012086.

[60] F. P. Alvarez Rabanal, J. Guerrero-Muñoz, M. Alonso-Martinez, and J. E. Martinez-Martinez, ‘Bending and Shear Experimental Tests and Numerical Analysis of Composite Slabs Made Up of Lightweight Concrete’, *J. Eng.*, vol. 2016, pp. 1–10, 2016, doi: 10.1155/2016/6819190.

[61] *Testing hardened concrete-Part 3: Compressive strength of test specimens*, 2002.

[62] *Eurocode 4: Design of Composite Steel and Concrete Structures - Part 1-2: General Rules—Structural Fire Design*, EUROPEAN STANDARD, 1989.